TECHNISCHE UNIVERSITÄT DARMSTADT

A Chemical Reaction Engineering Study on Non-Noble Metal Coordinated-Nitrogen Doped Carbon Catalysts for Liquid Phase Oxidation of Alcohols

From the Department of Chemistry
at the Technical University of Darmstadt

To obtain the degree

Doctor of Engineering
(Dr.-Ing.)

Dissertation

Catur Rini Widyastuti, M.Sc.

First reviewer : Prof. Dr. Bastian J.M. Etzold
Second reviewer : Prof. Dr. Marcus Rose

Darmstadt 2022

Erklärungen laut Promotionsordnung

§8 Abs. 1 lit. c PromO

Ich versichere hiermit, dass die elektronische Version meiner Dissertation mit der schriftlichen Version übereinstimmt und für die Durchführung des Promotionsverfahrens vorliegt.

§8 Abs. 1 lit. d PromO

Ich versichere hiermit, dass zu einem vorherigen Zeitpunkt noch keine Promotion versucht wurde und zu keinem früheren Zeitpunkt an einer in- oder ausländischen Hochschule eingereicht wurde. In diesem Fall sind nähere Angaben über Zeitpunkt, Hochschule, Dissertationsthema und Ergebnis dieses Versuchs mitzuteilen.

§9 Abs. 1 PromO

Ich versichere hiermit, dass die vorliegende Dissertation selbstständig und nur unter Verwendung der angegebenen Quellen verfasst wurde.

§9 Abs. 2 PromO

Die Arbeit hat bisher noch nicht zu Prüfungszwecken gedient.

Darmstadt, 04 April 2022

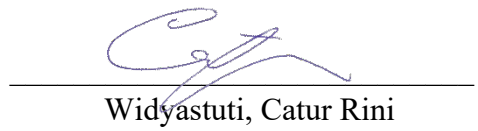

Widyastuti, Catur Rini

Acknowledgements

I would like to express my first gratitude to my supervisor Prof. Dr. Bastian Etzold, for the opportunity given to me for pursuing Doctoral in Germany. I really appreciate his guidance and kindness during my study; hence I finally managed all the difficulties and finished the dissertation.

I also thank Hon.-Prof. Dr.-Ing. Alfons Drochner, for the insightful feedback and valuable advice during my research. Your theoretical contribution leads me to search the in-dept answer.

Sincere thank goes to Dr.-Ing. Jan Gläsel for mentoring and advising during laboratory work. Same appreciation goes to Dipl.-Ing. Karl Kopp and Dr. Kathrin Hofmann for helping in XPS and XRD measurement. My gratitude also goes to Ali Shahraei from Prof. Kramm's group for the collaboration in the catalyst's synthesis and Niklas Oefner for proof-reading and discussion.

I would also like to thank everybody at the Etzold's group for the warm friendship. Being one of you is really my luckiness. Appreciation also goes to Marianne Blascak for her assistance in organizing the documents during my study. With everybody's help, I can turn the difficulties to ease.

Importantly, I would like to thank my family, Bapak Suratman Hadi Purwanto and Ibu Parjiyah, my sister and brother, Sri Rahayu Purwantiningsih, Dwi Any Wurjayanti, and Agung Tri Gunawan, and also my husband, Prabono H. Putranto, for your support and encouragement in going through the hard times. Especially to my dearest daughters, Aliya Kinanthi Larasati Prabono and Alina Kinasih Saraswati Prabono, I am grateful that you always make my life meaningful.

Lastly, I am grateful to the LPDP scholarship, the Indonesia Endowment Fund for Education, for financing my Doctoral study.

Table of contents

List of Figures

List of Tables

List of abbreviations and symbols

Abbreviations

M-N-C	Metal-Coordinated-Nitrogen Doped Carbon
Fe-N-C	Iron-Coordinated-Nitrogen Doped Carbon
Fe-N-Gra	Iron-Coordinated-Nitrogen Doped Graphene
Co-N-C	Cobalt-Coordinated-Nitrogen Doped Carbon
N-C	Nitrogen Doped Carbon
PANI	Polyaniline
PXP	Pyridoxine-5-phosphate
CoTMPP	Cobalt tetramethoxyphenylporphyrin
ZIF	Zeolitic Imidazolate Framework
MOF	Metal Organic Framework
MeIM	2-metylimidazole
APS	Ammonium Persulfat
WI	Wetness Impregnation
IWI	Incipient Wetness Impregnation
FTIR	Fourier Transform Infrared
ICP-AES	Inductively Coupled Plasma Atomic Emission Spectroscopy
XRD	X-Ray Diffraction
XPS	X-Ray Photoelectron Spectroscopy
TEM	Transmission Electron Microscopy
GC	Gas Chromatography
ORR	Oxygen Reduction Reaction
OER	Oxygen Evolution Reaction
HER	Hydrogen Evolution Reaction
CO_2RR	Carbon Dioxide Reduction Reaction
NRR	Nitrogen Reduction Reaction
a.u.	Arbitrary Unit
DMF	Dimethylfuran
RDE	Rotating Disc Electrode
PEMFCs	Proton Exchange Membrane Fuel Cells
CV	Cyclic Voltammetry
ECSA	Electrochemically Active Surface Area
DMF	Dimethylfuran
EDX	Energy-Dispersive X-Ray Spectroscopy
BA	Benzyl alcohol

BD	Benzaldehyde
MB	Methy benzoate
BB	Benzyl benzoate

Symbols

eV	Electronvolt	
CPS	Counts per second	
X	Conversion	%
Y	Yield	%
S	Selectivity	%
τ	Modified reaction time	min g_{cat} ml^{-1}
t	time	h
C_A	Concentration of component A	M
C_t	Concentration of component A at specified time	M
m_{cat}	Mass of catalyst	mg
k	Initial reaction rate constant	h^{-1}
k	Reaction rate constant	min^{-1} mL g_{cat}^{-1}
A	Frequency factor	
R	Gas constant	8.314 J mol^{-1} K^{-1}
E	Activation energy	kJ mol^{-1}
T	Temperature	°C or K
P	Pressure	Bar
ν_{ij}	Extent of reaction	
r	Reaction rate	mol g_{cat}^{-1} min^{-1}

Deutsche Zusammenfassung

Metallkoordinierte, mit Stickstoff dotierte Kohlenstoffkatalysatoren (M-N-C) wie Fe-N-C und Co-N-C wurden bereits erfolgreich für die Sauerstoffreduktionsreaktion (ORR) in Brennstoffzellen, sowie für die Umwandlung einer Vielzahl von organischen Stoffen eingesetzt. Die bisherigen Studien zeigen, dass diese Katalysatoren auch in der Oxidation von Benzylalkohol in flüssiger Phase aktiv und selektiv sind. Während bereits über die Selektivität bei Vollumsatz berichtet wurde, sind Untersuchungen der Kinetik, welche bei Teilumsätzen durchgeführt werden müssen, bisher nicht veröffentlicht. Dies ist für die Vergleichbarkeit der Performance der Katalysatoren von großer Wichtigkeit. In der vorliegenden Arbeit wurde ein geeignetes Protokoll zur Bestimmung der Kinetik von Katalysatoren auf der Grundlage einer reaktionstechnischen Studie entwickelt. Das Protokoll wurde für die Untersuchung der Kinetik verschiedener Arten von Co-N-C-Katalysatoren verwendet, die auf unterschiedlichen Wegen synthetisiert wurden. Diese kinetische Untersuchung wurde auch als Grundlage für eine Stabilitätsuntersuchung verwendet.

Die Co-N-C-Katalysatoren wurden durch verschiedene Imprägnierungsverfahren mit anschließender Pyrolyse bei 700-800 °C unter inerten Bedingungen synthetisiert. Die katalytische Aktivität wurde in der direkten oxidativen Veresterung von Benzylalkohol als Benchmark-Reaktion getestet. Die Reaktion wurde in einem Semi-Batch-Slurry-Reaktor mit kontinuierlicher Luftzuführung in die Flüssigphase bei einer Betriebstemperatur von 60 °C durchgeführt. Zusätzlich wurde für Orientierungsversuche ein kleinerer Batch-Slurry-Reaktor ohne kontinuierliche Luftzufuhr verwendet. Experimente in diesem Aufbau zeigten allerdings Stofftransportlimitierung in der Gasphase.

Für die kinetischen Untersuchungen wurde sichergestellt, dass der Reaktor im kinetisch kontrollierten Bereich ohne Stofftransportlimitierung arbeitet. Das Ergebnis zeigte, dass ein Kinetikmodell mit Potenzansatz erster Ordnung mit den optimalen Parametern eine gute Übereinstimmung mit den experimentellen Daten aufweist. Als kinetische Beschreibung erwies sich eine konsekutive Reaktion von Benzylalkohol zunächst zu Benzaldehyd und anschließend zu Methylbenzoat, beschrieben durch eine Kinetik nach dem Potenzansatz erster Ordnung, als effizient. Alle untersuchten Katalysatoren wiesen eine hohe Selektivität zu dem Esterprodukt auf. Die Studie zeigte, dass der erste Reaktionsschritt zu Benzaldehyd mehr als eine Größenordnung langsamer ist als die nachfolgende Reaktion zu Methylbenzoat. Bei allen untersuchten Katalysatoren wurden Aktivitätsunterschiede von fast einer Größenordnung beobachtet, wobei ein von Polyanilin abgeleiteter Katalysator mit einer zusätzlichen Säurebehandlung die höchste Aktivität aufwies. Während einer Variation der Basenkonzentration konnte eine starke Abhängigkeit der Aktivität von der Basenkonzentration festgestellt werden, wobei auch eine stärkere Desaktivierung zu beobachten war. Hierbei zeigte eine Basenkonzentration von 5

Mol-% bei ausreichender Katalysatorbeladung eine erhöhte Reaktionsgeschwindigkeit mit geringerem Einfluss auf die Katalysatorstabilität.

Abstract

Metal coordinated nitrogen doped on carbon (M-N-C) catalysts such as Fe-N-C and Co-N-C have been successfully implemented for oxygen reduction reaction (ORR) in fuel cell, to date these catalysts also demonstrated high activity for various organic transformation. The previous studies show that catalysts are active and selective in liquid phase benzyl alcohol oxidation. While selectivity was reported at full conversion, an assessment of the kinetics needing partial conversion is missing. This is important to truly compare the performance of different catalysts. In the present work, a proper protocol was developed to determine the kinetics of catalysts based on chemical reaction engineering study. The protocol was applied for evaluating the kinetics of several type of Co-N-C catalysts which were synthesized through different routes. This kinetic assessment was also used as the basis for a true stability investigation.

The Co-N-C catalysts were synthesized through different impregnation procedures prior to pyrolysis at 700-800 °C under inert conditions. The catalytic activity was tested in a benchmark reaction of direct oxidative esterification of benzyl alcohol. The reaction was carried out in a semi-batch of slurry reactor and with continuously bubbling air at operating temperature of 60 °C. A smaller scale set-up of slurry reactor with gas simply pressed up was used for orientation studies but showed gas-phase mass transfer limitations.

For the kinetic investigation it was ensured to operate in the kinetically controlled regime without mass transfer limitations. The result shows a simplified first order power law model with the optimum parameters were in a good agreement with the experimental data. As kinetic description, a consecutive reaction from benzyl alcohol to benzaldehyde and then methyl benzoate described with first order power law kinetics proofed to be efficient. All the investigated catalysts show high selectivity towards the ester product. The study shows that the first reaction step towards benzaldehyde is in minimum one magnitude slower compared to the consecutive reaction to methyl benzoate. Strong activity differences of nearly one order of magnitude can be observed for all the investigated catalysts, while a polyaniline derived catalyst employing an additional acid leaching, shows the highest activity. The catalyst stability was evaluated, showing strong dependency of catalytic activity on the base concentration, however, increasing in the deactivation behavior of the catalyst. Furthermore, base concentration of 5 mol% at sufficient catalyst mass loading was known to drive the reaction rate with less influence of catalyst deactivation.

1 Introduction

Catalysts are key components in chemistry from fundamental laboratory to industrial scale as it drives the chemical reaction. A suitable catalyst is required to decrease the activation energy, control reaction rate, and increase selectivity [1]. For instance, the catalyst helps to increase the sustainability of production processes, e.g., through reducing energy losses and ensuring high feedstock usage through high selectivity. The catalyst itself can be made out of critical materials such as precious metals, which are expensive, especially if used in large quantities. Reducing the amount of critical materials or substituting them with non-critical alternatives is a research gaining high interest in the past decade. Solely carbon as well as carbon with coordinated metals were shown to be suitable substitutes for noble metal catalysts. Especially the later one is studied as fuel cell catalyst intensively [2], but recently also as catalyst for liquid phase alcohol oxidation [3]. Furthermore, as it is a heterogeneous catalyst, its recyclability nature enables green and sustainable manufacturing and avoids the secondary pollution problem.

Non-noble metal coordinated carbons, such as Fe-N-C and Co-N-C, have been widely developed and applied in various industrial applications. Modification of such catalysts is possible in a relatively efficient way through various types of impregnation methods followed by heat treatment at high temperature. A suitable precursor support material, such as carbon black [4], polyaniline (PANI) [5], cobalt porphyrin (CoTMPP) [6], etc., is required to fabricate a catalyst with intended characteristics, i.e., high activity and selectivity in a specific reaction and high stability under reaction condition. The Fe-N-C type catalysts are commonly used as electrocatalysts in energy conversion systems, such as oxygen reduction reaction (ORR) [7], oxygen evolution reaction (OER) [8], hydrogen evolution reaction (HER) [9], carbon dioxide reduction reaction (CO_2RR) [10], and nitrogen reduction reaction (NRR) [11]. Besides the application as electrocatalysts [12][13], Co-N-C catalysts have recently been applied as thermal-catalysts in alcohol oxidation, i.e., in the oxidative esterification of benzyl alcohol [3]. Diverse organic transformations, such as reductive amination of aldehydes and ketones [14], alcohol dehydrogenation to acids [13], aerobic oxidative cross-coupling of secondary and primary alcohols to produce α,β-unsaturated ketones [15], etc., were also successfully conducted in the presence of the Co-N-C type catalysts.

Especially applied in the aerobic oxidative esterification reaction, such Co-N-C type catalysts showed high activity and selectivity. This reaction is commonly used as a benchmark reaction for screening various newly-developed novel catalysts due to mild operating conditions at temperature below 100 °C and atmospheric pressure with merely using molecular oxygen as oxidant agent [3], [4], [16]–[19]. Additionally, the main product of ester is an important building block for fine and bulk chemicals, such

as numerous pharmaceuticals, agrochemicals, fragrances, and polymers [3]. Esters were traditionally produced through reaction of alcohols and carboxylic acid or its derivatives via a multistep process in an acid catalyzed system or the presence of a dehydrating agent [20], [21]. Since the process results in unwanted side products and a significant amount of waste, an alternative pathway of the reaction that is more sustainable is required.

Different alternative pathways of the oxidative esterification process have been known. Direct esterification of alcohols with other readily available chemicals is feasible in the presence of a catalyst. Aldehydes are bulk chemicals that are widely used for the intended reaction (Scheme 1-1, path a). The reaction between the alcohol and the aldehyde occurs using oxidants and catalysts. Another possible pathway for the oxidative esterification process is the reaction between two alcohols (Scheme 1-1, path b). In this case, using two different alcohols is more favorable because aldehyde is usually an intermediate of alcohol oxidation. Inactivated alkanes have also been applied for oxidative esterification with alcohols (Scheme 1-1, path c). Alternatively, the ester can be synthesized by reacting organometallic compounds (R-M) or hydrocarbons (R-H) with CO through oxidative carbonylation (Scheme 1-1, path d) [20], [21].

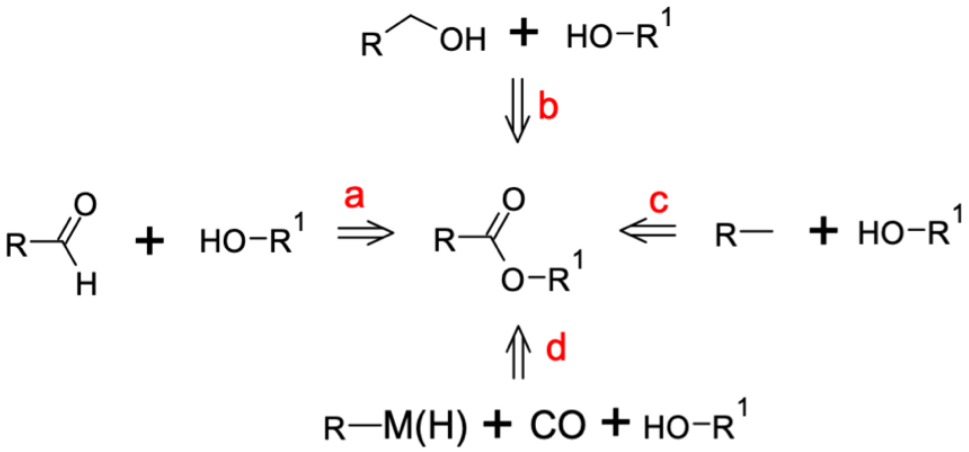

Scheme 1-1 Oxidative esterification of alcohols through different routes, i.e. the reaction between benzaldehydes and alcohols (path a), the reaction between two different alcohols (path b), the reaction between alkanes and alcohols (path c), the reaction between organometallic compounds (R-M) or hydrocarbons (R-H) with CO and alcohols [20]

As shown in Scheme 1-1 (path a and b), the esterification process can take place in the presence of oxidant and catalyst. As described previously, Co-N-C type catalysts may promote this path of reactions under mild conditions by merely using molecular oxygen as the oxidant. Furthermore, it has been observed that the direct transformation of aromatic alcohols to corresponding esters is easier compared to the aliphatic alcohols. In this case, benzylic alcohols are more reactive while aliphatic alcohols are

chemically stable; thus, the direct transformation under mild reaction conditions becomes more challenging.

A novel type of carbon-supported metal catalysts was reported to be superior in terms of their activity and selectivity, however, their stability under oxidative conditions is still a major concern [22]. The instability of the catalyst due to deactivation is generally associated with changes in the physical and chemical structure of the catalyst that is affected by the operating conditions applied. In many cases, Co-N-C catalysts showed less activity at the consecutive run of reaction in the liquid phase. Catalyst deactivation may be caused by the loss of the active component which usually results from leaching in liquid-phase reactions. Furthermore, the decay is not merely caused by the leaching but also another possible factor such as re-oxidation of cobalt after the recycling which diminished the active cobalt species [23]. Reported by *Li et al.*, the catalyst declining activity was also observed due to partially oxidized cobalt during the reaction by the air [24]. Also, they applied catalyst regeneration by H_2 treatment which was effective to restore the catalyst activity. Other possible parameters leading to deactivation suggested by *Koltunov et al.* [25], who studied the influence of bases, i.e., K_2CO_3, towards the activity of Co-N-C catalysts in the oxidative esterification of benzyl alcohol. Apparently, the base accelerates the reaction; however, the dependency effect of the base on its increasing concentration shows a pronounced deactivation behavior of catalyst.

Employing Co-N-C in a heterogeneous catalytic system involves multistep of mass transfer where diffusion may limit the rate of reaction as illustrated in Figure 1-1.

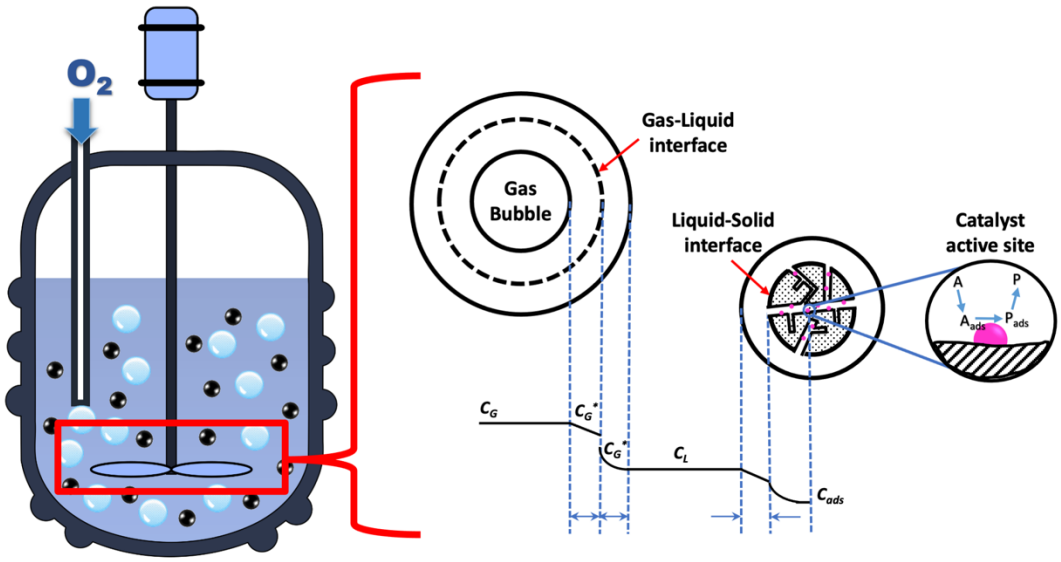

Figure 1-1 Illustration of mass transfer of substrate molecules to the active site in a heterogeneously catalyzed reaction system.

In a metal doped carbon catalyst, the active sites are located inside the pores, while the substrates enter the pores through diffusion. Minimizing the influence of diffusion limitation and confirming the surface reaction as the rate limiting step is a key for assessing a reliable kinetics. Proof of principle studies show that Co-N-C catalysts are active and selective e.g., in benzyl alcohol oxidation [3], [5], [26]–[28]. However, the activity and selectivity were reported at full degree of conversion, while a true kinetic assessment required partial conversion is missing. Hence in this work, a protocol was developed based on a chemical reaction engineering study to assess the kinetics of different catalysts. Given the reaction occurred in a heterogeneous system, the diffusion factor was taken into account for developing general procedure. The protocol was employed to assess the kinetic differences of the investigated Co-N-C catalysts and also as a basis for the stability assessment.

2 State of The Art of Research

2.1 Metal coordinated nitrogen doped carbon (M-N-C) catalysts

M-N-C based materials have exhibited excellent performance towards diverse catalytic reactions, including some typical sustainable fuel generation reactions, such as the oxygen reduction reaction (ORR) [29], [30], oxygen evolution reaction (OER) [13], hydrogen evolution reaction (HER) [9], carbon dioxide reduction reaction (CO_2RR) [31], nitrogen reduction reaction (NRR) [32], and have become promising alternatives to conventional noble metal or non-noble metal-based catalysts. Besides known as electro-catalyst, this composite material has wider application as thermal-catalyst for organic transformations. *Beller et al.* [3][4] have introduced a novel catalyst of Co-N-C for different kind of organic transformations, including aldehyde and ester production from the abundantly available alcohol substrate. Nitrogen-doped carbon (NC) has been considered as favorable support material, which shows strong interaction between N atoms in the carbon and the metal particles, good mechanical properties, large specific surface area, excellent conductivity, structural flexibility beyond atomic scale, low costs, and ideal stability under acidic or alkaline conditions [29]. The general synthesis strategy to prepare metal doped carbon catalysts is depicted in Figure 2-1. The properties of the catalyst can be tuned by changing the precursor material or by different treatment methods.

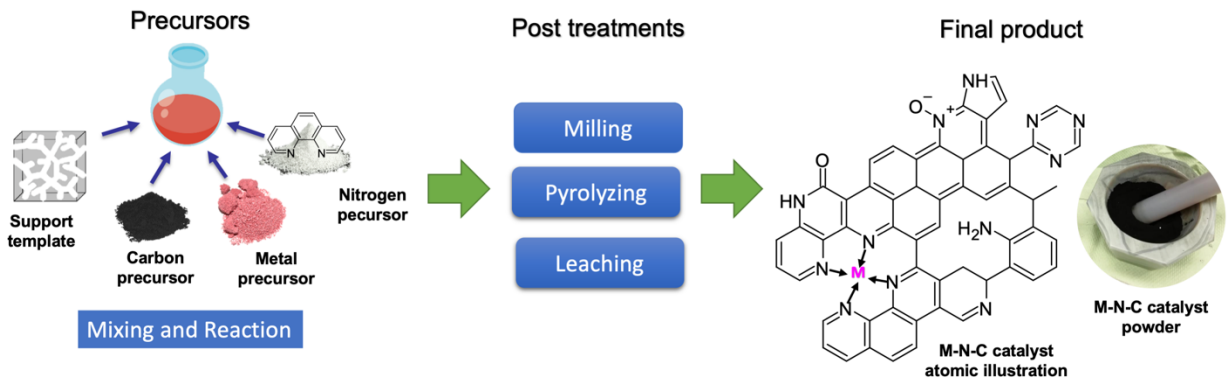

Figure 2-1 General synthesis procedure of M-N-C catalyst

Enhancement of the catalytic performance of M-N-C materials can be done by increasing the accessible number of active centers in catalyst. Controlling extrinsic and intrinsic factors associated with active centers is essential for highly efficient M-N-C catalysts with optimal electronic and geometric structure [33]. The extrinsic factors are generally correlated to the accessibility of the active metal site, in which the design strategy can be done by tuning the morphology of the carbon support. The construction of 3D hierarchical porous structures not only provides a large specific surface area to populate and stabilize

more single-atom active sites but also facilitates the diffusion of reactants, ions, and products [30], [31], [34]. Meanwhile, the intrinsic factors such as dopants and defects can interact with active centers by charge transfer effects and correspondingly alter the electronic structure of active centers [35]. The activity of a metal catalyst is intrinsically sensitive to their electronic structure, especially the d-band center of the metal species [36]. Dopants or molecules, either in the carbon support or coordinating the metal catalysts, are able to act as electron donors or acceptors, inducing electron redistribution around the metal active sites. Metal clusters embedded in the carbon support provide more active sites as well as modulates the d-band center with the charge transfer between the metal cluster and the single metal site [37], [38]. Additionally, defects in the carbon support or the change in the coordination number or type of active center that break the symmetry of the catalyst and shift the energy level of the d-band center of the metal atom, is another effective way to modulate the catalytic activity [39]. The synergistic effects between metal ion centers or between metal centers and other active sites, which are induced by extrinsic and intrinsic factors, also play an important role in boosting the catalytic performance. In brief, the extrinsic and intrinsic factors affect the activity and selectivity of active centers, electronic structure of active centers, and synergistic effects between active centers.

Among the recent studies of the non-noble-metal-based ORR catalysts, transition metal based M-N-C materials have been emerging as the most appealing platinum-free candidates [40], [41]. In particular Fe–N–C and Co–N–C nanomaterials have been recognized as the most promising non-precious ORR catalysts with higher electrochemical activities in both acidic and alkaline media. The study conducted by *Zelenay et al.* [42] has shown that iron based catalysts (PANI-Fe-C) exhibited higher ORR activity than the cobalt based catalyst (PANI-Co-C). Both Fe- and Co-N-C catalysts have been used as electrocatalyst, while the latter are also used as catalysts for various organic transformations. As reported by *Beller et al.* [3], the Co-N-C catalyst showed high activity in the oxidation reaction of alcohols.

2.1.1. Fe-N-C catalyst

As non-precious metal catalyst, iron has been widely used in oxidation reactions to replace platinum-based catalyst due to lower production costs. Iron as a heterogeneous catalyst is preferred with consideration of the ease in the separation process. In the fuel cell application, iron doped carbon has been introduced as an efficient ORR catalyst with excellent activity. The active catalyst can be prepared in several ways, commonly by impregnation of Iron (Fe) on the carbon support, followed the catalyst activation by heat treatment at high temperatures. Introduced by *Xu et al.* [43], they developed an iron-coordinated nitrogen-doped carbon catalyst (Fe-N/C) using a nitrogen-rich ligand 11,11′-bis(dipyrido[3,2-*a*:2′,3′-*c*]phenazinyl) (bidppz) as the nitrogen precursor. The ligand molecules

coordinate with iron to form a coordination polymer (Fe-bidppz) which hinders the agglomeration of iron species during the subsequent heat treatment. The concentration of highly thermally stable pyridinic nitrogen in bidppz is nearly 20 wt %, allowing a high degree of Fe-N coordination at a high pyrolysis temperature. The synthesis method of Fe-N/C catalysts follows the schematic illustration presented in Scheme 2-1. The synthesis method successfully doped the iron in the pyridinic N and pyrollic N as the metal-coordination sites due to their lone-pair electrons, in which the formed sites of Fe-N_x may act as the major active sites.

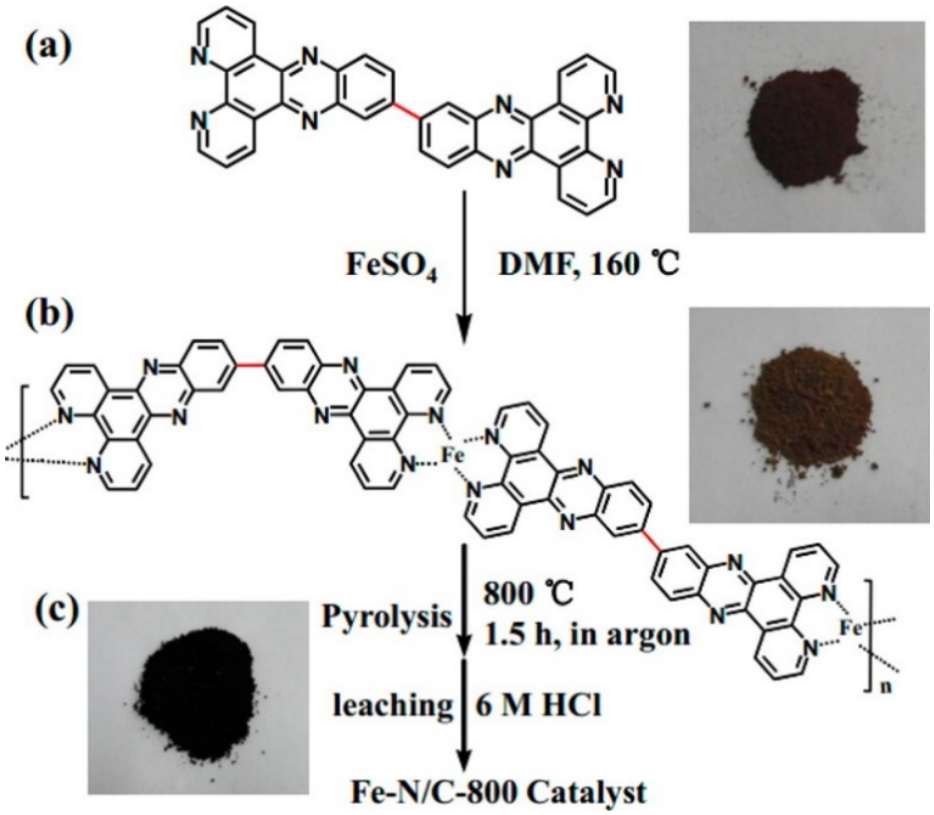

Scheme 2-1 Schematic illustration of the synthetic process of the Fe-N/C-800 catalyst: (a) chemical structure and photograph of bidppz, (b) chemical structure and photograph of the corresponding Fe-bidppz precursor, (c) photograph of the obtained Fe-N/C-800 catalyst. Reused figure with permission [43]. Copyright © 2014, American Chemical Society.

Another study conducted by *Tammeveski et al.* [44] investigated the influence of different support material precursors towards the activity of the obtained Fe-N-C as ORR catalyst. In their studies, commercially available graphene and graphene oxide were used as the carbon substrates. Their study revealed that graphene supported iron catalyst showed high ORR activity in alkaline media. In accordance with the report from *Xu et al.* [43], the highly active sites for ORR activity is Fe-N_x form which is also present in a large amount. In this case, graphene provides more nitrogen atoms used for coordination with iron atoms. In addition to the presence of high amount active sites, the activity of iron

coordinated nitrogen doped graphene (Fe-N-Gra) is also attributed to the higher surface area and micro/mesoporous nature of the support material.

Besides graphene, polymer-based carbon has also been widely developed as a support material. The combination of nitrogen-containing compounds, transition-metal salts, and carbons ultimately leads to considerable increase in ORR activity but relatively little progress in stability [42]. Polyaniline (PANI) has been known as a promising template since it represents a favorable combination of aromatic rings connected via nitrogen-containing groups. The polyaniline structure has similarity with graphite, in which the heat treatment could facilitate the incorporation of nitrogen-containing active sites into the partially graphitized carbon matrix. The use of polyaniline as a nitrogen precursor provides a more uniform distribution of nitrogen sites on the surface and an increase in the active-site density. Additionally, PANI-derived formulations appear to combine high ORR activity with relatively high-performance durability for heat-treated non-precious metal catalysts. A schematic diagram describing the catalyst synthesis as studied by *Wu et al.* [42] is shown in Scheme 2-2.

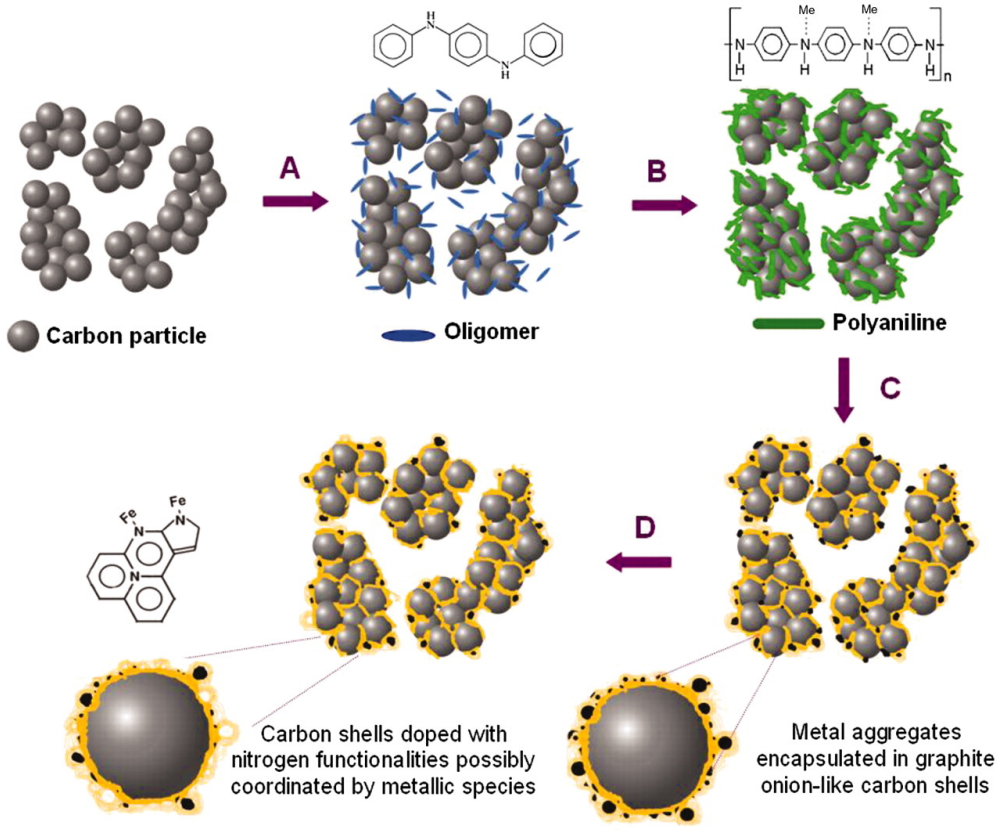

Scheme 2-2 Schematic diagram of the synthesis PANI-M-C catalyst. (A) Mixing of high-surface area carbon with aniline oligomers and transition-metal precursor (M: Fe and/or Co). (B) Oxidative polymerization of aniline by addition of APS. (c) First heat treatment in N_2 atmosphere. (D) Acid Leaching. Reused figure with permission from Wu et al. [42]. Copyright (c) 2011, American Association of the Advancement of Science.

According to synthesis approach conducted by *Wu et al.* [42], a short-chain aniline oligomer was first mixed with high-surface area carbon material and transition metal precursor (i.e., iron(III) chloride), followed by the addition of $(NH_4)_2S_2O_8$ (ammonium persulfate, APS) as an oxidant to completely polymerize the aniline [42]. After polymerization, water was evaporated from the suspension and the remaining solid phase was heat treated in the range of 400 to 1000 °C under N_2 atmosphere. Subsequently, a leaching procedure was applied using 0.5 M H_2SO_4 at 80 to 90 °C for 8 hours to remove any unstable and non-reactive phases. The second heat treatment was conducted under N_2 as the final step of the synthesis. The synthesized PANI-Fe-C catalyst was applied as electro-catalyst in a fuel cell and showed high ORR activity. The pyridine, pyrrollic, and quaternary nitrogen centers are present in the heat-treated PANI-C, which play a role in donating electrons to the carbon, hence facilitating the ORR. While the incorporated iron leads to an enhancement in the ORR activity and four-electron selectivity of the catalyst. Furthermore, the catalytic activity and the performance stability were highly influenced by the heat treatment temperature. As confirmed using FTIR spectra of PANI-Fe-C, between 400 - 600 °C the benzene-type (1100 cm^{-1}) and quinone-type (1420 cm^{-1}) structures on the main PANI chain break into smaller fragments, such as C=N (1300 cm^{-1}), which was believed as precursor states for ORR-active sites. At higher heat treatment temperature, starting from 900 °C, the PANI structures become more graphitic. An even higher temperature above 1000 °C, the particles morphology becomes highly non-uniform and substantially surface area loss were detected [42].

The influence of the combination of iron and coordinated nitrogen on the carbon framework towards the ORR activity has also been studied by *Zhang et al.* [45]. A catalyst with complete atomic dispersion of FeN_4 was synthesized by tuning the doped Fe content in zeolitic imidazolate framework (ZIF)-8 precursors. The catalyst synthesis was principally conducted by chemical doping to replace a small fraction of Zn ions in ZIF-8 precursors with Fe ions, allowing precise control of the Fe content. By applying subsequent high-temperature treatment, chemically doped ZIFs are directly converted into a high surface area carbon, co-doped with Fe and nitrogen [46], [47]. The high ORR activity was confirmed in fuel cell testing, in which the key factor behind the high ORR activity of the Fe-N-C catalyst is the optimum Fe content in the ZIF-8 precursor. The Fe content in the precursor also affects other key catalyst properties such as the particle size, porosity, nitrogen-doping level, and carbon microstructure. The best activity of the Fe-N-C catalyst was achieved using 1.5 at% of Fe content due to the highest density of atomically dispersed Fe sites in the ORR. Whereas further increase of iron loading led to the formation of Fe clusters or nanoparticles which are less active. The optimum Fe content benefits from the conversion of all available Fe in the precursor to FeN_4 active sites, rather than to Fe clusters or nanoparticles. Moreover, studied by advanced spectroscopy, the best performing catalyst has the highest

total and pyridinic nitrogen content. This is correlated to the highest concentration of FeN_4 sites which likely involves pyridinic nitrogen atoms.

2.1.2. Co-N-C catalyst

Cobalt is one of the well-known non-noble metal catalysts with high activity and selectivity in oxidation reactions [3], [4], [48]. Cobalt can be used in a homogeneous and heterogeneous catalytic system. Different types of cobalt catalysts in the form of nanoparticles have been prepared by *Mondal et al.* [33], which works effectively in dichloromethane solvent for aerobic oxidation of various alcohols. The catalyst was synthesized at room temperature from cobalt sulfate as the metal salt and tetrabutyl ammonium bromide as surfactant. Due to its magnetic property, the catalyst can be recycled with equal activity. Recently, Beller and co-workers have established an efficient synthesis method of Co-N-C catalyst by combining wetness impregnation method using ligated complexing agent and subsequent pyrolysis at high temperature, as seen in Scheme 2-3 [3], [4], [49]. The resulting catalyst shows cobalt nanoparticles with varying sizes of 2-20 nm, as well as particles and agglomerates in the range of 20-200 nm. These particles are encapsulated by individually nitrogen-enriched graphene-type layers, which the formation occurred during the pyrolysis process by carbonization of the nitrogen ligand. The catalyst has been successfully applied in the liquid phase for oxidative esterification of alcohols using molecular oxygen under relatively mild conditions. Different aliphatic alcohols undergo oxidative self-esterification in the presence of this catalyst using only 1 bar of molecular oxygen. The bulk chemical ethyl acetate can be obtained from ethanol in good yield (65 %) under such mild conditions (P: 1 bar, T: 90 °C). The self-esterification of benzylic alcohols was also carried out, and the catalyst showed high selectivity towards the corresponding benzyl benzoate in up to 85% yield [3].

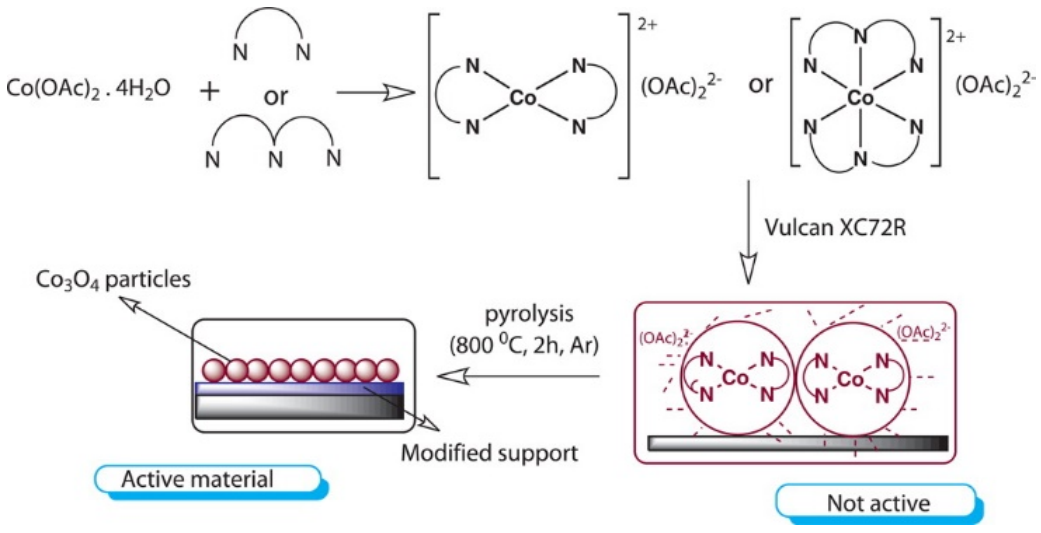

Scheme 2-3 Preparation of Co_3O_4-N@C material. Reused figure with permission [3]. Copyright © 2013, American Chemical Society.

Another report has been conducted by *Liu et al.* [50] in which they synthesized cobalt catalysts embedded in N-doped carbon derived from cobalt porphyrin via a one-pot synthesis method. The catalyst showed good performance for selective oxidation of ethylbenzene under a solvent-free condition with molecular oxygen and a stable activity after six runs of reactions. The stability of the catalytic performance was attributed to the stable N-doped graphitic carbon, the synergistic effect of the N-C structure and cobalt oxide, and the stability of the carbon-encapsulated Co nanoparticles. The N-C was designed to improve catalytic performance by preventing the growth of Co particles and stabilizing the Co valance state via the ability of N-C to donate and accept electrons [50].

Li et al. [27] also reported that single metal atom can be stabilized on carbon matrix by introducing N atoms as an anchor, since the C-N bond is highly stable. Another way to synthesize of Co-N-C catalyst was done by *Zhong et al.* [24] by simple thermolysis of the Co-containing metal-organic framework (MOF), ZIF-67 ($Co(MeIM)_2$, MeIM = 2-methylimidazole) as illustrated in Scheme 2-4. The precursor is an ordered porous materials consisting of metal ions and organic ligands. The MOF-derived materials have shown excellent performance in oxidative esterification with a broad substrate scope for aromatic and aliphatic alcohols as well as diols. During the pyrolysis, the MeIM linkers are carbonized gradually and the resulting carbon-nitrogen composites play an important role in isolating the Co species.

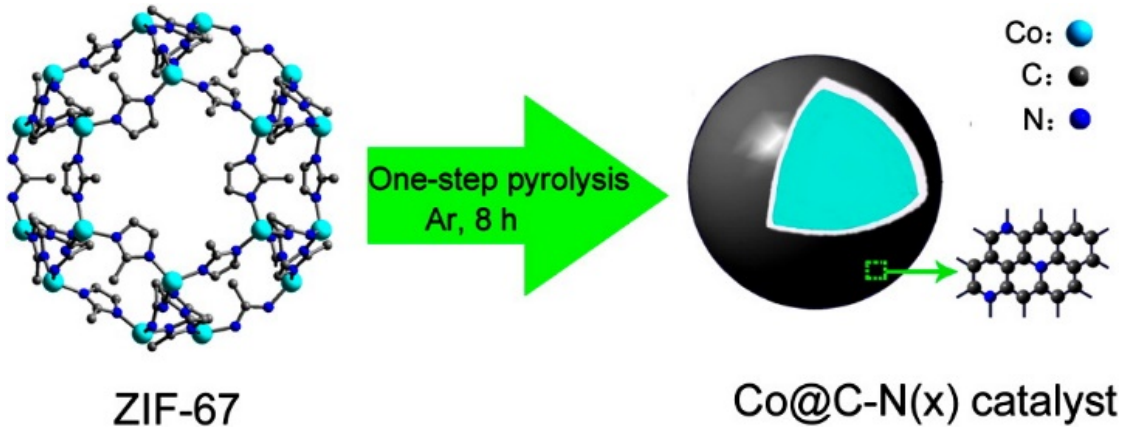

Scheme 2-4 Schematic illustration of the formation of a nitrogen doped graphite embedded Co catalyst from one-step pyrolysis of ZOF-67. Reused figure with permission [24]. Copyright © 2015, American Chemical Society

Different precursor materials of polymer derived carbons were previously introduced by *Jain et al.* [5]. They prepared a Co-N-C catalyst via pyrolysis of polyaniline (PANI) grafted cobalt(II)acetate at 600 °C for 2 h under inert atmosphere. The presence of nitrogen atoms in the developed catalyst was found to be essential for improving catalytic activity as well as stability due to strong interaction between nitrogen atoms and cobalt ions. The schematic preparation of PANI derived catalyst can be seen in Scheme 2-5.

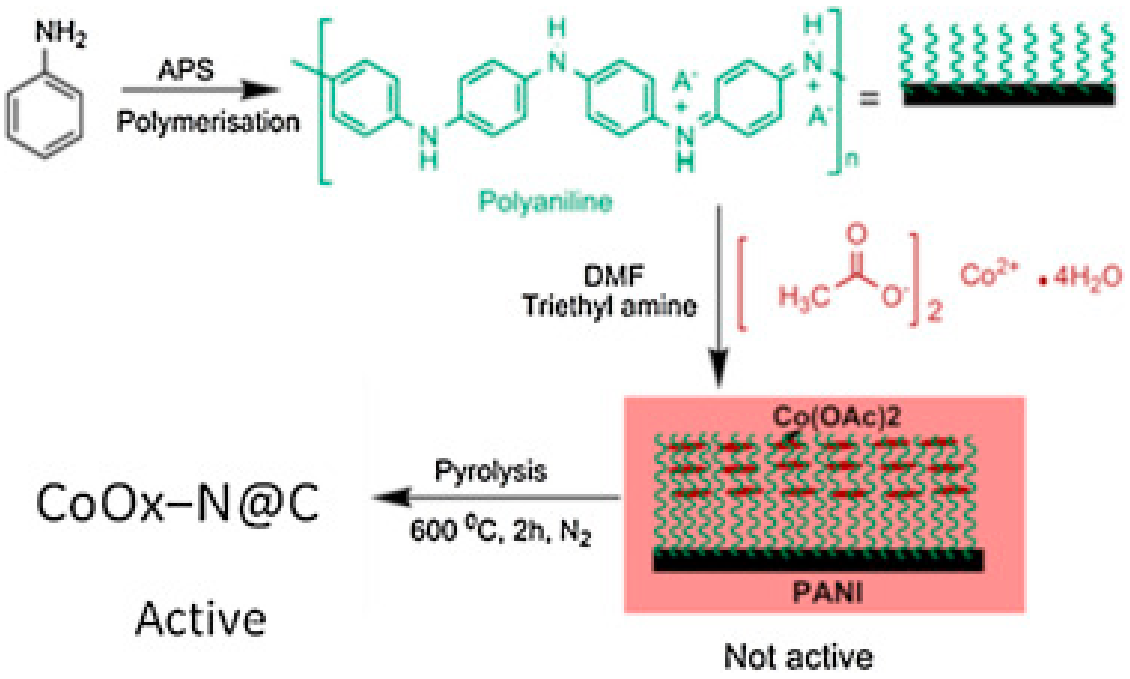

Scheme 2-5 Preparation of CoOx-N@C, PANI catalyst. Reused figure with permission [5].

According to Scheme 2-5, the PANI derived catalyst was prepared by mixing cobalt (II) acetate tetrahydrate, triethylamine, and polyaniline in DMF solvent, followed by heating at 80 °C with continuous stirring. After employing filtration and washing, the obtained powder was subjected to pyrolysis at 600 °C under nitrogen atmosphere. The HR-TEM analysis revealed nano-sized (20-40 nm) particles, while the FTIR analysis confirmed the presence of cobalt oxide polymer in the polymer matrix, thus the catalyst was termed as nano-powder CoOx-N@C, PANI. Further XRD analysis showed considerably high intensity peaks of Co_3O_4 nanoparticles. Also, the thermal decomposition (TGA) analysis showed high thermal stability of the catalyst. The PANI derived catalysts was evaluated for the oxidative esterification of alcohol using molecular oxygen as oxidant. The catalyst was active and selective to the corresponding methyl benzoate without evidence for formation of any by-products [5].

Combining the Co-N-C catalyst synthesis with a hard template approached was also demonstrated. *Yu et al.* [6] has developed a method for preparing a group of meso-porous Co-N-C materials by pyrolysis of cobalt porphyrin (CoTMPP) with silica nanoparticle templates under different temperatures and used the materials as heterogeneous catalysts in organic reactions and electro catalysis. Their findings shown that varying the pyrolysis temperature leads to a material with different active centers. The CoTMPP pyrolized at 400 to 500 °C results in a Co-N-C material with uniformly distributed atomically cobalt coordinated to nitrogen (Co-N) centers. At increased pyrolysis temperatures from 600 to 700 °C, bigger nanoparticles are formed due to agglomeration. The CoTMPP pyrolized at 700°C possesses two

coordination configurations of Co-N and Co-Co. In the higher range of pyrolysis temperature of 600 °C to 800 °C, the Co-N centers are partially destroyed to form less active metallic Co nanoparticles. Furthermore, they classified the catalysts according to the containing active center as result from different pyrolysis temperatures, i.e., pyrolized Co-TMPP at 500 °C as thermal catalyst and pyrolized Co-TMPP at 700 °C as electro catalyst (Scheme 2-6).

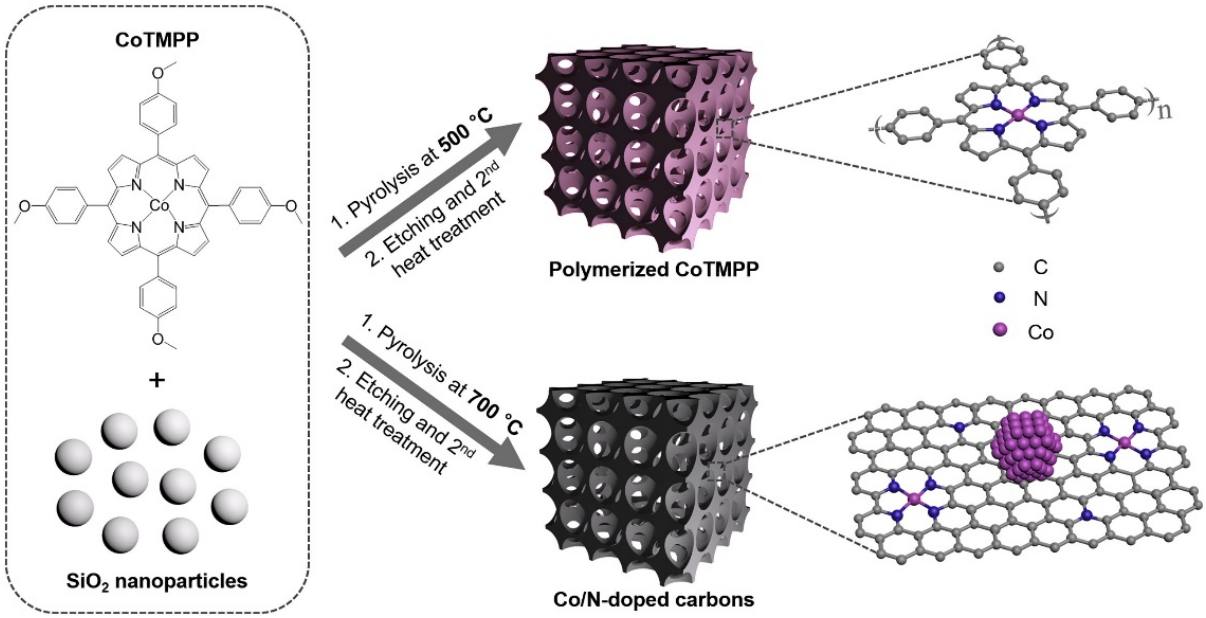

Scheme 2-6 Schematic illustration of the preparation of mesoporous polymerized CoTMPP and Co/N-doped carbons from CoTMPP and SiO2 templates. Reused figure with permission [33]. © 2019 The Author(s).

Another development of carbon supported Co catalyst has been done by *Xiao et al.* [51] in which a simple one-pot hydrothermal synthesis in a solution of NH_3 was used to prepare a sandwich-like N-doped graphene/Co_3O_4 hybrid catalyst (Co_3O_4/RGO_{-N}). The characterization of the catalyst showed the Co_3O_4 nanoparticles are formed on both sides of well-exfoliated N-doped graphene. N-dopants in the carbon matrix may strengthen the interaction between Co_3O_4 and the graphene matrix, prevent re-graphitization of graphene, and improve the dispersion of Co_3O_4. They revealed abundantly presence of Co(III) species on the surface of RGO_{-N} which indicated a strong interaction exists between Co_3O_4 and RGO_{-N} sheets through interfacial Co-O-C and Co-N-C bonds.

Liu et al. [50] has prepared Co-N-C derived from cobalt porphyrin via a one-pot method at different heating treatments ranging from 600 to 800 °C. The morphology and structure of the Co-N-C composites were examined by transmission electron microscopiy (TEM) which showed the presence of nanoparticles in different sizes (Figure 2-2). The particle size followed the order: 6 nm (600 °C) < 20 nm (700 °C) < 43 nm (800 °C), which showed that the particle size of cobalt nanoparticles becomes larger as the heating

temperature increased. High treatment temperature may cause the aggregation of cobalt nanoparticles. Further observation using TEM showed that cobalt nanoparticles were embedded in N-doped carbon architecture and surrounded by few graphitic layers (Figure 2-2g), which is generally correlated to the stability of catalyst. In their study using TEM, XRD, and XPS, *Liu et al.* [50] determined that their catalyst with very small particles are oxidic, while the bigger particles contain a Co core and a cobalt oxide shell. They concluded that the oxidic surface layer consists of Co_3O_4, while CoO and Co (identified by XRD) are enriched in the bulk. Additionally, different methods for preparation of Co-N-C catalyst with well-dispersed active metal on the carbon support are summarized in Table 2-1.

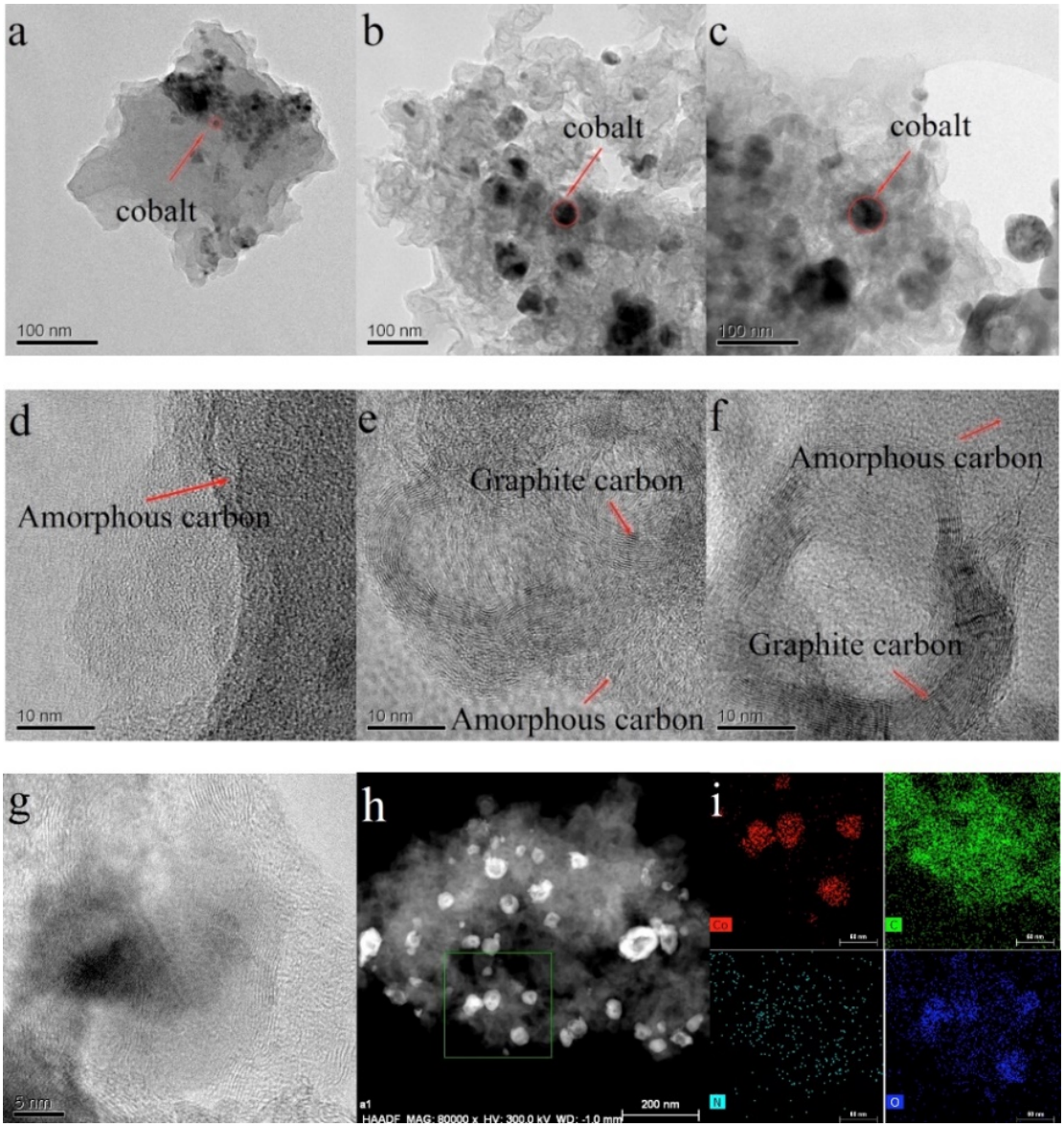

Figure 2-2 TEM and HRTEM images of Co-N-C catalyst. (a, d) Co-N-600, (b, e) Co-N-C-700, (c, f, g) Co-N-C-800), (h) STEM image and (i) elemental mapping of Co-N-C-800. Co-N-C-x, x represents heating temperature. Reused figure with permission [50].

Table 2-1 Different methods for the synthesis of Co-NC catalysts

Catalyst	Carbon precursor	Preparation method	Co species, particle size, and dispersion	Ref.
Co_3O_4/N@C	Vulcan XC72R	Wetness impregnation followed by pyrolysis at 800 °C.	Mostly 2-10 nm in size, few larger particles are present in range 20-80 nm which consist of a Co core and a CoO and/or Co_3O_4 shell. The particles are well dispersed	[3], [52], [53]
CoO_x-N@C, PANI	Polyaniline derived carbon	Wetness impregnation followed by pyrolysis at 600 °C.	Metallic Co and Co_3O_4 with diameter of 20-40 nm are well dispersed on C-N matrix	[5]
Co-N/C-700	Carbon XC-72	Wetness impregnation followed by pyrolysis at 700 °C.	CoO and metallic Co found in sub-nanometer clusters or single atom and homogeneously dispersed on the carbon support	[54]
Co-NG-750	Graphene oxide	Wetness impregnation followed by pyrolysis at 750 °C	Metallic Co is uniformly dispersed onto the framework of N-doped graphene.	[27]
Co_3O_4/AC	Activated carbon	Wetness impregnation followed by pyrolysis at 350 °C.	Co_3O_4 with average particle sizes below 5 nm are homogeneously dispersed	[55]
CoNC/CNT	Carbon nanotubes	Wetness impregnation with subsequent HCl acid leaching followed by pyrolysis at 800 °C.	CoNx in the form of subnanometer clusters or single atoms are highly dispersed in the carbon framework	[56]
Co-g-C_3N_4	Graphitic carbon nitride (g-C_3N_4)	Wetness impregnation following by heating treatment at 550 °C.	Co is homogeneously distributed in the g-C_3N_4 matrix in the form of Co-N bond.	[57]
Co-TMPP-500	CoTMPP	Polymerization at 500 °C using SiO_2 templates	Co coordinated to N (Co-N) is uniformly distributed.	[6]
Co-TMPP-700	CoTMPP	Polymerization at 700 °C using SiO_2 templates	Consisted of atomic Co coordinated to nitrogen (Co-N_x) and metallic cobalt phase (Co nanoparticles)	[6]

Catalyst	Carbon precursor	Preparation method	Co species, particle size, and dispersion	Ref.
Co@NC	ZIF-67-Co	One step pyrolysis at 600 °C.	Metallic Co with sizes of about 8 nm uniformly distributed in the carbon frameworks.	[58]
Co@NC	cobalt nitrate hexahydrate, 1,4-benzenedicarboxylic acid, and triethylene diamine, and g-C_3N_4	Direct polycondensation of organic molecules and inorganic metal salts in the presence of g-C_3N_4 as pore template and nitrogen source, followed by pyrolysis at 900 °C.	Metallic Co nanoparticles in the size range of 28-30 nm are well distributed in the carbon framework.	[28]
Co_3O_4/RGO_{-N} hybrid	Graphene oxide	One-pot hydrothermal reaction in a solution of NH_3 at 150 °C.	Co_3O_4 nanoparticles (formation of interfacial C-O-Co and C-N-Co as the anchor) are displayed on the surface of few layer RGO_N sheets.	[51]
Co_3O_4/AC	Activated carbon Aerosorb LR4	Incipient wetness impregnation followed by thermal treatment at 350 °C in N_2 atmosphere	Co_3O_4 with average particle sizes below 5 nm are highly dispersed on the AC support.	[59]
Co-N-C/ CMK-3	CMK-3 (modified mesoporous carbon)	Wetness impregnation followed by pyrolysis at 800 °C in N_2.	Co(0), CoO_x, and CoN_x nanoparticles encapsulated by graphitic carbon.	[15]
Co/C-N700	MOF	One-pot thermal decomposition of a Co-containing MOF at 700 °C in Argon.	Co nanoparticles are dispersed on the N-doped carbon with uniform particle size of 9.8± 2.6 nm.	[60]
Co-N-C	Co-TPP	One-pot pyrolysis at 600 - 800 °C	Metallic Co as core and CoO and/or Co_3O_4 in the shell. Particle size is dependent to pyrolysis temperature, as follow the order: 6 nm (600 °C) < 20 nm (700 °C) < 43 nm (800 °C).	[50]

The role of nitrogen dopants in enhancing the activity of Co-N-C catalyst has been studied by *Chen et al.* [28]. They designed a Mott-Schottky-type heterogeneous catalyst which boosts the activity of a transition-metal nanocatalyst through electron transfer at the metal/nitrogen-doped carbon interface. The catalyst was prepared through direct polycondensation of simple organic molecules and inorganic metal salts in the presence of g-C_3N_4 which act as template and as nitrogen source. The g-C_3N_4 mass loading was varied to obtain catalysts with different content of nitrogen dopants. They found a gradually depressed electron density of Co particles in Co-N-C samples with the introduction of more nitrogen dopants. Electronic structure of the carbon framework could be controlled by introducing nitrogen atoms to lower the valence band and elevate the conduction band. Nitrogen-rich carbon, as an ambipolar support acting in the Metal/NC heterojunction, is dominated by the work function of two components. The work function of Co is located close to that of N-doped carbon, so that the flow of electrons sensitively depends on the nitrogen content and the structure. Nitrogen-rich carbon with a relatively higher flat band potential or work function than that of metallic Co material, will accept electrons from Co nanoparticles until reaches equilibrium. This electron transfer is described as Mott-Schottky effect (Figure 2-3).

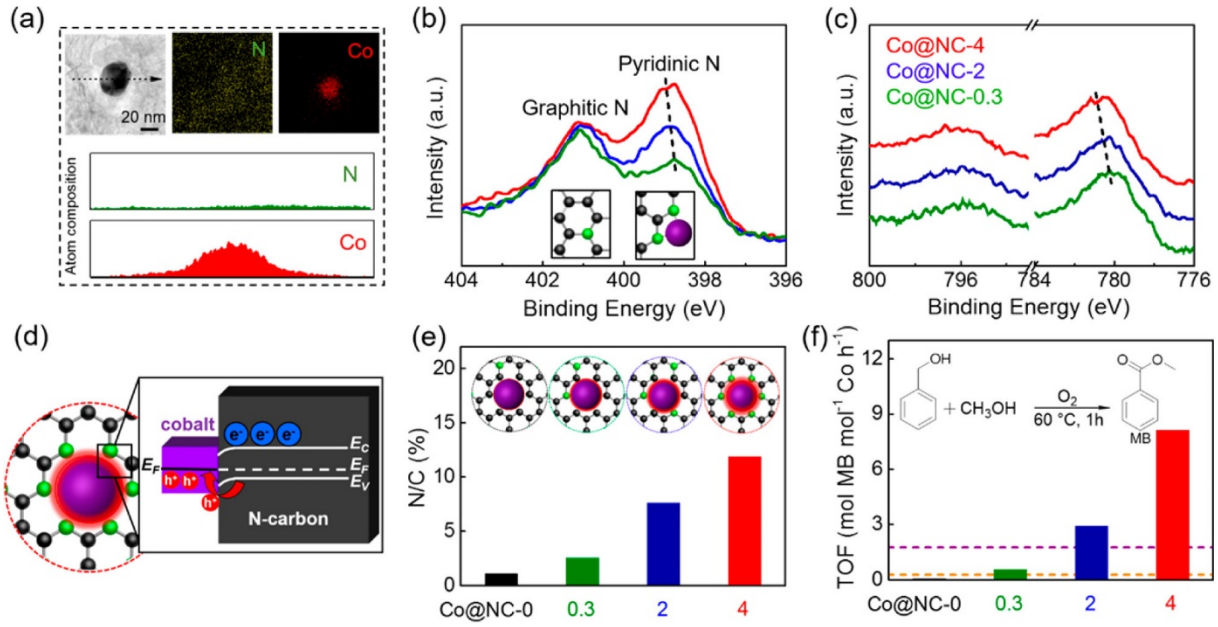

Figure 2-3 Mott-Schottky effect on the catalytic performance of the Co@NC-x catalysts. (a) Nitrogen (green) and cobalt (red) elemental-mapping images and the corresponding line profile of a typical Co@NC-4 sample. (b) N 1s and (c) Co 2p XPS spectra of Co@NC-x. (d) Schematic illustration of Mott-Schottky-type contact of Co@NC. (e) The N/C mole ratio of Co@NC-x samples as determined by elemental analysis and the corresponding schematic structures (inset of e). (f) TOF values for methyl benzoate (MB) production via aerobic esterification of benzyl alcohol and methanol over Co@NC-x in this work and the highest TOF values over a Co-based heterogeneous catalyst with (purple line) or without (orange line) the addition of base. Reused figure with permission [28]. Copyright © 2017, American Chemical Society.

The barrier of this effect will cause an electron redistribution at the interface of cobalt and nitrogen-doped carbon and enrich the positive charges on the side of the Co nanoparticles accordingly. The XPS peaks of pyridinic nitrogen and Co gradually shift to higher binding energy values as the nitrogen content increases. The electron density at the nitrogen decreases with increasing nitrogen content supports the electron transfer over Mott-Schottky heterojunction at the interface of metallic cobalt and carbon. The catalyst was applied in the oxidation of benzyl alcohol and it was shown that Co-N-C based Mott-Schottky catalysts not only boost the oxidative power of the Co-nanoparticles, but also enable the reaction to proceed in the absence of base.

The impact of the nitrogen content on the catalytic performance was also studied by *Liu et al.* [61] using cobalt coordinated nitrogen doped carbon nano-tubes (Co-N-CNTs) as probe catalyst. The pyridinic N is most likely to form coordination structures with cobalt (Co-Nx) which stabilizes Co nanoparticles and prevents them from agglomeration, hence facilitates the dispersion of Co nanoparticles. As in a good agreement with the previous literature, the synergistic effect between cobalt and pyridinic N tunes the spin density, charge density and π-state density of C atoms, resulting in more C atoms being activated and more active sites being generated, which further promotes the adsorption/desorption of intermediates for enhancing the catalytic performance. Hence, the Co-Nx sites are essentially related to the performance of the catalyst.

2.2 Application of M-N-C catalyst in fuel cell

Transition metal and nitrogen co-doped carbonaceous catalysts (M-N-C) are a category of non-noble metal catalyst which are most promising substitutes for the expensive platinum-based catalysts currently used for proton exchange membrane fuel cells (PEMFCs). Early study conducted by *Jasinski et al.* [62] confirmed that cobalt cooperated with nitrogen to yield catalytic activity toward the ORR in an alkaline medium. Further study showed that transition metal catalyst coordinated with nitrogen and carbon through heat treatment could enhance the ORR performance [63].

The fuel cell has been developed in order to produce clean energy with high energy efficiency. In principle, the electric power is directly produced from a fuel and air via two electrochemical reactions obtaining higher efficiency than if the same fuel was combusted [7]. The application of fuel cells for transportation, such is in a car, requires low working temperature. As for this purpose, there are two main possible types of fuel cells, i.e., proton exchange membrane (PEM) and anion exchange membrane (AEM) fuel cells. The key chemical-to-electrical energy conversion process in proton exchange membrane fuel cells (PEMFC) is simply described in a formula: $2H_2 + O_2 \rightarrow 2H_2O$, where the reaction

takes place in two different parts, including an anode where H_2 is oxidized (hydrogen oxidation reaction, HOR), a cathode where O_2 is reduced (ORR), and a proton exchange membrane through which H^+ is transferred from the anode to the cathode as illustrated in Figure 2-4 [64].

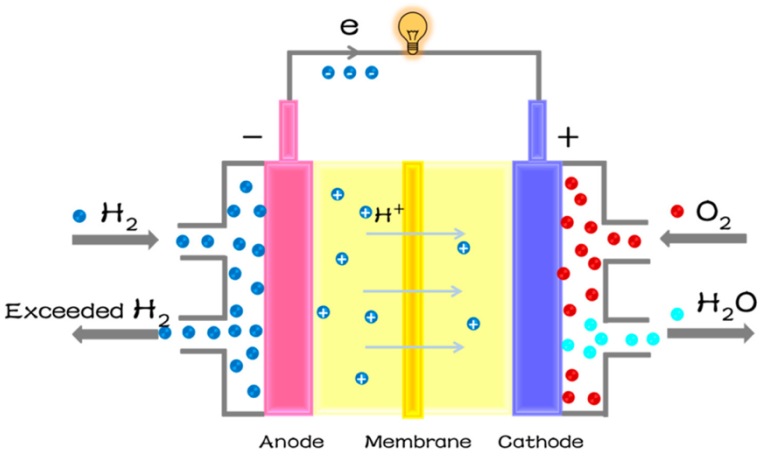

Figure 2-4 Schematic illustration of the proton exchange membrane fuel cells (PEMFC). Reused figure from Wu et. al. [2]. Copyright © MDPI.

The reaction on the cathode, the ORR, can proceed through two pathways: a direct four-electron way or an indirect two-electron way, varying with the electrode material and pH of the electrolyte as presented in Figure 2-5. In the two-electron pathway, the O_2 molecules receive two electrons to be reduced to H_2O_2 (in acid and neutral solution) or HO_2^-, and then adsorb another two electrons to be transferred into H_2O or OH^- [65], [66]. While in the four-electron pathway, the oxygen molecules can accept four electrons to be reduced to H_2O (in acid solution) or OH^- (in alkaline solution), without any detectable intermediates (H_2O_2) in the final electrolyte. Since generation of H_2O_2 in electrolyte causes damages to the catalysts and the proton exchange membrane which lead to reducing the PEMFCs lifetime, hence the most ideal mechanism of fuel cells is the four-electron pathway. Instantly, the ORR proceeds via two-electron pathway, since the dissociation energy of the O-O bond in O_2 is much higher than that on H_2O_2. To drive the reaction following the four-electron pathway, a catalyst to decrease the activation energy of ORR is required. An effective catalyst is developed to selectively reduce the bond energy of O_2, therefore promoting the four-electron process [67].

Despite cathode and anode require catalysts to lower the electrochemical overpotential and to achieve higher voltage output, the cathodic oxygen reduction reaction (ORR) is a multielectron, multistep reaction with very slow kinetics. In this case, the ORR reaction represents the critical limiting step and requires the most catalyst material. Platinum (Pt) has been widely explored as ORR electrocatalyst due to its excellent catalytic performance. Development of cost-effective material with high performance,

such as non-noble metal-based catalysts, to improve the ORR kinetics is essential in reducing the costs of PEMFCs.

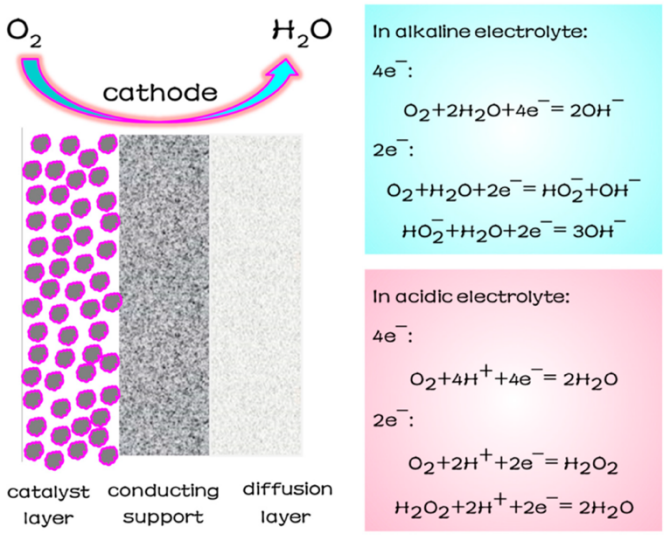

Figure 2-5 The structure of the cathode in PEMFCs and the oxygen reduction reaction (ORR) pathways on the cathode. Reused figure from Wu et. al. [2]. Copyright © MDPI.

Generally, examination of the electrocatalytic activity can be conducted by cyclic voltammetry (CV) measurements in O_2- or N_2-saturated alkaline and acidic electrolytes at the same catalyst loading. The noble-metal-based catalysts (or commercially available Pt/C) are used as a benchmark to evaluate the activity of the developed non-noble metal catalyst. A typical voltammograms in alkaline media is shown in Figure 2-6a and in acidic media is shown in Figure 2-6c. From the voltammograms, the peak current of the investigated metal catalyst is compared with the peak current of the benchmark catalyst.

Another method for measuring the ORR activity is by conducting the rotating disk electrode (RDE) experiments at 1600 rpm and 10 mV s^{-1}. The typical polarization curves are shown in Figure 2-6b and Figure 2-6d, which show the onset potential and half-wave potential of the investigated catalyst compared to the benchmark noble metal (Pt/C) catalyst. The curves also show the limiting current densities (j_L) of the investigated catalyst which is approached to the theoretical value determined by the Koutecky-Levich equation [68]. While durability of the electro-catalyst can be measured by conducting a cycling durability test in O_2-saturated electrolyte for 10,000 cycles. The recorded polarization curves after 10,000 cycles can be used for comparison the catalyst activity, in which a negative shift of the half-wave potential ($E_{1/2}$) recorded after 10,000 cycles indicate the stability of the catalyst.

Lin et al. [43] has reported that Fe-N/C pyrolyzed at 800 °C showed excellent performance with onset and half-wave potentials of 0.923 V and 0.809 V in 0.1 M KOH, respectively, which are comparable to

those of Pt/C (half-wave potentials 0.818 V vs RHE) at the same catalyst loading. Also, in the acidic media (0.1 m $HClO_4$), the Fe-N/C-800 showed comparable activity with onset and half-wave potentials only 39 and 59 mV less than those of the Pt/C catalyst. Despite having relatively not so high surface area (56 $m^2\ g^{-1}$), the catalyst possessed excellent activity, indicating a high density of surface-active sites. The electrochemical measurement of the Fe-N/C catalyst showed that the ORR reaction in both alkaline and acidic media follow the effective four-electron-transfer pathway. Additionally, they performed a durability test of the Fe-N/C catalyst which can be seen in Figure 2-6 e-f. The polarization curves recorded after 10,000 cycles show a negative shift of $E_{1/2}$ of 30.4 and 28.5 mV in alkaline and acidic electrolytes, respectively, indicating its durability is superior to that Pt/C. Additionally, they observed the obvious deactivation behavior of the Pt/C catalyst, indicated by large negative shifts of the onset potential (E_{onset}) and half-wave potential ($E_{1/2}$) without obvious decrease in limiting current densities (j_L).

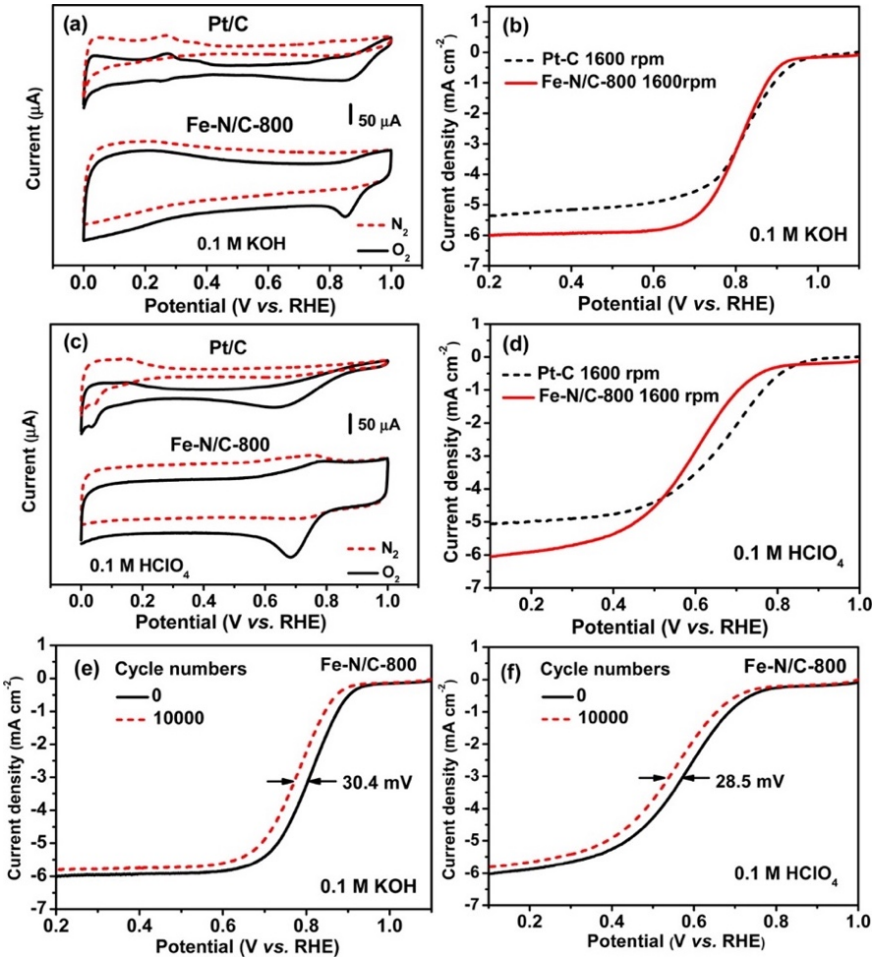

Figure 2-6 Cyclic voltamograms (a) and RDE voltamograms (b) of Pt/C and Fe-N/C-800 in O2-saturated 0.1 M KOH. Cyclic voltamograms (c) and RDE voltammograms (d) of Pt/C and Fe-N/C-800 in O_2-saturated 0.1 M $HClO_4$. Endurance test of the Fe-N/C-800 catalyst for 10,000 cycles in O_2-saturated 0.1 M KOH (e) and 0.1 M $HClO_4$ (f) with 0.1 mg cm^{-2} of the catalyst loading for all conducted tests and the scan rate of 10 mV s^{-1}. Reused figure with permission [43]. Copyright © 2014, American Chemical Society

Platinum doped carbon (Pt/C) catalysts are commercially available, while the more cost-effective M-N-C catalyst based on non-noble metals, such as Fe and Co, are recently developed to reduce the price of fuel cells system in general. Comparison of different type of M-N-C catalysts applied for the ORR system in acidic and alkaline media are summarized in Table 2-2 and Table 2-3. The data shows a significant progress on the activity of M-N-C catalysts in alkaline and acidic medium, and the half-wave potential with a rotating disk electrode (RDE) is close to that of a commercial Pt/C catalyst (E_{onset} = 1.01 V; $E_{1/2}$ = 0.90 V) [69], thus establishing a foundation for the application of M-N-C in PEMFCs.

Table 2-2 Comparison of the ORR and PEMFC performance of Co-/Fe- based electrocatalyst in acidic media

Catalyst	Electrolyte	E_{onset} (V)	$E_{1/2}$ (V)	Open-cell voltage (V)	Maximum power density (W cm^{-2})	Ref.
CoN_x/C	0.5 M H_2SO_4	0.81	0.67	0.82	0.20	[70]
PANI-Co-C	0.5 M H_2SO_4	0.82	0.75	0.95	0.35	[42]
Co-N-C	0.5 M H_2SO_4	0.89	0.79	-	-	[71]
Co-N-C	0.1 M $HClO_4$	0.82	0.761	-	-	[72]
Co corrole/CNT	0.5 M H_2SO_4	0.85	0.78	-	-	[73]
Co-NC-1100	0.5 M H_2SO_4	0.93	0.80	0.95	0.56	[74]
Co-N-C@F127	0.5 M H_2SO_4	0.93	0.84	0.92	0.87	[75]
Co-N/CNFs	0.1 M $HClO_4$	0.82	0.70	0.91	0.016	[76]
Fe-N/C-800	0.1 M $HClO_4$	0.918	0.759	-	-	[43]
1.5Fe-ZIF	0.5 M H_2SO_4	0.95	0.88	0.98	0.65	[45]
Fe-SNC-0.45	0.1 M $HClO_4$	0.95	0.81	-	-	[69]

Table 2-3 Comparison of the ORR performance of Co-/Fe- based electrocatalysts in alkaline media

Catalyst	Electrolyte	E_{onset} (V)	$E_{1/2}$ (V)	Ref.
Co-N-C	0.1 M KOH	1.05	0.90	[77]
Co-C_3N_4/CNT	0.1 M KOH	0.90	0.85	[78]
CoZIF-VXC72	0.1 M KOH	0.92	0.84	[79]
Co-N-C	0.1 M KOH	0.982	0.881	[72]
Hollow Co/NC	0.1 M KOH	1.0	0.87	[80]
Co-N-CNTs	0.1 M KOH	0.97	0.90	[81]
Fe-N/C-800	0.1 M KOH	0.923	0.809	[43]
Fe-N-Gra	0.1 M KOH	0.94	0.77	[44]
FeNPC	0.1 M KOH	0.88	1.03	[82]
Fe-SNC-0.55	0.1 M KOH	1.05	0.92	[69]
Zn/Co/Fe-S-NC-900	0.1 M KOH	-	0.87	[83]

2.3 Application of M-N-C catalysts in heterogeneous catalysis

Esterification is a fundamental transformation in organic synthesis to convert alcohols into esters. Commonly procedures to prepare esters involve the reaction of carboxylic acids or activated acid derivatives, i.e., acid chlorides or anhydrides with alcohols. The reaction requires a multistep process along with the use of mineral acid catalyst, i.e., HCl and H_2SO_4, which generates a lot of waste, thus leading to environmental problems. Therefore, finding alternative methods for ester synthesis has become the main research focus in organic chemistry for few decades. Continuous efforts have been made towards the direct esterification of alcohols with others readily available chemicals, such as other alcohols or aldehyde, in the presence of oxidants and catalysts. Cobalt coordinated nitrogen doped on carbon support material (Co-N-C) has been investigated recently as highly active and selective catalyst for direct esterification of different kind of alcohol substrates, including aromatic and aliphatic alcohols.

2.3.1 Oxidative esterification of aromatic alcohols

Direct oxidative esterification of benzylic alcohol to the corresponding ester using Co-N-C catalysts has been successfully conducted under mild reaction condition. As reported by *Jagadeesh et al.* [3], different benzylic alcohols were successfully transformed to the corresponding methyl ester over Co_3O_4-N@C catalyst using 1 bar O_2 at relatively mild condition (T: 60 °C, P: 1 atm). Their result also confirms the importance of both the oxidant (O_2) and base for the oxidative esterification process. The diverse direct oxidative esterification of benzylic alcohol over different Co-N-C catalyst is summarized in Table 2-4.

Table 2-4 Oxidative esterification of benzyl alcohol into ester over Co-N-C catalyst

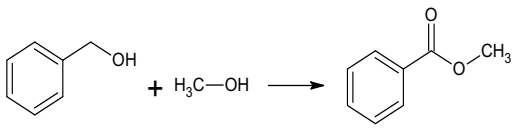

Entry	Catalyst	Reaction conditions	X (%)	S (%)	Y (%)	Ref.
1	Co_3O_4/N@C	0.5 mmol benzyl alcohol, 4 mL CH_3OH, 60 °C, 1 bar O_2, 24 h, 0.1 mmol K_2CO_3, 25 mg catalyst (2.5 mol% Co).	>99	-	97	[3]
2	CoOx-N@C, PANI	1 mmol benzyl alcohol, 4 mL CH_3OH, 0.1 mmol K_2CO_3, 1.5 g catalyst (2.5 mol% Co), 60 °C, 24 h	92	-	-	[5]
3	CoNC/CNT-HCl CoNC/CNT-CB	0.4 ml benzyl alcohol, 32 ml of CH_3OH, 0.1 g of K_2CO_3, 0.2 g of catalyst, 60 °C, 2 MPa O_2, 12 h.	88.1 91.4	- -	91.6 97	[56]
4	Co-CoO@NC-700-3h	1 mmol benzyl alcohol, 8 ml CH_3OH, 25 mg catalyst, 0.2 mmol K_2CO_3, 1 bar O_2, 80 °C, 12 h	100	100	-	[84]

The oxidative esterification of benzylic alcohol into esters is usually done in the presence of a base to boost the catalytic activity. The reaction without a base can be challenging, but it is also possible to occur over Co-N-C catalyst with special support. The work reported by *Chen et al.* [28] shows the influence of the concentration of nitrogen dopants in the carbon support on the activity of Co@NC catalysts in promoting aerobic esterification of benzyl alcohol and methanol. The concentration of nitrogen dopants in the resulting catalyst were varied and it could be shown that in the presence of a catalyst without nitrogen dopants, only trace amounts of benzyl alcohol were oxidized to benzaldehyde. In contrast, catalysts with nitrogen dopants could promote the formation of methyl benzoate, giving the highest conversion and selectivity achieved by the catalyst with the highest concentration of nitrogen dopants. This result indicates the important of the nitrogen-rich carbon support in generating the catalytic activity of Co nanoparticles in Co@NC for the aerobic esterification of alcohols using molecular oxygen under base-free conditions.

Selective oxidation of benzyl alcohol may occur without methanol to transform benzaldehyde over Co-N-C catalyst using molecular oxygen under mild reaction condition as summarized in Table 2-5.

Table 2-5 Oxidative esterification of benzyl alcohol into benzaldehyde over Co-N-C catalyst

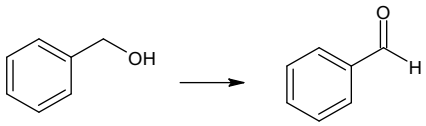

Entry	Catalyst	Reaction conditions	X (%)	S (%)	Y (%)	Ref.
1	Co_3O_4/AC	20 mL toluene, 20 µL benzyl alcohol, 0.1 g catalyst, oxygen flowrate 50 mL min^{-1}, 80 °C, 3 h.	~100	87.3	-	[55]
2	Co_3O_4/AC	20 µL benzyl alcohol, 20 mL toluene, oxygen flowrate 50 mL min^{-1}, 80 °C, 3 h.	~100	-	-	[59]
3	Co_3O_4/G60	0.2 mmol benzyl alcohol, 20 ml toluene, 0.1 g catalyst, oxygen flowrate 50 ml min^{-1}, 80 °C, 6 h.	100	>99	-	[85]
4	Co-N-C/700	1 mmol benzyl alcohol, catalyst (10 mol% Co), 5 ml toluene, O_2 balloon, 100 °C, 36 h.	92	-	92	[26]

Oxidative methyl esterification of a series of structurally diverse benzylic alcohols can be carried out in the presence of Co-N-C catalyst. *Beller et al.* [3] have performed the reaction of alkyl-substituted benzyl alcohols, also halide-, trifluoromethyl-, nitro-, ether-, and even thioether-substituted benzylic alcohols with yields ranging from 80 to 99 % and high selectivity to the corresponding methyl esters. Another summary of different reactions of benzylic alcohol with methanol in catalyzed base or base-free systems is listed in Table 2-6.

Table 2-6 Oxidative esterification of structurally diverse benzylic alcohol over Co-N-C catalyst

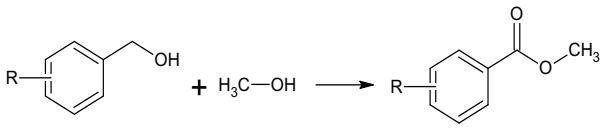

Entry	Catalyst	Reaction conditions	X (%)	S (%)	Y (%)	Ref.
1	Co_3O_4/N@C	0.5 mmol benzylic and heterocyclic alcohol, 4 mL CH_3OH, 60-80 °C, 1 bar O_2, 24 h, 0.1 mmol K_2CO_3, 25 mg catalyst (2.5 mol% Co)	>99	-	80-97	[3]
2	CoO_x-N@C, PANI	1 mmol substrate, 0.15 g catalyst (2.5 mol% Co), 0.1 mmol K_2CO_3, 4 mL CH_3OH, O_2, 60°C, 24h	92	-	90	[5]
3	Co@C-N(800)	Aromatic alcohol (0.5 mmol), CH_3OH (1 mL), n-hexane (4 mL), catalyst (15 – 25 mol% Co), P = 1 atm in air, 25 °C, 96 – 120 h	-	-	80-99	[24]

Similar to cross esterification of methanol with various benzylic alcohols, such selective oxidative couplings for different alkyl esters have been conducted in the presence of Co-N-C catalysts. Cross esterification of various benzylic alcohols and aliphatic alcohols were done to obtain the respected ester, such as propyl, butyl, pentyl, and hexyl benzoates in high yield at slightly higher temperature. Different reports are summarized in Table 2-7.

Table 2-7 Oxidative esterification of benzylic alcohol with aliphatic alcohol over Co-N-C catalyst

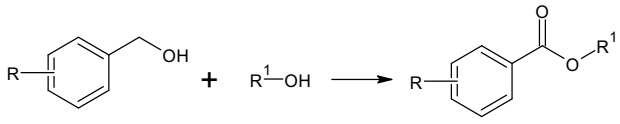

R^1—OH = aliphatic alcohol

Entry	Catalyst	Reaction conditions	X (%)	S (%)	Y (%)	Ref.
1	Co_3O_4-N@C	0.5 mmol benzylic alcohol, 1 ml aliphatic alcohol, 0.25 mmol K_2CO_3, 25 mg catalyst (2.5 mol% Co), 4 mL n-heptane, 70-110 °C, 24 h.	-	-	77-92	[3]
2	Co@NC-4	0.1 mmol substrates, 4 mL of aliphatic alcohol, 40 mg of Co@NC-4, 70-110 °C, 12 h, and 1 bar O_2	46-99	-	45-87	[28]

Another work has been conducted by *Li et al.* [24] to investigate the activity of Co-N-C catalysts in the oxidative cross esterification of *p*-nitrobenzyl alcohol and methanol under basic and base-free conditions. It was shown that the catalyst was able to promote the transformation of alcohol into the corresponding ester with yield above 99% as presented in Table 2-8.

Table 2-8 Oxidative esterification of p-Nitrobenzyl alcohol with methanol

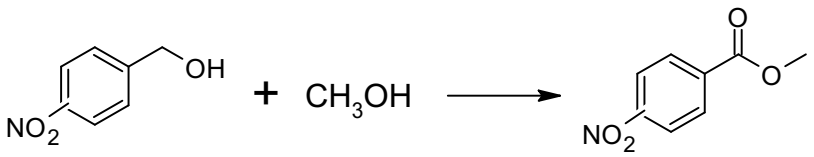

Entry	Catalyst	Reaction conditions	X (%)	S (%)	Y (%)	Ref.
1	Co@C-N(800)	0.5 mmol *p*-nitrobenzyl alcohol, 1 mL CH_3OH, 4 mL n-hexane, catalyst (15 mol% Co), P = 1 atm, 25 °C, in air, 96 h.	>99	-	>99	[24]
2	Co@C-N(800)	0.5 mmol *p*-nitrobenzyl alcohol, 1 mL CH_3OH, 4 mL n-hexane, catalyst (15 mol% Co), 0.1 mmol K_2CO_3, P = 1 atm, 25 °C, in air, 48 h.	>99	-	>99	[24]

Li et al. [24] also developed the catalytic system for the oxidative esterification of long-chain aliphatic alcohols. Various linear aliphatic alcohols including ethyl, n-propyl, n-butyl, n-pentyl, n-hexyl, n-heptyl, and even n-octyl alcohol underwent the esterification to the corresponding esters in good to excellent yields at room temperature and base-free conditions (Scheme 2-7). The product yield decreased when the carbon chain length of the aliphatic alcohol increased. The catalytic system was also applicable to the oxidative esterification of branched alcohols. The desired ester was obtained with a yield of 81% yield when isobutyl alcohol was employed. The yield to the cross-esterification product decreased as the steric hindrance of alcohol increased, i.e., for *tert*-butyl alcohol, the ester product was obtained in 62% yield under identical conditions.

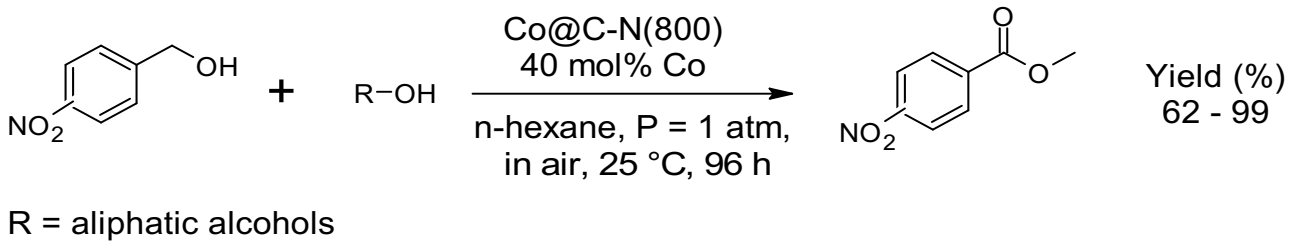

Scheme 2-7 Oxidative esterification of p-nitrobenzyl alcohol with various aliphatic alcohols [24].

The catalytic system using Co-N-C catalysts has also been demonstrated for self-esterification of benzylic alcohol. *Beller et al.* [3] have successfully transformed a different of substituted benzylic alcohols into corresponding esters under such typical reaction conditions in relatively high yields (Scheme 2-8). The catalyst is highly selective and the corresponding substituted benzyl benzoates can be obtained in up to 85% yield.

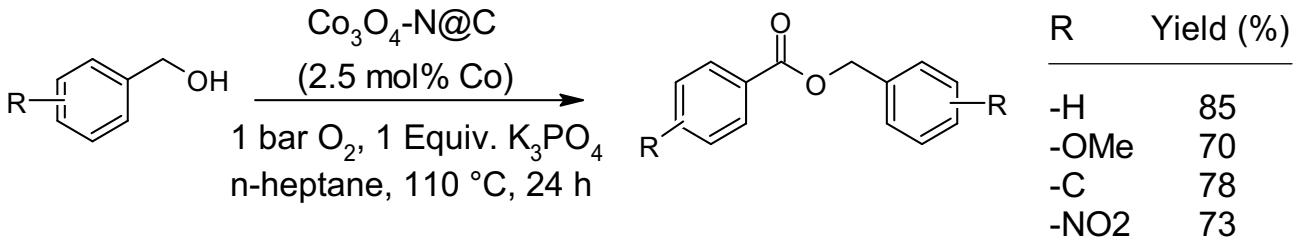

Scheme 2-8 Co_3O_4-N@C-catalyzed oxidative self-esterification of benzylic alcohols [3].

Li et al. [60] investigated a wide range of different substrate within the selective alcohol oxidation over Co/C-N catalysts with air in a base-free conditions. The developed catalytic system was applicable to the oxidation of primary alcohols, giving the corresponding aldehydes in excellent yields as presented in Scheme 2-9.

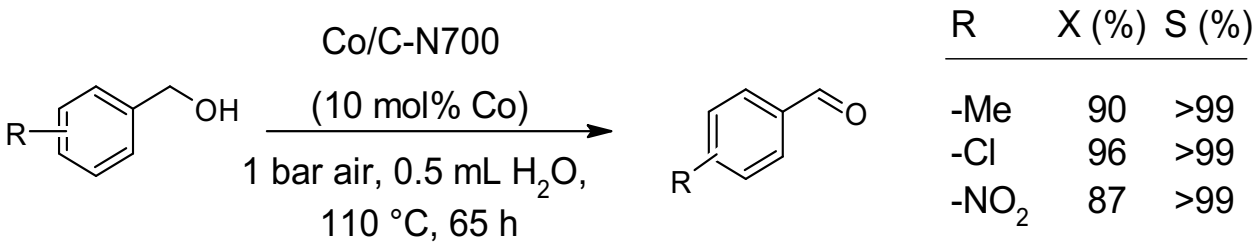

Scheme 2-9 Aqueous selective oxidation of primary alcohols catalyzed by Co/C-N700 [60]

2.3.2 Oxidative esterification of aliphatic alcohols

Direct self-esterification of aliphatic alcohols has been known to be more challenging than aromatic alcohols due to the high stability of the substrates. Previously reported by Beller and co-workers [86], they initially implemented the catalytic system using palladium catalyst for the self-esterification of 1-octanol and ethanol to produce octyl octanoate and ethyl acetate. Later, they developed a Co_3O_4-N@C catalyst which promotes the oxidative self-esterification for different aliphatic alcohols using only 1 bar of molecular oxygen (Scheme 2-10). The bulk chemical acetate can be obtained from ethanol in good yield under such mild conditions. The oxidative self-esterification of longer chain aliphatic alcohols was achieved in a straightforward manner and the corresponding esters can be obtained in 71-75% yield.

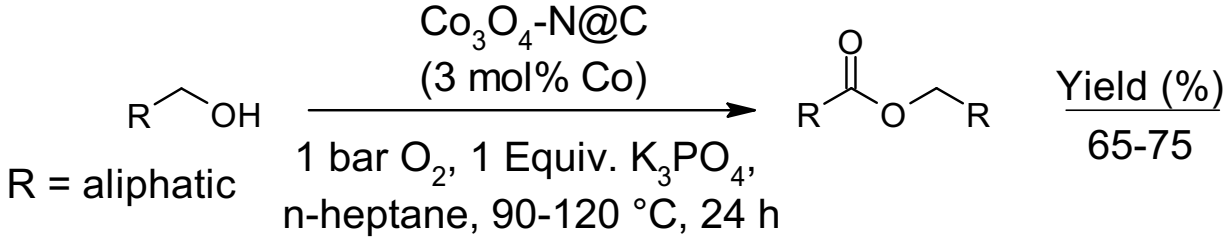

Scheme 2-10 Co_3O_4-N@C catalyzed oxidative esterification of aliphatic alcohols [86].

2.3.3 Proposed mechanisms of selective oxidation of benzyl alcohol

Guan et al. [27] have demonstrated Co coordinated nitrogen doped graphene support (Co-NG-750) catalyst for the oxidation of benzyl alcohol to benzaldehyde and a mechanism for the selective oxidation of benzyl alcohol with molecular oxygen has been postulated. The oxygen molecules can be chemically adsorbed and activated on the Co-N_x structure to form superoxide species, which abstracts the hydrogen of benzyl alcohol to yield benzaldehyde (Figure 2-7). Variety of substituted benzyl alcohol were investigated which showed good catalytic performance on the benzyl alcohol derivatives. The conversion of *p*-chlorobenzyl alcohol and *p*-methoxy benzyl alcohol were achieved up to 93.5 % and 90.3 % respectively. Transformation of 2-methyl heptanol to 2-methyl heptaldehyde can be obtained with 71.3 % conversion after reaction for 6 h at 120 °C. The reaction occurred in the base-free catalytic system using oxygen as oxidant and DMF as solvent.

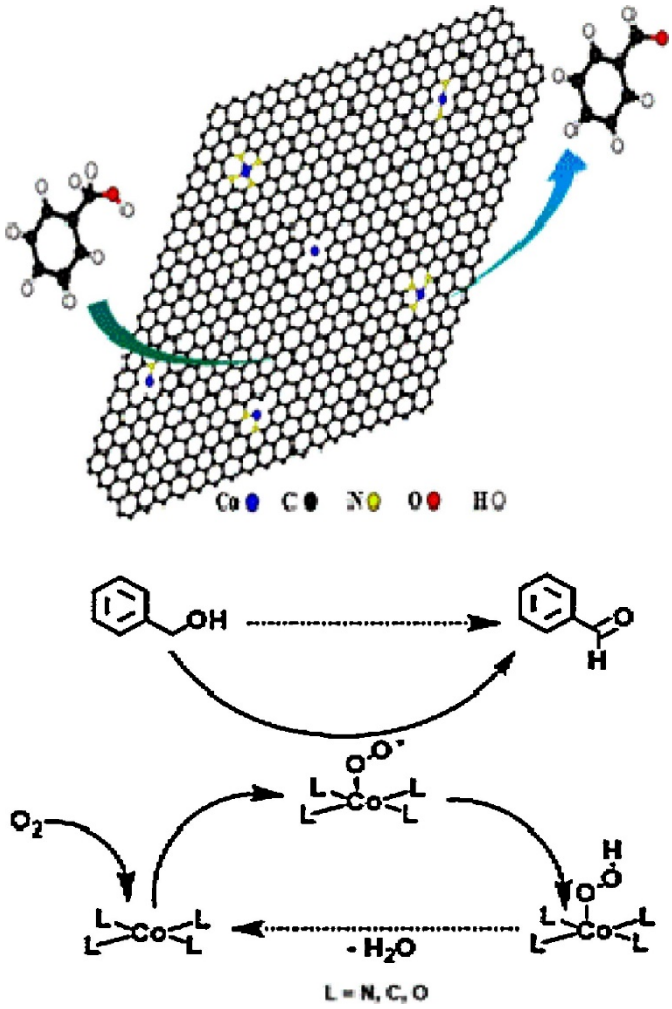

Figure 2-7 The proposed mechanism for aerobic oxidation of benzyl alcohol over Co-NG catalyst. Reused figure with permission [27]. © 2017 Elsevier B.V. All rights reserved.

The proposed mechanism of aerobic oxidation of alcohols conducted on a Co_3O_4/AC catalyst has also been developed by *Thomas et al*. [59]. The oxygen activation and regeneration take place on the surface of the activated carbon support, while Co_3O_4 catalyzes the dehydrogenation reaction step. It is assumed that the carbon support offers the site for oxygen adsorption and activation, whereas Co_3O_4 acts as the site for alcohol dehydrogenation, as illustrated in Figure 2-8. Initially, molecular oxygen is adsorbed and activated on the defects originated from thermal decomposition of the surface groups on the carbon support, forming an activated oxygen species. It is postulated that O_2 interacts with activated carbon to form carboxyl groups. Next, the adsorption and activation of the alcohol occurs, producing the target aldehyde and leaving two hydrogen atoms on the metal oxide. This step is essential, which requires strong ability of the metal oxide towards alcohol dehydrogenation. Finally, oxygen atoms on the carbon surface react with the H atoms to form H_2O, regenerating the defects and starting a new catalytic cycle.

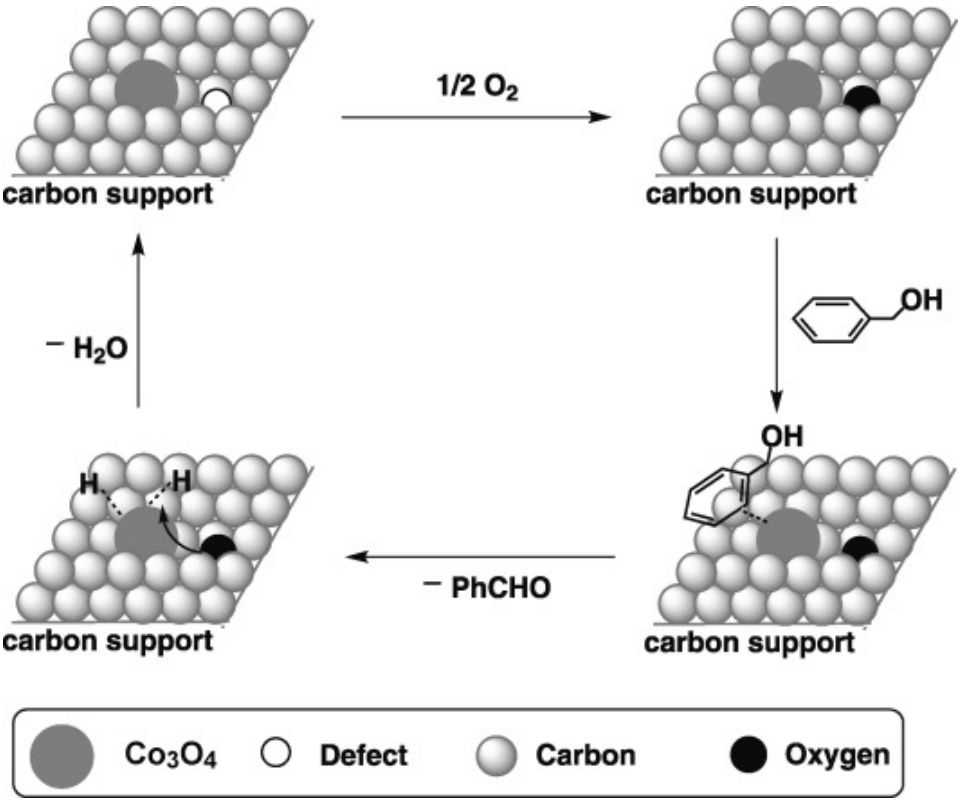

Figure 2-8 A proposed mechanism of alcohol oxidation by using molecular oxygen over Co_3O_4/AC catalyst. Reused figure with permission [59]. Copyright © 2011 WILEY-VCH Verlag GmbH & Co. KGaA, Weinheim.

2.3.4 Function of base in Co-N-C catalyzed oxidative esterification of alcohols

In a typical reaction condition of oxidative esterification of benzyl alcohol into the ester product, a base is usually used to boost the catalytic activity. *Astrakova et al.* [25] have studied the influence of different bases and their concentrations on catalytic properties of Co-N-C in the oxidative esterification of benzyl

alcohol with methanol. Their results have shown that different bases influenced the conversion of benzyl alcohol and the selectivity of the reaction with respect to benzaldehyde and methyl benzoate. As shown in Figure 2-9, the strongest promoter is K_2CO_3 and to a lesser extent, Na_2CO_3. The catalytic activity is determined by the generation of bases well soluble in methanol, such as CH_3ONa and CH_3OK, respectively.

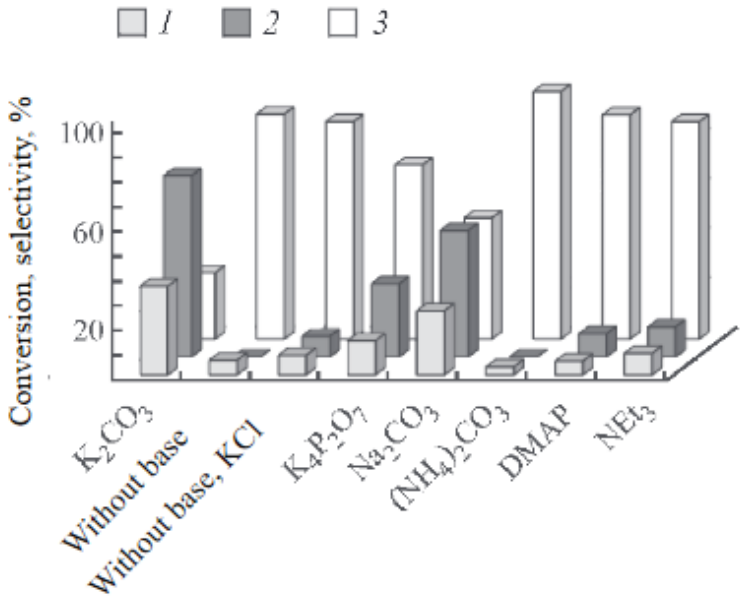

Figure 2-9 Effect of bases on the oxidative esterification of benzyl alcohol with methanol on Co-N@C-850 catalyst in 4 h. Reaction conditions: T = 60°C, P(O2) = 1 atm, Co : BnOH : MeOH : base molar ratio = 1 : 11 : 470 : 1.3. (1) Conversion of benzyl alcohol, (2) selectivity with respect to methyl benzoate, (3) selectivity with respect to benzaldehyde. Reused figure with permission [25]. Copyright © 2019 Springer Nature.

The consecutive steps in the oxidative esterification of benzyl alcohol are shown in Scheme 2-11. By analogy with the reactions of oxidative esterification on gold-containing catalysts, the influence of the base promoter on the catalytic activity of Co-N-C is possibly due to the need to preliminarily deprotonate benzyl alcohol into benzaldehyde in the oxidation step [23]. In the second step of the reaction, a base can catalyze the formation of a hemiacetal of benzaldehyde with methanol, which is the key intermediate of the oxidative esterification [3], [84]. In addition, the base may remove the by-product of reaction, i.e., benzoic acid, from the catalyst surface since capable of deactivating the catalyst [87].

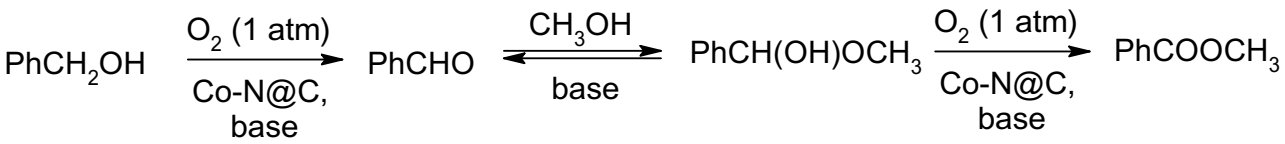

Scheme 2-11 Sequence of steps in the oxidative esterification of benzyl alcohol [23].

Further discussed by *Astrakova et al.* [25], the catalytic activity of the investigated Co-N@C-850 catalyst is strongly dependent on the K_2CO_3 concentration in reaction mixture as seen in Figure 2-10. The addition of K_2CO_3 accelerated both, the first and the second steps of the consecutive reaction. However, the dependency of the promoting effect of K_2CO_3 on its increasing concentration shows deactivating behavior of catalyst. In order to obtain a strong effect on the catalytic activity, they suggested that to use 5 mol % K_2CO_3 relative to benzyl alcohol, instead of an equimolar ratio.

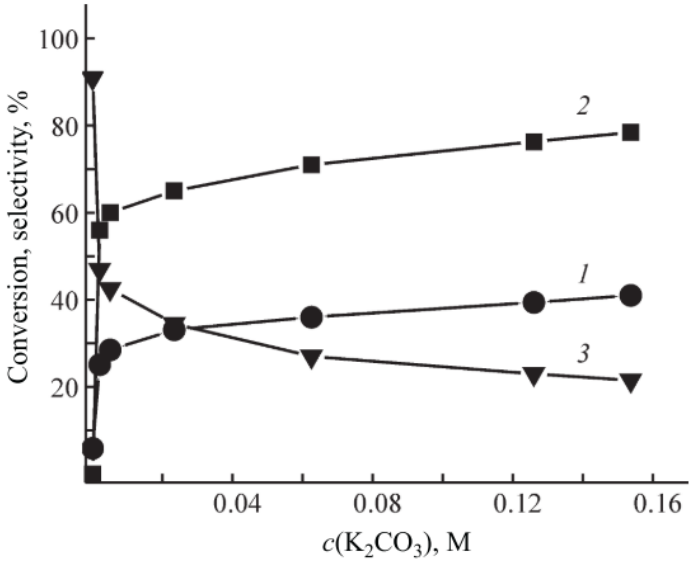

Figure 2-10 Conversion of benzyl alcohol (1) and selectivity with respect to (2) methyl benzoate and (3) benzaldehyde vs. concentration of K_2CO_3 on Co-N@C-850 catalyst. Reaction duration 4 h, T = 60°C, P(O2) = 1 atm, Co : BnOH : MeOH : K_2CO_3 = 1 : 11 : 470 : (0, 0.05, 0.1, 0.5, 1.3, 2.5, 3). Reused figure with permission [25]. Copyright © 2019 Springer Nature.

The described promoter effect of the base could also be achieved by a high concentration of basic sites on the catalyst surface. As investigated by *Leng et al.* [88] using a bimetallic Co/Cu@NC catalyst for the oxidative esterification of alcohols to esters, they successfully achieved full conversion of benzyl alcohol and complete selectivity to the respected ester product under base-free condition. In their finding, the highest activity and selectivity of the catalyst was strongly dependent on the N-content which can be adjusted by tuning the melamine content during the CoCu@NC_n synthesis. It has been known that N-doped carbon could act as built-in and strengthened Lewis base to accelerate the deprotonation process [89]–[91]. Leng and co-workers confirmed the finding by CO_2-TPD analysis which shows a positive relationship between the amount of basic sites on the catalyst surface and the peak area of CO_2-TPD, in which the amount of desorbed CO_2 increased significantly after the N-doping in the catalyst, revealing that the basic sites were mainly referred to the N-doping. The highest N-dopant containing catalyst not only enable the oxidative esterification of alcohols to proceed in a base additive-free reaction system, but also exhibit high activity and selectivity [88].

3 Scope of This Work

Metal coordinated nitrogen doped carbons (M-N-C) based on non-precious metal catalysts have been developed and become alternative candidates for replacing the noble metal-based catalysts. Iron and cobalt are among all of the known non-noble metal catalysts which show superior activity to the noble metal such as Pt based catalysts. Both type of Fe- and Co-N-C catalysts have been widely implemented as electro-catalyst for fuel-generation reaction, such as ORR in the fuel cell. For Co-N-C catalysts, a proof of principle was given that they are active and selective as thermal catalyst in oxidation reaction for organic synthesis. The state of the art makes also clear, that the catalytic studies on Co-N-C in thermal catalysis are mainly results where selectivity at full degree conversion is compared. Thus, a lack of data as also a lack of true stability insights are available. Furthermore, it is unclear how far the experimental findings up to now are influenced by mass transfer effects. The aim of this study is to close this gap on true kinetic evaluation of Co-N-C catalysts in the heterogeneously catalyzed alcohol oxidation. Thus, experiments and a protocol to assess the activity of Co-N-C catalyst based on kinetic evaluation and a subsequent stability assessment shall be deduced.

In this sense the work is divided into three main steps as follow: catalyst preparation, physical characterization, and catalytic testing in oxidative esterification of benzyl alcohol. The catalysts were prepared through different synthesis routes with nomenclature as follow: (1) Co-N-C, (2) Co-N-C/AL, (3) Co-N-C-PANI/AL, (4) Co-N-C-CoTMPP/AL, (5) Co-N-C-PXP, and (6) Co-N-C-PXP/AL. The investigated catalysts number 1 and 2 were prepared within the thesis following methods developed by Beller's group, while the catalyst number 3, 4, 5 and 6 were prepared by Prof. Kramm's Catalyst and Electro-Catalyst Group (Department of Chemistry, TU Darmstadt).

Within this thesis, the physical properties of all catalyst were characterized by applying several methods, including N_2 sorption, XRD, XPS, TEM, and ICP-AES. After conducting the physical characterization, the investigated catalysts were tested in a benchmark reaction of oxidative esterification of benzyl alcohol. As in the multi-phase catalytic system, the transport step from gas-to-liquid phase and finally the solid surface more critical. Hence, to investigate the chemical properties of the catalysts, ensuring surface reaction as the rate-limiting step, the mass transfer barriers are minimized. A set of experiments was conducted to confirm an absence of mass transfer limitations. The kinetics were conducted following an apparent first-order power-law model for consecutive reaction. Parameter estimation was performed simultaneously using the time-concentration data by minimizing the objective function in Presto Kinetics. The stability of the catalysts was analyzed at long-run reaction time in the kinetics region. Also, the experiment was conducted to confirm the influencing deactivation parameters.

4.1.1 Co-N-C (Vulcan XC72R carbon black)

The preparation method was adapted from *Beller et al.* [4] with an additional step of acid leaching. The catalyst was synthesized by impregnating *in situ* generated amino-ligated cobalt (II) acetate complexes on carbon black (Vulcan XC72R) as support material prior to pyrolysis under inert gas. Typical composition of the precursor materials used during the impregnation steps are listed in Table 4-1.

Table 4-1 Composition of the precursor materials during impregnation steps.

Entry	Co-N-C (g)	$Co(OAc)_2 \cdot 4H_2O$ (g)	1,10-Phenanthroline (g)	Vulcan XC72R (g)	Ethanol (ml)
1	1	0.124	0.18	0.696	20
2	5	0.62	0.9	3.48	150-200
3	10	1.24	1.81	6.96	350-400

The reaction mixture containing an appropriate amount of $Co(OAc)_2 \cdot 4H_2O$, 1,10-Penanthroline, and Vulcan XC72R carbon were stirred in ethanol. Firstly, the appropriate amount of $Co(OAc)_2 \cdot 4H_2O$ is dissolved in ethanol for 10 minutes at room temperature leading to a clear purple solution. Then, 1,10-penanthroline was added to the solution and stirred at 60 °C under refluxed conditions for 120 min by keeping a constant stirring speed of ~800 rpm. The color of the solution changes immediately to the dark yellow cobalt-penanthroline complex. Subsequently, an appropriate amount of Vulcan XC72R carbon black powder was added slowly and stirred at room temperature for 18h. Next, the solvent was evaporated under reduced pressure using a rotary evaporator at 40 °C and the immobilized material was dried for 4h *in vacuo*. Slowly solvent removal is beneficial for a homogeneous dispersion of the adsorbed solvated chelate. The obtained powder was ground prior to pyrolysis at 800 °C for 2 h under inert gas (N_2 or Ar) in a tubular furnace as illustrated in Figure 4-1 and the set-up is shown in Figure 4-2.

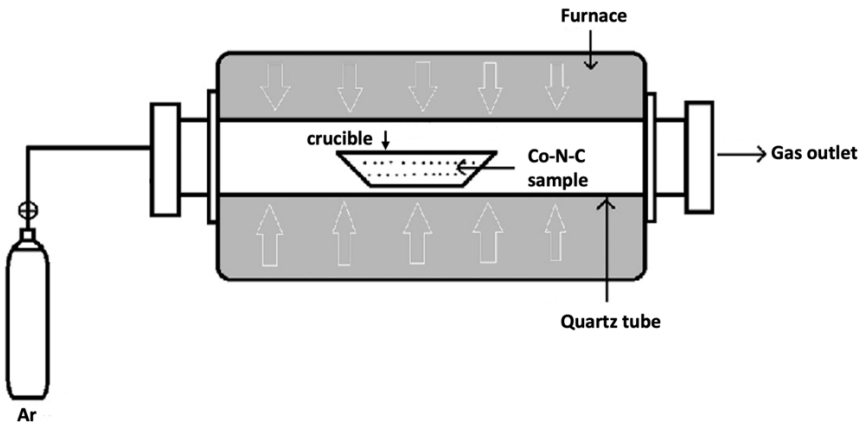

Figure 4-1 Schematic of tubular furnace for pyrolysis of Co-N-C catalyst

Figure 4-2 Tubular furnace used for pyrolysis of Co-N-C catalyst

For preparing the Co-N-C/AL catalyst, an additional step of acid leaching (AL) after the first pyrolysis was applied using 2 M HCl overnight followed by filtration and washing until the neutral pH of filtrate was achieved. Then, the second pyrolysis was conducted with the same procedure.

4.1.2 Co-N-C-PANI/AL (Polyaniline derived carbon)

Polyaniline (PANI) was prepared via polymerization reaction of aniline using Ammonium persulfate (APS) in 0.5 M HCl at 0 °C. The molar ratio of aniline to APS is 1:3. Then, the residual solvent was removed by evaporation under reduced pressure. For the catalyst synthesis, Co acetate, PANI, and dicyandiamide (DCDA) were mixed in a mortar with 5 wt% of cobalt within the mixture. Subsequently, the obtained powder was pyrolyzed under inert conditions in a step-wise heating procedures as follow:

300 °C for 30 min, 500 °C for 30 min, and 800 °C for 60 min. A typical acid leaching step was conducted followed by second pyrolysis at 800 °C for 3 h under inert condition.

4.1.3 Co-N-C-CoTMPP/AL (HZB route)

The precursor materials for preparing this catalyst consisted of 12.51 g Cobalt oxalate dehydrate, 1.95 g Cobalt tetramethoxyphenylporphyrin (CoTMPP), and 0.60 g sulfur. All the components were homogeneously mixed in a porcelain mortar. The mixture of the precursor materials was subsequently pyrolyzed with a step-wise heating procedure as follow: 450 °C for 30 min and 750 °C for 1 h. A typical acid leaching procedure was applied with subsequent washing to neutral pH. Next, the obtained material was dried in the oven at 80 °C for 24 h.

4.1.4 Co-N-C-PXP

A mixture of the precursor materials, consisting of 300 mg CoTMPP and 500 mg diphosphine ligand PXP (Pyridoxine-5'-phosphate), were ground in a porcelain mortar until a homogeneously mixture was obtained. The resulting powder was pyrolyzed at 750 °C for 1 h under inert conditions. The same synthesis procedure was applied for preparing Co-N-C-PXP/AL with an addition of a typical acid leaching procedure and washing to achieve neutral pH.

The preparation of Co-N-C-PANI/AL, Co-N-C-CoTMPP/AL, and Co-N-C-PXP were conducted by the research group of Prof. Ulrike Kramm in the Catalysts and Electrocatalysts, Department of Chemistry, TU-Darmstadt.

4.2 Characterization of the catalysts

4.2.1 N_2 sorption measurement

N_2 sorption isotherms were measured at 77K to determine the specific surface area using a Quadrasorb Evo from Quantachrome Instruments. Prior to the adsorption measurement, the catalyst samples were degassed using FLOVAC Degasser (Quantachrome) instruments at 350 °C for 18 h. The Brunauer-Emmett-Teller (BET) model was used to determine specific surface areas (S_{BET}) and the pore volume (V_t).

4.2.2 ICP-AES (Inductively Coupled Plasma Atomic Emission Spectroscopy)

Analysis of cobalt loading was conducted by Mikroanalytisches Labor Kolbe in Mülheim an der Ruhr, Germany.

4.2.3 XRD (X-ray Diffraction Analysis)

The XRD analysis of Co-N-C catalyst was conducted in the Eduard-Zintl-Institut für Anorganische und Physikalische Chemie, TU Darmstadt. The measurements were carried out in a capillary in Debye-Scherrer geometry, either with Cu-radiation (λ=1.54060 Å) or Mo-radiation (λ=0.70930 Å), Ge[111]-monochromator using detector Mythen 1K for Cu-radiation and small PSD for Mo-radiation. The catalyst powder of Co-N-C, Co-N-C/AL, Co-N-C-PXP, and Co-N-C-PXP/AL were measured with Cu-radiation. While the Co-N-C-PANI and Co-N-C-CoTMPP/AL powder catalysts were measured using Mo-radiation.

4.2.4 XPS (X-Ray Photoelectron Spectroscopy)

The measurement and deconvolution of the XPS spectra of the investigated Co-N-C catalysts were conducted in Eduard-Zintl-Institut für Physikalische Chemie, TU Darmstadt.

4.2.5 TEM (Transmission Electron Microscopy)

The TEM measurements were carried out in Ernst-Berl-Institut für Technische und Makromolekulare Chemie, TU Darmstadt, using a device with the series number of JEOL JEM 2100F. The standard measurement procedure was applied with the acceleration voltage of 200 kV.

4.3 Catalytic test

4.3.1 Preliminary screening reaction procedure

The screening tests of the catalysts were conducted using a standard balloon experiment according to protocols developed by *Beller et al.* [4]. Firstly, 52.6 mg of benzyl alcohol (0.5 mmol) was mixed with 4 ml of MeOH solvent in a glass reaction tube. Then, 13.8 mg of K_2CO_3 (0.1 mmol) and 25 mg of Co-based catalyst (1.3 mol % Co in Co-N-C/AL and 2.6 mol % Co in Co-N-C) to the solution. The glass tube was fitted with a septum and connected to the balloon containing 1 bar oxygen. The glass tube was placed in a heating block. Next, the tube was preheated to 60 °C, followed by mixing it for 24 °C at constant stirring speed of 750 rpm. After the reaction was completed, the glass tube containing reaction mixture was cooled down to room temperature, and then the remaining oxygen was discharged. To analyze the sample, an aliquot (1 ml) of filtrate was taken using a syringe and the solid catalyst was filtered out through the connected milipore membrane syringe filter. Hexadecane solution of 5 mg/ml was added as internal standard with the ratio of 1:1 to the reaction sample. Then, the chemical composition of the product was analyzed using GC-TCD.

4.3.2 General experimental procedure in semi-batch reactor system

The reaction of oxidative esterification was carried out in a slurry reactor with the scheme as presented in Figure 4-3.

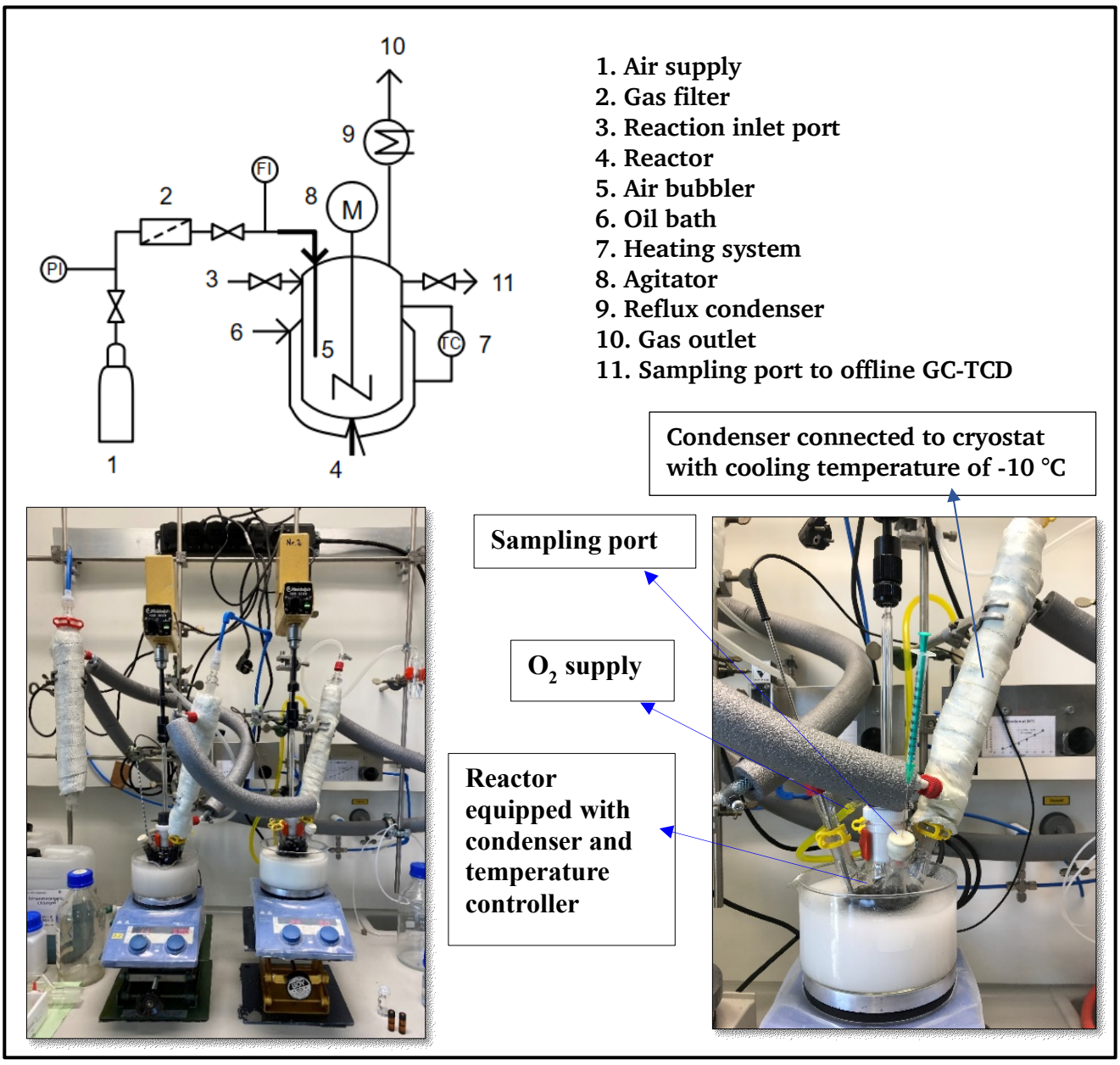

Figure 4-3 Semi-batch reactor set-up

The reactor was equipped with sampling port, air bubbles, temperature controller, and condenser connected to cryostat with cooling temperature of -10 °C. The reaction was conducted according to procedure as follow: 2 mmol K_2CO_3 were dissolved in 80 mL methanol (pH 11-12) with vigorous stirring for ~30 min. Next, 10 mmol of benzyl alcohol were added and stirred for ~10 min. The catalyst was

suspended into the solution while agitation was off. Then, the reaction mixture was preheated to 60 °C, followed by starting the air bubble. The mixture was stirred at 60 °C for 7 hours with constantly bubbling air at 20 ml/min. The initial time (t_0) of the reaction was considered when the air bubble and stirring started. The chemical product analysis was conducted every hour with the typical procedure described in the next section. For characterization of the catalyst after being used, the catalyst was removed from the liquid mixture by centrifugation with subsequent washing with methanol and water. The catalyst was dried at 80 °C in the oven under air condition for 24 hours.

The chemical product analysis was performed using gas chromatograph (GC-2010 Shimadzu) with a thermal conductivity detector (TCD) and N_2 as gas carrier. A representative method for monitoring the reaction is as follow: the oven temperature was set at 60°C and held for 1 min upon injection. Then, temperature was increased to 240°C with the temperature ramp of 10 °C/min and held at 240°C for 10 min. GC samples were prepared as follow: 500 µL of the solution were taken out from the oxidation reaction system and placed in a vial. Then, 500 µL of internal standard solution (5 mg/mL Hexadecane in methanol) were added. The organic compound was characterized by Gas Chromatography (Shimadzu GC-2010) with TCD detector. A multiple point internal standard method was used for quantification of the results. A control experiment without the presence of catalyst showed no alcohol oxidation was occurring over 24 h.

4.3.3 Calculation and determination of components involved in the experimental part

Calculation for calibration

The calibration of benzyl alcohol, benzaldehyde, methyl benzoate, and benzyl benzoate using hexadecane as internal standard were calculated according to the following formula:

Equation 4-1

$$R_{x/is} = \frac{A_x / A_{is}}{c_x / c_{is}}$$

Where R is the response factor (determined from linear plot of calibration standard), A_x is the analyte area, A_{is} is the internal standard area, C_x is the concentration of analyte, and C_{is} is the concentration of internal standard.

Rearrangement the Equation 4-1 leads to the following equation to calculate the concentration of the unknown species:

Equation 4-2

$$C_x = C_{is} \times \frac{A_x / A_{is}}{R_{x/is}}$$

Calculation for determining product quantity

The conversion, selectivity, and yield of the reaction product are calculated according to the following formula:

Equation 4-3

$$X_A = \frac{n_{A(t=0)} - n_{A(t)}}{n_{A(t=0)}} = 1 - \frac{n_{A(t)}}{n_{A(t=0)}}$$

Equation 4-4

$$S_P = \frac{n_P}{n_{A(t=0)} - n_{A(t)}}$$

Equation 4-5

$$Y_P = X_A \times S_P$$

Where X_A is the conversion of component A, S_P is the selectivity of product P, Y_P is the yield of the product P, $n_{A(t=0)}$ is the initial amount of component A, $n_{A(t)}$ is the amount A at time t, and n_P is the amount of the product P.

Calculation for determining modified reaction time

The modified reaction time (τ) is calculated according to the following formula:

Equation 4-6

$$\tau = t \times \frac{m_{cat.}}{V_{sol.}}$$

Where τ is the modified time (min g ml^{-1}), t is the reaction time (min.), $m_{cat.}$ is the catalyst mass (gram), and $V_{sol.}$ is the volume of the solution (mL).

The reaction rate constant (k) for 1st order modified time was deduced from the following step:

Equation 4-7

$$k = k_i^0 exp - \frac{E}{RT}$$

$$\ln k = -\frac{E}{R}\left(\frac{1}{T}\right) + \ln k_i^0$$

$$\ln k = \ln k_i^0$$

For the 1st order of reaction, $k = \frac{1}{t}$

By using time modified reaction time, the rate constant can be calculated as follow:

Equation 4-8

$$k_i^0 = \frac{1}{\tau} = \frac{1}{t} \times \frac{V_{sol}}{m_{cat}} (min^{-1} mL\ g_{cat}^{-1})$$

Where k is the rate constant and k_i^0 is the modified rate constant.

Data evaluation of initial rate constant

The reaction rate constant is calculated by combining mass balance and rate law according to power law model for the first order of reaction.

Equation 4-9

$$-r_A = k_1 C_A$$

Where $-r_A$ is the rate of decreasing of benzyl alcohol (M h^{-1}), C_A is the concentration of benzyl alcohol in solution (M); and k_1 is the reaction rate constant of the first order power law model (h^{-1}).

Arrhenius equation

The activation energy was calculated following the Arrhenius equation:

Equation 4-10

$$\ln k_A = \ln A - \frac{E}{R}\left(\frac{1}{T}\right)$$

Where k_A is the rate constant, E is the activation energy, A is the frequency factor, and R is the gas constant (8.314 J mol^{-1} K^{-1}).

Evaluation of internal mass transfer

The evaluation is used to check whether the reaction is internal diffusion limited or not. The Weisz-Prater parameter is calculated according to the following equation:

Equation 4-11

$$C_{WP} = \frac{-r'\rho_s R^2}{D_e C_{AS}}$$

The summary of parameters to calculate the Weisz-Prater Criterion are listed in Table 4-2.

Table 4-2 Parameters for calculating the Weisz-Prater Criterion

Parameter	Description	Unit
$-r'$	Observed reaction rate	$mol\ g_{cat}^{-1}\ min^{-1}$
ρ_s	Solid catalyst density	$g\ cm^{-3}$
R	Average catalyst particle radius	cm
C_{AS}	Concentration of A (benzyl alcohol) at catalyst surface	$mol\ cm^{-3}$
D_e	Effective diffusivity of solute into solvent at 333 K (60 °C)	$cm^2\ min^{-1}$
∅	Catalyst porosity	unitless
σ	Constriction factor	unitless
τ	Tortuosity	unitless

The internal diffusion is negligible when $C_{WP} \ll 1$. The effective diffusivity, D_e, can be calculated following this formula:

Equation 4-12

$$D_e = \frac{D_{AB}\emptyset\sigma}{\tau}$$

D_{AB} is the diffusion coefficient which can be calculated using the Wilke-Chang equation [92] for dilute solution as follows:

Equation 4-13

$$D_{AB} = 7.4 \times 10^{-8} \frac{(\varphi M_B)^{1/2} T}{\eta V_m^{0.6}}$$

Where φ is the association parameter of the solvent, M_B is the molecular weight of solvent, T is the temperature, η is the viscosity of the solution, V_m is the molar volume of solute (benzyl alcohol) at normal

boiling point. The molar volume of substance i is defined as its molar mass divided by its density ρ_i^0 as follow:

Equation 4-14

$$V_{m,i} = \frac{M_i}{\rho_i^0}$$

Parameter estimation in the kinetic study

The parameter estimation implemented in PRESTO using the measured data in order to fit selected rate coefficient of model. The reaction coefficients were determined by minimizing the distance between simulation results and experimental data using a fitting algorithm, i.e., Damped Gauss-Newton-algorithm. The success of a parameter estimation depends on the model and its ability to predict the real condition, which in the present study, is the reaction network from benzyl alcohol to aldehyde and ester. The performance of parameter estimation essentially depends on the chosen coefficient to be fitted as well as its initial values.

The information of fit can be obtained by analyzing the derivatives of the model responses with respect to parameters. The sensitivity of the parameter estimation, which shows the goodness of fit, is evaluated by confidence interval (alpha = 0.95), t-value, standard error, and residual. The confidence interval is the interval, where the parameter has the same sensitivity as in the model achieved. A small confidence interval means that the achieved value has a significant effect on the solution, while a large confidence interval indicates that the parameter can also spread around this value indicating the same effect. The t-value calculated from statistical procedure shows the significancy of parameter. Hypothesis H_0 is assumed that the parameter has no significance. If t-value is close to 0, that H_0 is true and that parameter has no significant effect. While if t-value is large, it is likely that H_0 is not true.

The residual describes the deviation between the experimental values and the computation's results. The weighted residual sum of squares is calculated according to Equation 4-15.

Equation 4-15

$$SS_E = \sum_{j=1}^{r} \sum_{i=1}^{n_j} \frac{\left(m_{i,j} - s_{i,j}\right)^2}{w_{i,j}^2}$$

There are multiple experiments for a total number r of species or derived quantities, each of them measured at arbitrary times under arbitrary conditions, which should be used to fit distinct coefficients

of a model. In general, it is considered a model with r responses and an individual number of data points n_j for each response, i.e., for the measurements $m_{i,j}$

$m_{i,j}$ for $j = 1, \dots r$ and $i = 1, \dots n_j$

The simulated responses are denoted by $s_{i,j}$ and the weighting factor is denoted by $w_{i,j}$.

$w_{i,j} = max(scale_j, m_{i,j}) > 0$

With a scaling threshold $scale_j$ for each response.

Based on SS_E the relative total residual r_{rel} is given by Equation 4-16.

Equation 4-16

$$r_{rel} = \frac{1}{\sqrt{N}}\sqrt{SS_E}$$

$$N = \sum_{j=1}^{r} n_j$$

where N is the total number of data and r_{rel} is the residual value mentioned in PRESTO and defines the objective function.

In order to get successful parameter estimation, the residual must finally converge. This residual depends on the predicted model, if the model describes the underlying process, the residual will converge to zero. The value also gives hints which component differs slightly or heavily from the measured data.

5 Results and Discussion

5.1 Characterization of Co-N-C catalyst

5.1.1 N_2-physisorption

The N_2 adsorption-desorption isotherms curves of all Co-N-C catalyst samples are shown in Figure 5-1.

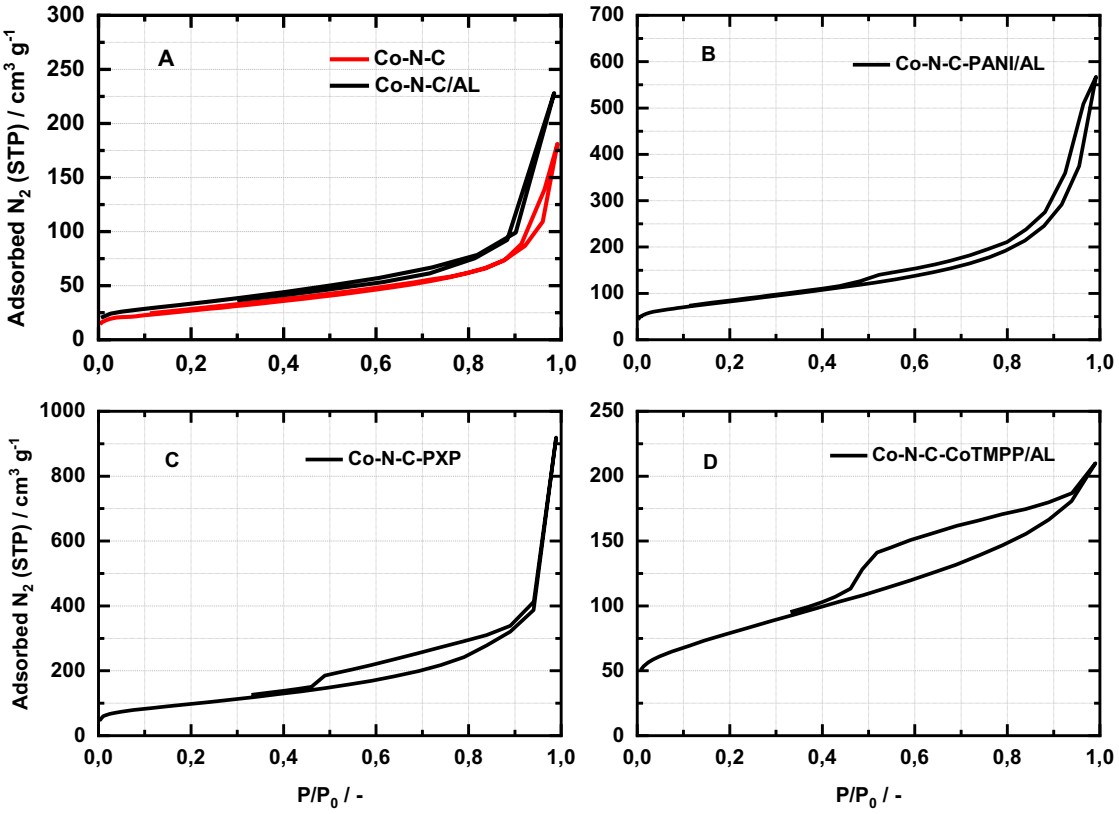

Figure 5-1 N_2 adsorption desorption isotherm plots of Co-N-C catalysts

The filling of micropores is a continuous process that occurs at low relative pressures ($p/p°$<0.015) [93]. According to the IUPAC classification, microporosity leads to Type I(a) and Type 1(b) isotherms [94]. The N_2 sorption of Co-N-C and Co-N-C/AL catalysts are presented in Figure 5-1A which shows a combination of isotherm type I and II. The steep uptake in low relative pressure indicates the filling of micropores as in the case of isotherm type I. A high-volume uptake is also seen at high relative pressure ($p/p°$<0.9), indicating unrestricted monolayer-multilayer adsorption [93], [94]. This shape belongs to type II isotherms which is given by the physisorption of most gases on macroporous adsorbents. While the N_2 sorption isotherms of Co-N-C-PANI/AL (Figure 5-1B), Co-N-C-PXP (Figure 5-1C), and Co-N-C-CoTMPP/AL (Figure 5-1D) are more suitable to be classified as type IV shape which indicates the

presence of mesopores. Also, a hysteresis loop of H3 type can be seen in the N_2 sorption curve of Co-N-C-PANI/AL and Co-N-C-PXP at a relative pressure above 0.4. The H3 type-hysteresis loop existed because of the capillary condensation of N_2 in the complex pore system, as in the slit-shaped nanopores [50]. While the presence of H4 type-hysteresis loop can be seen in the N_2 sorption isotherm of the Co-N-C-CoTMPP/AL catalyst as indication of material with a combination of micro-mesoporous structure [94].

From the N_2-physisorption isotherms, the specific surface areas and the total pore volumes of the investigated Co-N-C catalysts can be determined as can be seen in Table 5-1. The surface area was calculated using the BET method, while the total pore volume was estimated from the N_2 adsorption at $p/p^\circ = 0.8$ by considering pores with dimeters less than 10 nm.

Table 5-1 Surface morphology of the investigated Co-N-C catalysts

Catalysts samples	N_2 sorption	
	S_{BET}[a] ($m^2\ g^{-1}$)	V_{tot}[b] ($cm^3\ g^{-1}$)
Co-N-C [4]	92	0.076
Co-N-C/AL	116	0.096
Co-N-C-PANI/AL	288	0.297
Co-N-C-PXP	351	0.374
Co-N-C-PXP/AL*	346	0.361
Co-N-C-CoTMPP/AL	280	0.227

*N_2 sorption of used catalyst

The Co-N-C reference catalyst has the lowest specific surface area, in which an additional acid leaching step during the synthesis may increase the surface area as the cobalt blocking is removed from the pore opening. This is in agreement with the result reported by *Liu et al.* [95] that by applying acid leaching on the Co-N-C catalyst sample, the metallic cobalt cores were easily removed, resulting in more accessible pore volume.

In the present study, different derived carbon precursors result in catalysts with a relatively higher surface area and total pore volume. High surface area would be favorable to display more active sites and thus enhancing the catalytic performance of the as-prepared catalysts [96], [97]. It is worth noting that all the catalysts were prepared by heat treatment above 750 °C; however, the surface area and total pore volume were not directly influenced by the elevation of heating temperature as suggested in the reported literature [50]. In this case, the reason may be more complex since the catalysts were prepared from different precursor material which may also influence the morphology of the resulting catalyst. Also, the amount of metal loading was varied, as the higher metal loading would lead to a reduced of surface area [98].

5.1.2 ICP-AES analysis

The cobalt loading of the investigated Co-N-C catalysts determined by ICP-AES are presented in Table 5-2.

Table 5-2 Cobalt loading of Co-N-C catalyst

Catalysts samples	ICP-AES Cobalt content (wt%)
Co-N-C [4]	3.09
Co-N-C/AL	1.53
Co-N-C-PANI/AL	31.86
Co-N-C-PXP	2.86
Co-N-C-PXP/AL	2.26
Co-N-C-CoTMPP	22.73

In all of the investigated catalyst sample, Co-N-C-PANI/AL and Co-N-C-CoTMPP have the highest cobalt content. Worth noting that the investigated catalysts, i.e., Co-N-C, Co-N-C-PANI, Co-N-C-PXP, and Co-N-C-CoTMPP, were prepared using different amount of cobalt precursors. The influence of acid leaching treatment was observed from the Co-N-C and Co-N-C-PXP catalysts, in which the catalyst employed acid leaching treatment were denoted by the addition of -AL in their nomenclature. After acid leaching treatment, as in the Co-N-C/AL and Co-N-C-PXP/AL, the cobalt content was reduced which is believed that the residual Co-containing nanoparticles in the leached samples are encapsulated in graphitic nanoshells which protect them from acid leaching as in accordance with the report from *Zhang et al.* [15].

Another study reported by *Liu et al.* [95] also found a significant reduced cobalt content in the prepared Co-N-C catalyst after acid leaching due to removal of metallic cobalt core. In their finding, during the pyrolysis process, the cobalt ions reduced to Co(0) crystallites and aggregated together to form a larger size, while some Co atoms diffused into the graphene shell and bonded with nitrogen and carbon to form Co-N-C structure. Formation of numerous pore structures implies that the Co-N-C provides abundant oxygen and substrate diffusion channel for the intended reaction.

5.1.3 XRD analysis

The XRD measurement were conducted for analysis of crystallinity and detection of different cobalt phases present in the catalyst. X-ray powder diffractograms of the investigated Co-N-C catalysts are presented in Figure 5-2.

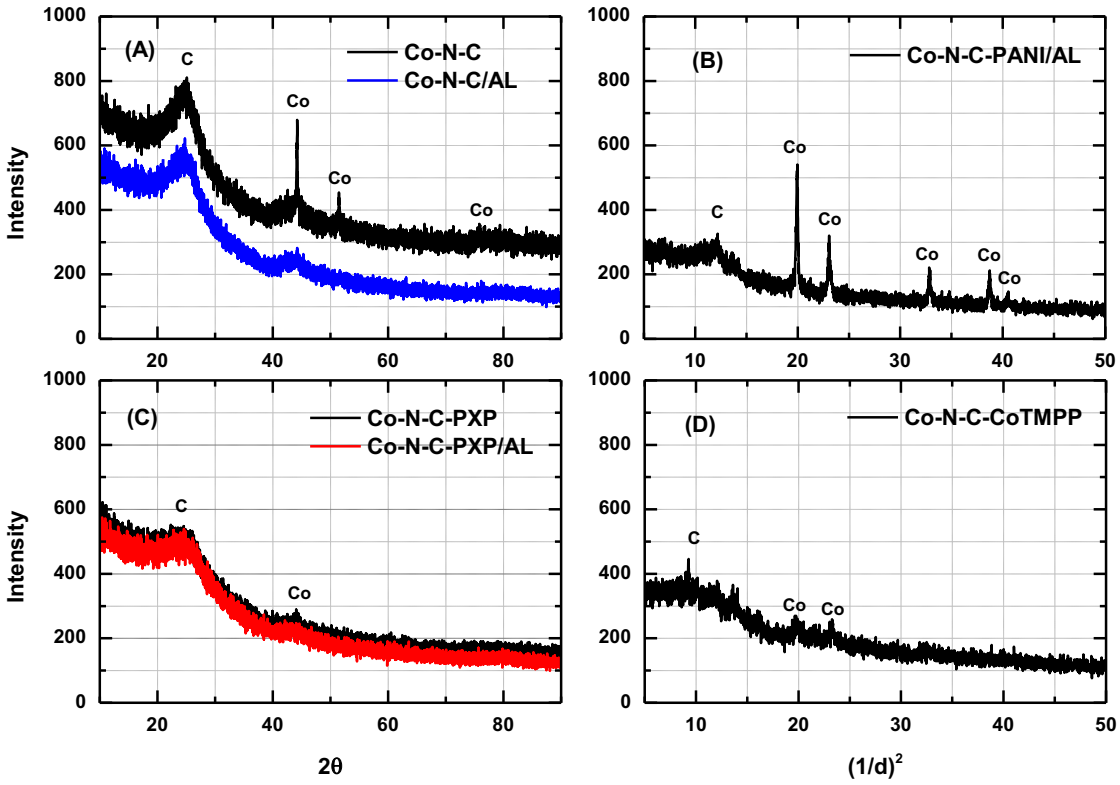

Figure 5-2 XRD pattern of the Co-N-C catalyst

From XRD results, most of the investigated catalysts are relatively amorphous and only show minor crystallinity as can be seen in Co-N-C and Co-N-C-PANI/AL powder. The reflections in these spectra (Figure 5-2A and Figure 5-2B) can be assigned to elemental cobalt (cubic modification) [ICDD-No. 15-806]. The very weak signal at ~44 °/2θ in Co-N-C/AL and Co-N-PXP cannot be assigned clearly, but it appears at the same position as the strongest reflection of cubic cobalt modification. For Co-N-PXP/Al measured by Cu/radiation and Co-N-C-CoTMPP powder recorded by Mo-radiation, small signals in the X-ray powder pattern cannot be assigned (Figure 5-2C and Figure 5-2D).

As for identification of different cobalt phases in the catalyst samples, the expected cobalt oxide was not detected, which is either due to inability of XRD to detect nanoparticles in a low amount or as only amorphous oxide phases were present. To be able to detect Bragg-reflections of the additional phase, there must be at least 2-5 wt % of a phase within a phase mixture. This is limitation of the instrument used for detection of mixed material with standard procedure. The analysis showed that cobalt cubic was the only dominant species within the mixture.

5.1.4 XPS analysis

The atomic percentage of the elemental surface composition of Co-N-C, Co-N-C/AL, Co-N-C-PANI/AL, and Co-N-C-CoTMPP/AL are shown in Table 5-3.

Table 5-3 Elemental surface composition of the investigated Co-N-C catalyst determined by XPS

Catalyst	Element surface composition (at%)				
	C 1s	O 1s	N 1s	Co 2p	S 2p
Co-N-C	92.7	2.4	4.0	0.5	0.3
Co-N-C/AL	95.1	1.4	2.8	0.5	0.2
Co-N-C-PANI/AL	73.0	11.6	11.1	3.1	1.2
Co-N-C-CoTMPP/AL	68.0	19.8	4.8	4.1	3.4

From the survey spectrum, the presence of C, N, Co, O, and S elements can be identified in all the investigated catalysts. Polyaniline and CoTMPP derived carbons are likely to have 20 at % carbon less than the carbon black support material. Deconvolution of the high-resolution spectra of different element regions in the Co-N-C is presented in Figure 5-3.

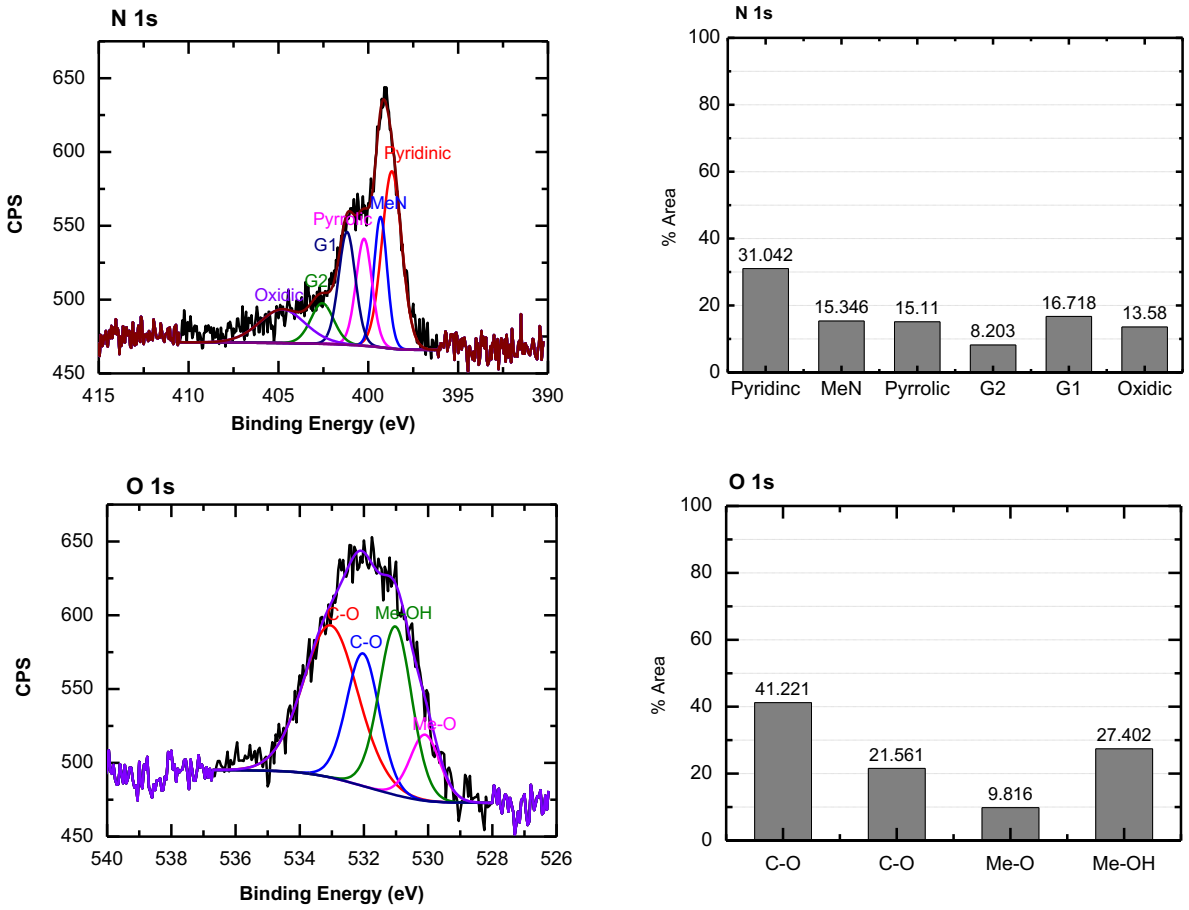

Figure 5-3 High resolution XPS spectra of the N 1s and O 1s region with deconvolution and quantification of the different nitrogen and oxygen species on the Co-N-C catalyst.

In Figure 5-3, the XPS spectrum shows that the Co-N-C catalyst consists of 92 % carbon and the remaining 8 % are heteroatoms, including cobalt. The N 1s spectra can be deconvoluted into C-N with 30 % pyridinic, 15 % pyrollic, and 24 % graphitic nitrogen species. Additionally, the spectra show photo emission around a binding energy of 339 eV which refers to M-N. From the spectra, it can be deduced that in maximum 15 % of nitrogen facilitates the formation of Co-N_x site. In the O 1s deconvolution spectra, peaks at binding energies of 530 and 531 eV can be seen which refer to M-O and M-OH, respectively. Hence, it reveals the formation of cobalt oxide on the catalyst surface. In conclusion, different cobalt phases are present on the Co-N-C catalyst, which is in agreement with the study conducted by *Beller et al.* [3], [4]. Trace amount of sulfur is also detected on the catalyst sample.

Deconvolution of the high-resolution spectra of the O 1s, N 1s, C 1s, and Co 2p in the Co-N-C/AL catalyst is presented in Figure 5-4.

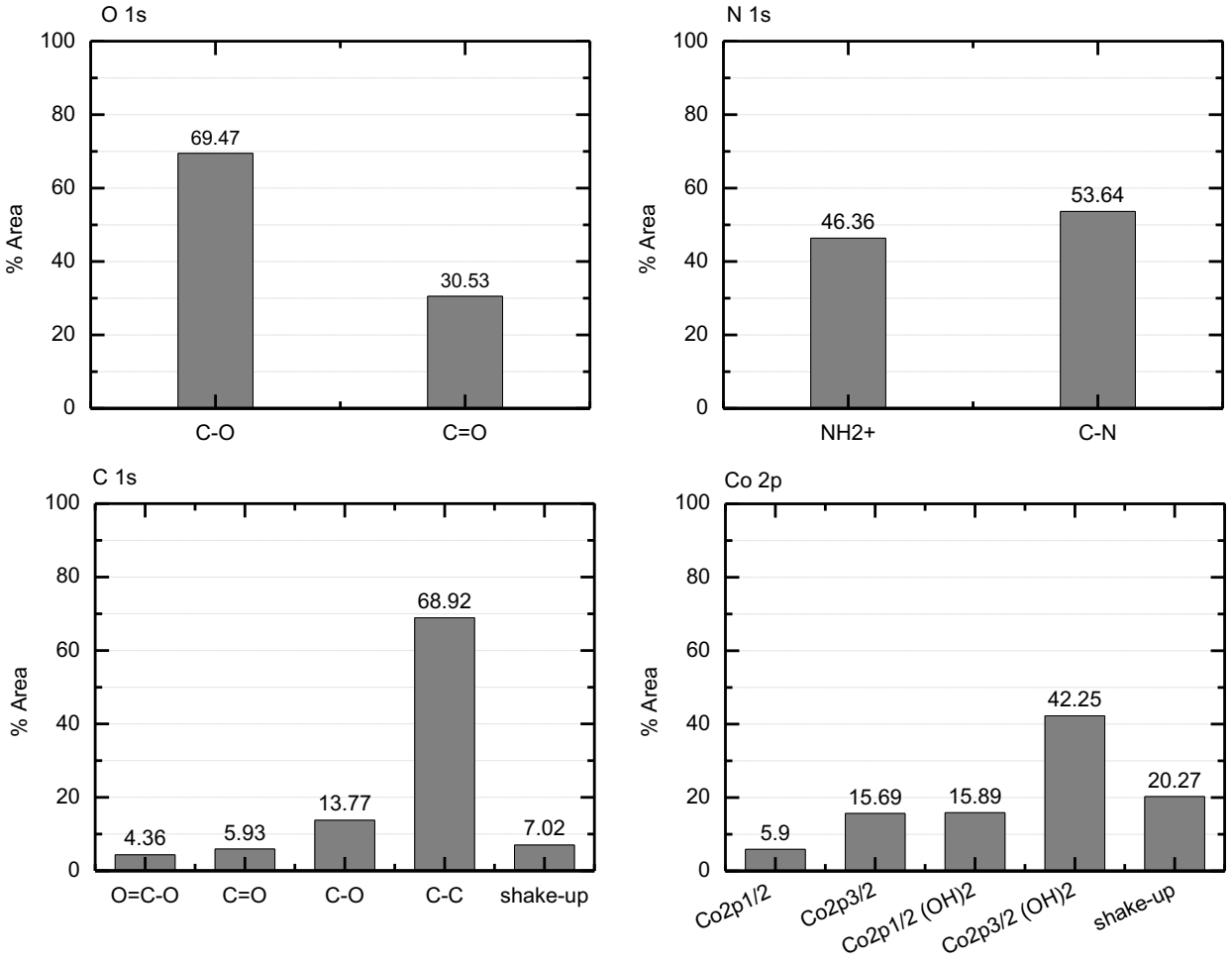

Figure 5-4 XPS spectra and deconvolution of the elemental composition on Co-N-C/AL catalyst

The C 1s and N 1s region shows that the carbon structure is dominantly graphitic, where nitrogen atoms are successfully attached into the carbon framework, which results in C-N_x site formation. The Co 2p spectra reveals two distinct energy bands profile, i.e., a high energy band at 798.3 eV and 796.3 eV and a low energy band at 783.1 eV and 780.8 eV which attributed to Co 2p ½ and Co 2p 3/2 respectively. These energy bands profile referred to the presence of Co_3O_4 and $Co(OH)_2$ [99].

Deconvolution XPS spectra of the Co-N-C-PANI/AL catalyst can be seen in Figure 5-5.

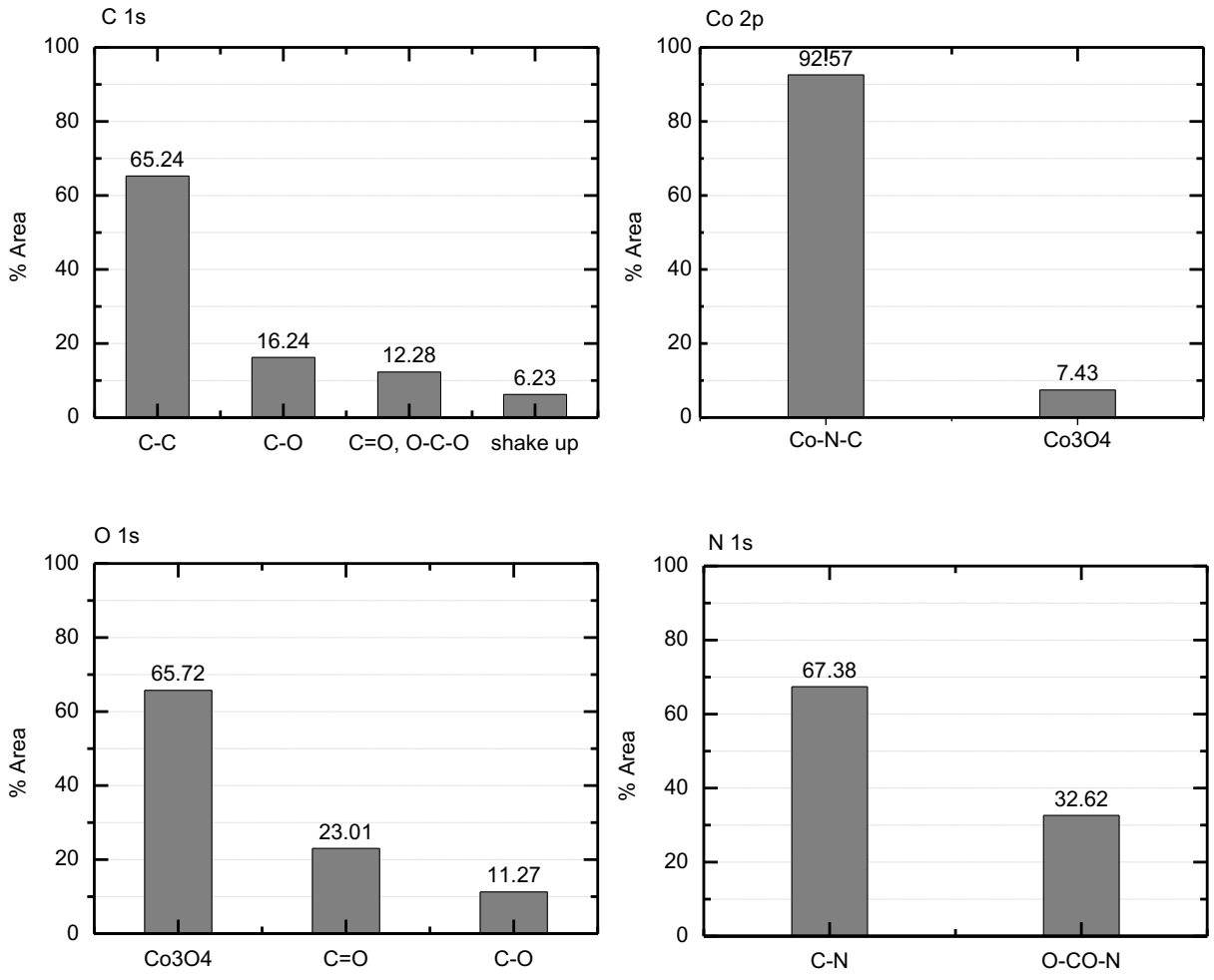

Figure 5-5 XPS spectra and deconvolution of the elemental composition on Co-N-C-PANI/AL catalyst

The deconvolution of C 1s spectra shows that the carbon is dominated by graphitic structure. Hence, polyaniline derived carbon is suitable as support material with comparable morphology to carbon black. As the content of cobalt is relatively high according to ICP-AES analysis data, it can be clearly distinguished between the phases formed on the catalyst structure. From the deconvolution of the spectra of the Co 2p region, well dispersed Co-N-C sites are present as much as 92 % and the remaining cobalt is present as Co_3O_4 nanoparticles.

5.1.5 TEM analysis

The TEM image of Co-N-C/AL, Co-N-C-PXP, and Co-N-C-CoTMPP catalysts are presented in Figure 5-6.

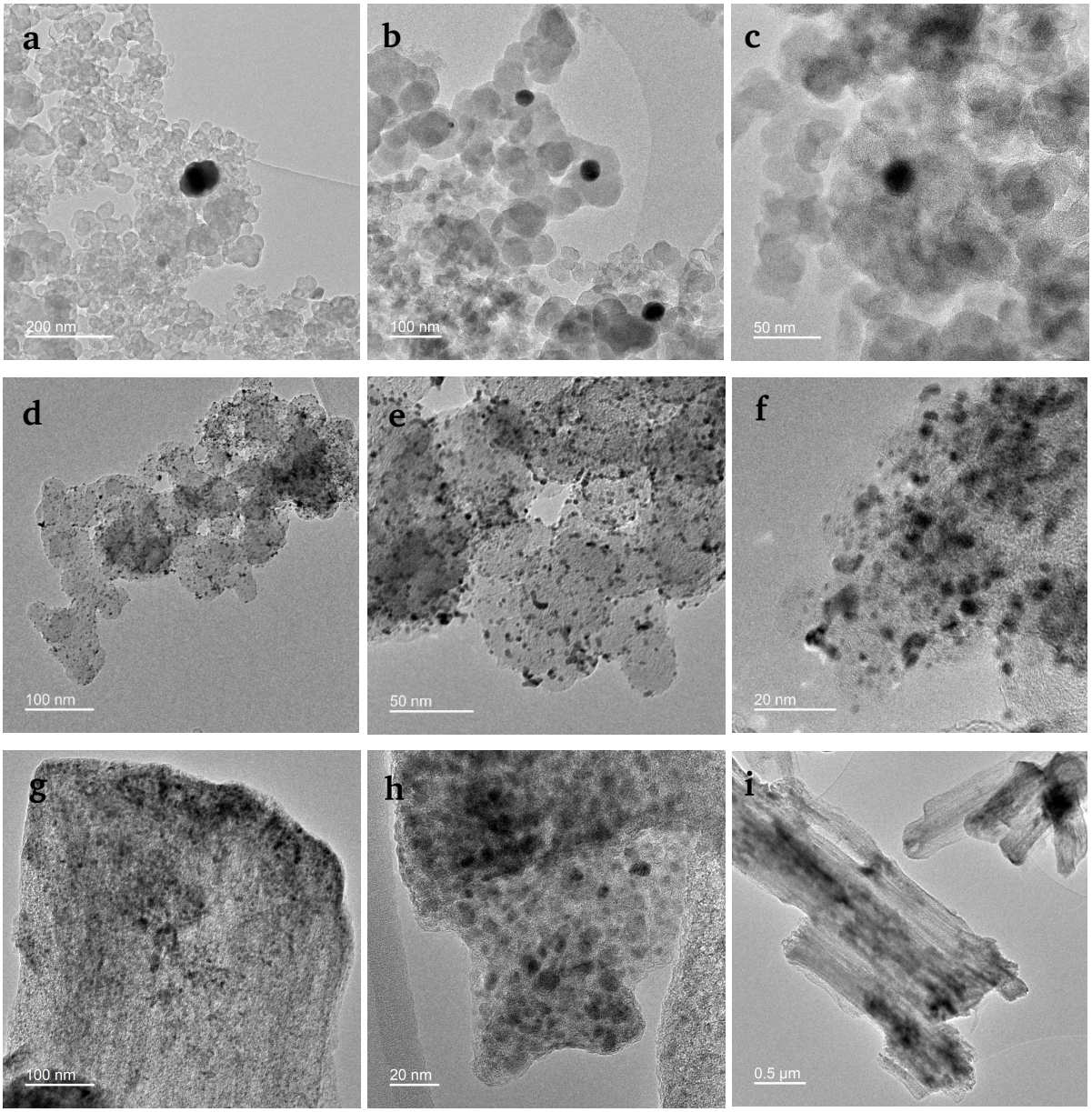

Figure 5-6 TEM image of Co-N-C/AL (a, b, c), Co-N-C-PXP (d, e, f), and Co-N-C-CoTMPP (g, h, i) catalysts with enlarged images of cobalt particles. The black dot particles are Co (checked with STEM EDS)

The influence of the different synthesis routes on the structure of the catalysts were investigated using high-resolution transmission electron microscopy (HRTEM). The three representative catalysts, i.e., Co-N-C/AL, Co-N-C-PXP, and Co-N-C-CoTMPP/AL, were chosen as their cobalt loading are relatively contrast. Large particles of cobalt up to 100-200 nm were observed in the Co-N-C/AL catalyst sample

(Figure 5-6a-c). In accordance with *Beller et al.* [3], the synthesized Co-N-C catalyst following their procedure revealed the preferential formation of small (2-10 nm) Co_3O_4 particles on a carbon-nitrogen-based support surface. They also found a few larger particles of 20-80 nm and occasionally of up to 800 nm in size are also present which consisted of a Co and/or CoO core and a Co_3O_4 shell. The large Co particles in the Co-N-C/AL sample, could be caused by the low nitrogen content measured by XPS. Nitrogen doping facilitates an enhanced cobalt dispersion leading to smaller particles, while a lower nitrogen content leads to agglomeration and thus resulting in larger Co nanoparticles [61].

TEM analysis of the presence of cobalt nanoparticles in Co-N-C/AL catalyst sample is in agreement with the analysis using XPS. The TEM image of Co-N-C-PXP shows the presence of smaller cobalt particles of about ~20-50 nm which are well dispersed on the carbon support (Figure 5-6d-f). In the Co-N-C-CoTMPP catalyst sample, cobalt particles were identified smaller than 20 nm and more dispersed on the carbon framework (Figure 5-6g-i). In the latter sample, the cobalt content based on the ICP analysis showed the highest amount of cobalt loading, but this did not lead to the formation of cobalt clusters or agglomerations. Worth noting that these catalysts were prepared using different impregnation method and heat treatments, thus the parameters chosen for the preparation seems to significantly influence the properties of catalysts.

5.2 Orienting studies and development of experiment procedure

5.2.1 Orienting studies

The employed Co-N-C catalysts were screened initially in the liquid phase oxidative esterification of benzyl alcohol. The usage of aromatic alcohols as reactant resulted in high conversions with over 90 % of yield (see Table 5-4).

Table 5-4 Degree conversion and selectivity of oxidative esterification of benzyl alcohol to methyl benzoate over Co-N-C catalysts

Entry	**Catalyst**	**Oxidant**	**X (%)**	**Y (%)**
1[a]	Co-N-C	O_2	92	90
2[a]	Co-N-C	air	65	59
3[a]	Co-N-C/AL	O_2	>99	>99
5[b]	Co-N-C	air	99	99
6[b]	Co-N-C/Al	air	99	99

Reaction conditions: (a) 0.5 mmol initial alcohol substrate, 0.1 mmol K_2CO_3 (0.2 equiv. to substrate), 4 ml methanol (solvent), 25 mg of catalyst (1.3 mol % Co in Co-N-C/AL and 2.6 mol % Co in Co-N-C), 1 bar, 60 °C, 750 rpm of sirring, 24 h; (b) 10 mmol initial alcohol substrate, 2 mmol K_2CO_3 (0.2 equivalent to substrate), 80 ml methanol (solvent), 500 mg catalyst (1.3 mol % Co in Co-N-C/AL and 2.6 mol % Co in Co-N-C), gas flowrate of 20 ml/min, 1 bar, 60 °C, 300 rpm of stirring, 24 h. X is referred to conversion of Benzyl Alcohol and Y is referred to yield of methyl ester.

Two different catalyst samples, Co-N-C (benchmark catalyst) and Co-N-C/AL were chosen for reaction screening with different experiment protocols. Firstly, the Co-N-C catalyst was tested under two different reaction conditions, using pure oxygen and air as the oxidant in a standard balloon experiment. The results show that using pure oxygen leads to a higher ester yield (Y = 90 %) than experiments using air (Y = 59 %). Next, the Co-N-C/AL catalyst was tested under the same conditions using oxygen as the oxidant. The result shows that both catalysts are active in the reaction with comparable activity at full conversion. The reaction was carried out also using a semi-batch reactor system where air is bubbled continuously into the liquid phase. The result shows that the air bubbling increases the yield to 99 % even if air was employed and the activity is comparable with using pure oxygen in the standard balloon experiment. Reason for this observation might be the presence of mass transfer limitation from the gas to the liquid phase in the simple balloon setup. Hence, in this case, the semi-batch reactor system is more reliable for assessing the activity of catalyst.

5.2.2 Development of experiment procedure

To develop an experimental procedure, which allows to deduce kinetics, a batch reactor in which the gas is bubbled through the solution was employed. The reaction was carried out for two hours in the presence of the catalyst, then continued without catalyst for another 7 hours (Figure 5-7).

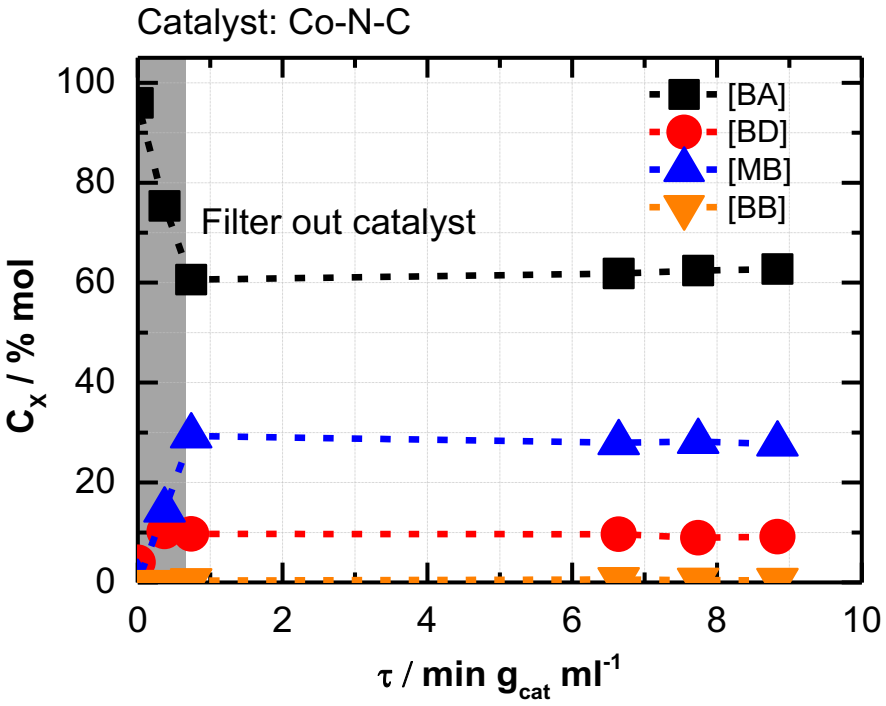

Figure 5-7 Oxidative esterification of benzyl alcohol with and without the presence of the Co-N-C catalyst. Reaction conditions: 9.2 mmol Benzyl Alcohol, 73.6 ml methanol, 1.84 mmol K_2CO_3, 460 mg Co-N-CB catalyst, F_{air} = 20 ml min^{-1}, stirring speed = 300 rpm.

The experiment was conducted to check the system is heterogeneous catalysis and no cobalt is going into the solution and catalyzes the reaction homogeneously. The results as can be seen in Figure 5-7 showed that the reaction took place with the promotion of a catalyst; while no conversion is achieved without catalyst.

As the reaction occurred heterogeneously, confirmation of the absence of mass transfer limitation in the reaction system was required. Subsequently, a set of experiments is described where the stirring rate, the catalyst loading, reaction temperature and grinding of the catalyst was varied to minimize the diffusion, both external and internal (pore diffusion) and to identify conditions ensuring the catalytic activity measurement was conducted in kinetic region.

5.2.2.1 Variation of stirring rate

The effect of agitation rate on the reaction rate was investigated by varying the rotation speed of stirrer. A set of experiments with typical reaction conditions were carried out at different agitation rates of 300-700 rpm. The result can be seen in Figure 5-8.

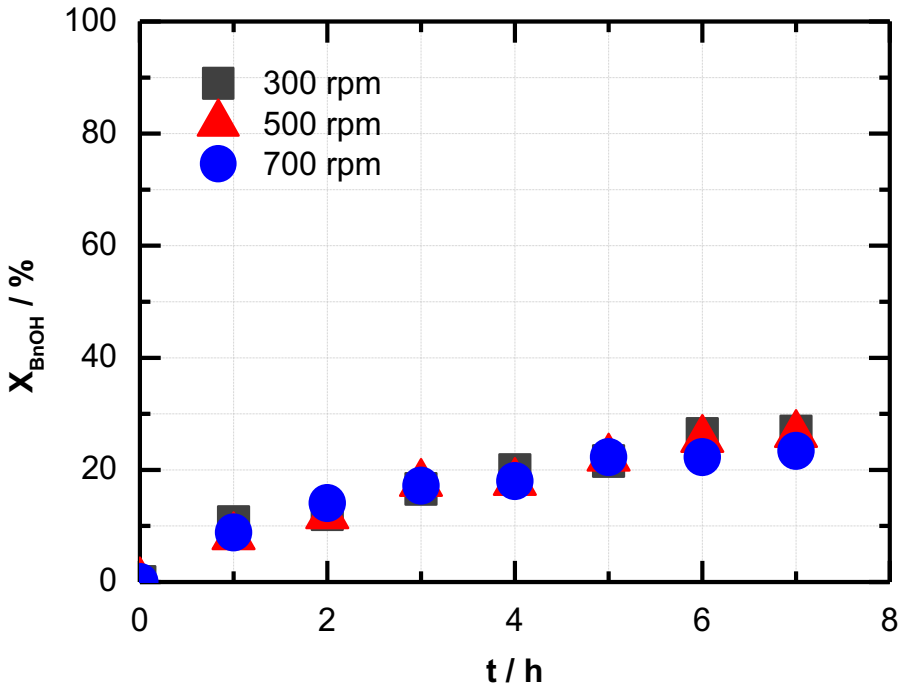

Figure 5-8 Conversion profile of oxidative esterification catalyzed by Co-N-C/AL catalyst with varying speed of stirring. Reaction conditions: 10 mmol Benzyl alcohol, 2 mmol K_2CO_3 (0.2 equivalent to substrate), 80 ml methanol, 100 mg Co-N-C/AL catalyst, T: 60 °C, F_{air}: 20 ml min^{-1}, speed of stirring: 300, 500, and 700 rpm.

The result shows a constant reaction rate while the agitation speed was varied, which is a strong indication that the gas-liquid transport is not limiting. As a slurry is employed the relative speed between the liquid and solid must not change, thus no conclusion on the liquid-solid film transport can be made.

5.2.2.2 Variation of catalyst loading

The influence of catalyst loading on the reaction rate was observed by varying the catalyst mass, i.e., 100, 150, 250, 400 and 600 mg. The experiments were carried out in the reaction mixture containing a certain amount of Co-N-C/Al catalyst under typical reaction conditions with 0.1 M initial concentration of benzyl alcohol at constant stirring speed of 300 rpm. The concentration-time data is used for calculating the rate constant following Equation 4-9. A plot of the reaction rate constant vs. catalyst loading is presented in Figure 5-9.

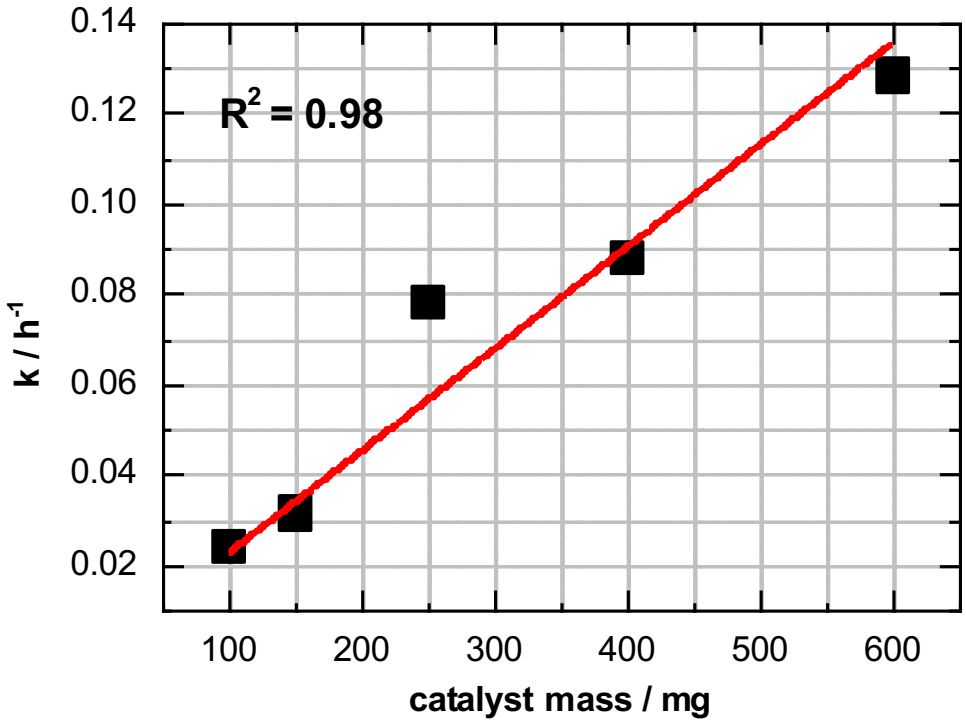

Figure 5-9 Reaction rate dependency towards the catalyst loading evaluated at the first 1-hour reaction. Reaction conditions: 10 mmol Benzyl alcohol, 2 mmol K_2CO_3, 80 mL methanol, 100 mg Co-N-C/AL catalyst, T: 60°C, F_{air}: 20 ml min^{-1}, speed of stirring: 300 rpm

From the result presented in Figure 5-9, the reaction rate is increasing linearly with the catalyst loading, indicating the active surface area is proportional to the amount of catalyst. Furthermore, variation of the catalyst loading shows a linear relation with the reaction rate which is another strong indication that there is no limitation of gas-liquid mass transfer.

5.2.2.3 Internal mass transfer

The Weisz-Prater criterion was calculated according to Equation 4-11, Equation 4-12, and Equation 4-13 to evaluate the influence of internal diffusion within the catalyst pores [100]. The detailed calculation, assumptions, and simplification which were made are provided in the Appendix 8.6. The calculated Weisz-Prater criterion is 0.0916, and thus by two orders of magnitude less than 1, which indicates that effects of internal diffusion limitation can be neglected.

5.2.2.4 Variation of temperature

A set of experiments with typical reaction condition using 150 mg Co-N-C/AL catalyst and 10 mmol benzyl alcohol in 80 ml methanol was conducted by increase of temperature from 25-60 °C. The result is shown in Figure 5-10.

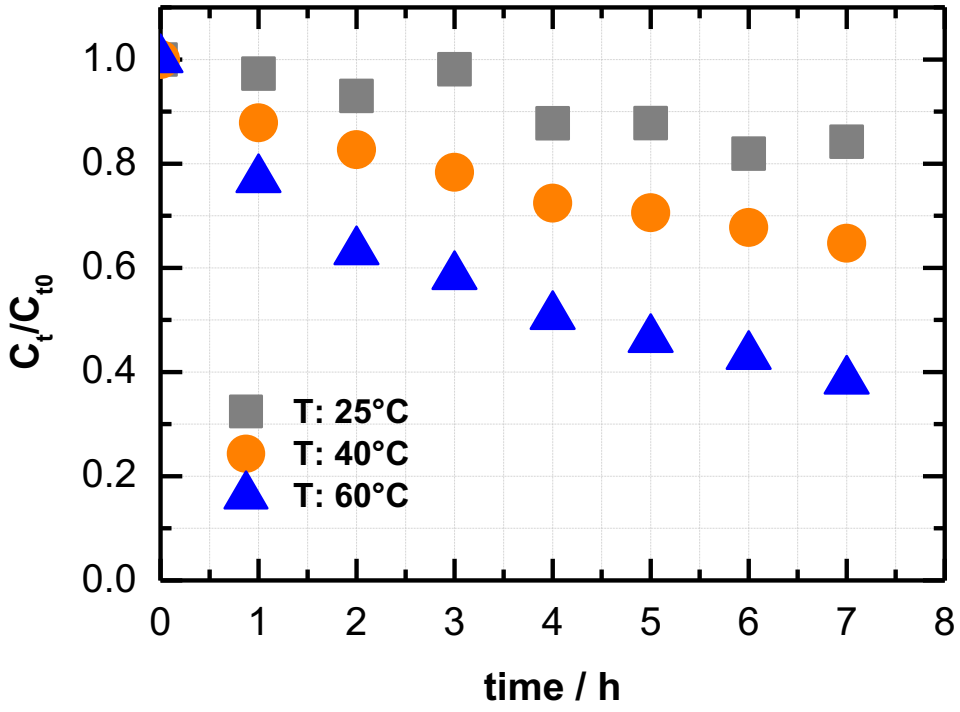

Figure 5-10 Concentration profile of oxidative esterification of benzyl alcohol using Co-N-C/AL catalyst with varying reaction temperature. Reaction conditions: 10 mmol Benzyl alcohol, 2 mmol K_2CO_3, 80 mL methanol, 150 mg Co-N-C/AL catalyst, T: 25, 40, 60 °C, F_{air}: 20 mL min^{-1}, speed of stirring: 700 rpm.

Figure 5-10 shows the reaction rate increases by the elevated temperature; thus, giving insights that the reaction is not controlled by internal and/or external diffusion steps but chemical reaction steps since chemical change is more temperature sensitive than physical steps.

5.3 Evaluation of kinetics

5.3.1 Simplified reaction network and kinetic model

Initial observation was made to see the chemical compounds formed during oxidative esterification of benzyl alcohol. The reaction was conducted in a typical reaction condition described in section 4.3.2 using semi-batch reactor set-up for 52 hours. The formation of different chemical compounds during the course of reaction were analyzed using Gas Chromatography as presented in Figure 5-11.

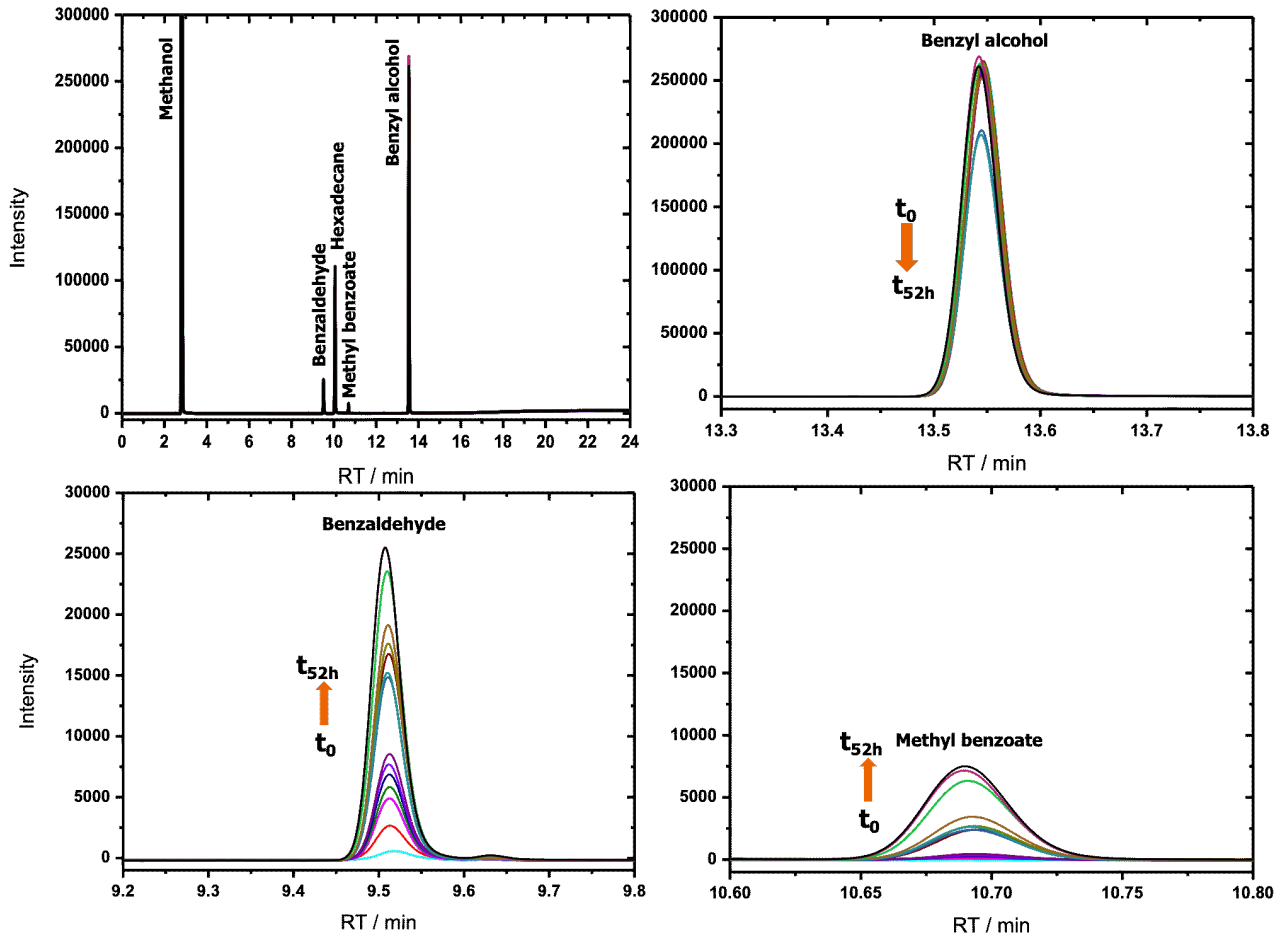

Figure 5-11 Different products formed during oxidative esterification of Benzyl Alcohol. Reaction conditions: 10 mmol Benzyl Alcohol, 100 mg Co-N-C catalyst, 80 ml methanol, F_{air}: 20 ml min^{-1}, T: 60 °C, P: 1 bar, speed of stirring: 300 rpm, t : 52 h.

As can be seen in Figure 5-11, the chromatograph shows different chemical compounds involved in the reaction, i.e., methyl benzoate (Retention time: 10.752) and benzaldehyde (Retention time: 9.56). In addition, only trace amount of benzyl benzoate (Retention time: 21.71) was identified in the product reaction. There was no significant amount of side product observed from reaction, thus suggesting that the catalyst was selective towards the expected product of reaction.

Further experiment was conducted using higher loading of catalyst, i.e., 500 mg of Co-N-C catalyst. The change of reactant and products concentration during the course of reaction were observed as presented in Figure 5-12.

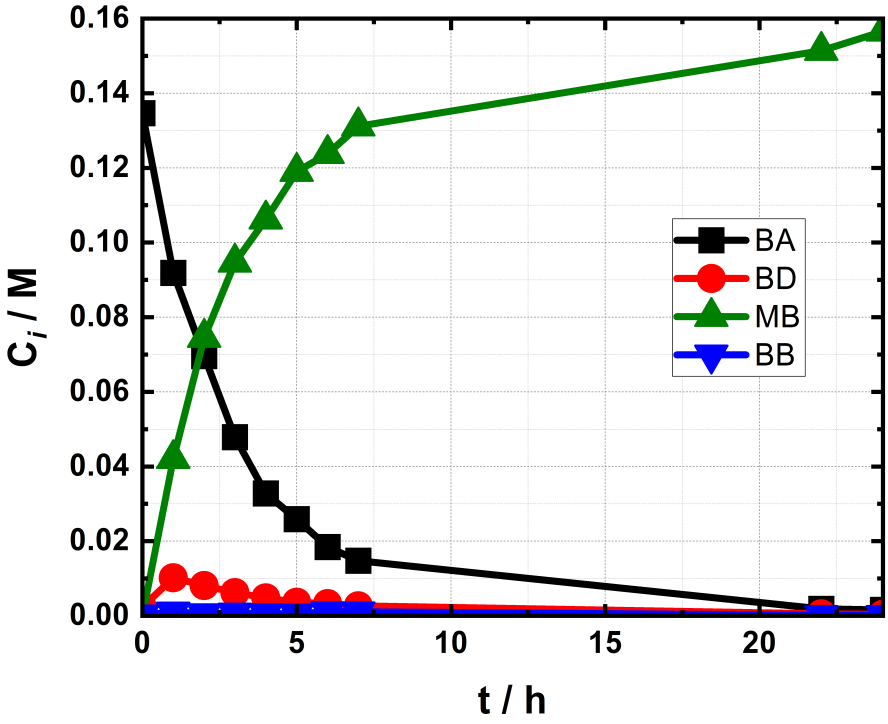

Figure 5-12 Concentration changes of Benzyl Alcohol (BA), Benzaldehyde (BD), Methyl Benzoate (MB), and Benzyl Benzoate (BB) over the time. Reaction conditions: 10 mmol Benzyl Alcohol, 2 mmol K_2CO_3, 500 mg Co-N-C catalyst, 80 ml methanol, F_{air}: 20 ml min^{-1}, P: 1 bar, t; 24 h

This result shows that reaction steps occurred in series, indicated by the presence of intermediate product, i.e., Benzaldehyde. The first step is the formation of benzaldehyde from benzyl alcohol, followed by the formation of methyl benzoate. From the Figure 5-12 can be seen that the peak of intermediate product (benzaldehyde) is lower than the main targeted product (methyl benzoate) at any time observed, thus suggesting that the 2^{nd} step of reaction is relatively faster than the 1^{st} step of reaction. It is in agreement with the literature proposed by *Beller et al.* [3], that the reaction occurred consecutively by selective oxidation of the alcohol to the aldehyde, formation of hemiacetal from the aldehyde and methanol, and further oxidation of the hemiacetal to the methyl ester. While benzyl benzoate was found as side product, which has been known as derivative of benzyl alcohol. One of the possible routes of benzyl benzoate formation is by transesterification of methyl benzoate with benzyl alcohol in the presence of an alkali benzyl oxide [101].

According to the initial observation on various products formation over the time, the reaction network can be proposed in this study as presented in Scheme 5-1.

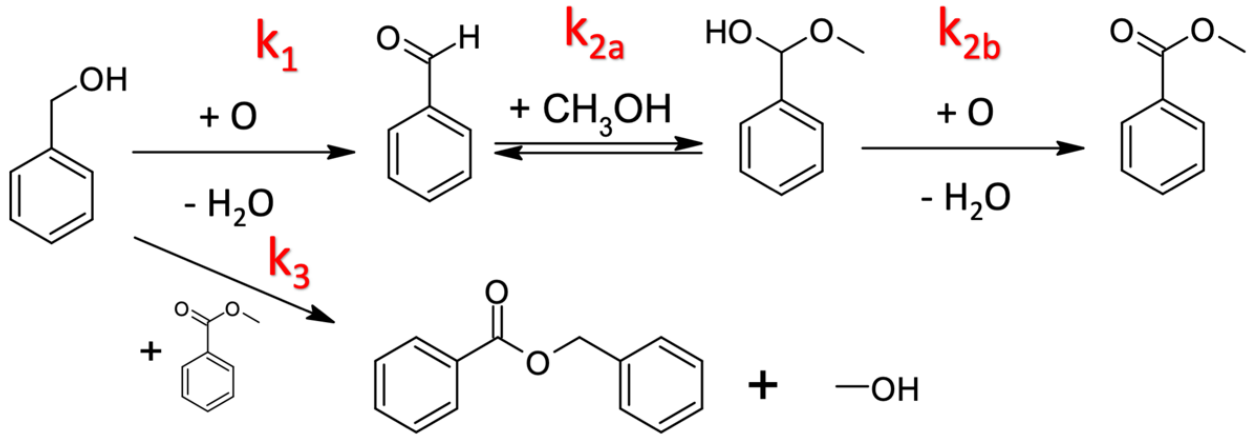

Scheme 5-1 Reaction scheme of the oxidative esterification of benzyl alcohol over Co-N-C catalyst

Based on the reaction network shown in Scheme 5-1 the subsequent chemical reactions and stoichiometries are employed for the kinetic modelling, while Equation 5-1 to Equation 5-4 describe the main reactions and Equation 5-5 the side reaction.

Equation 5-1 Reaction of Benzyl Alcohol to Benzaldehyde

$$C_7H_8O + \frac{1}{2}O_2 \xrightarrow{k_1} C_7H_6O + H_2O$$

Equation 5-2 Reaction of Benzaldehyde to Hemiacetal

$$C_7H_6O + CH_3OH \overset{k_{2a}}{\longleftrightarrow} C_8H_{10}O_2$$

Equation 5-3 Reaction of Hemiacetal to Methyl Benzoate

$$C_8H_{10}O_2 + \frac{1}{2}O_2 \xrightarrow{k_{2b}} C_8H_8O_2 + H_2O$$

As formation and decomposition of hemiacetal ($C_8H_{10}O_2$) occurs very fast, the reaction can be simplified as follow:

Equation 5-4 Reaction of Benzaldehyde to Methyl Benzoate

$$C_7H_6O + CH_3OH + \frac{1}{2}O_2 \xrightarrow{k_2} C_8H_8O_2 + H_2O$$

Equation 5-5 Side reaction of Benzyl Alcohol and Methyl Benzoate to Benzyl Benzoate

$$C_7H_8O + C_8H_8O_2 \xrightarrow{k_3} CH_3OH + C_{14}H_{12}O_2$$

A batch reactor data achieved by measuring concentration as a function of time was used to determine the rate law parameters. The reactor was equipped with a refluxed-condenser with -10 °C cooling system making the rate of evaporation is negligible, thus the liquid volume was considered to be constant. In addition, the air was continuously bubbled and methanol was used as the solvent, so that the concentration of oxygen and methanol in the solution remains constant over time. Therefore, the reaction rate is only a function of the benzyl alcohol concentration, which is also the limiting reactant.

A combination of material balance for a batch reactor and a rate law can be used for expressing the rate of formation and depletion of products and reactants (Equation 5-6 and Equation 5-7).

Equation 5-6

$$\frac{dc_i}{d\tau} = \sum_j \nu_{ij}\, r_j$$

Equation 5-7

$$r_j = k_j C_i$$

Where r_j is the rate of reaction (mol g_{cat}^{-1} min^{-1}), $\nu_{reactant} < 0$ and $\nu_{product} > 0$; C_i is the concentration of species i in solution (M); τ is the modified time (min g_{cat} ml^{-1}), and k_i is the apparent first order rate constant (ml min^{-1} g_{cat}^{-1}).

The change of concentration over time can be calculated by solving differential equation in Presto Kinetics according to the following equations:

Equation 5-8

$$\frac{d[C_7H_8O]}{dt} = -k_1[C_7H_8O] - k_3[C_7H_8O][C_8H_8O_2]$$

Equation 5-9

$$\frac{d[C_7H_6O]}{dt} = k_1[C_7H_8O] - k_2[C_7H_6O]$$

Equation 5-10

$$\frac{d[C_8H_8O_2]}{dt} = k_2[C_7H_6O] - k_3[C_7H_8O][C_8H_8O_2]$$

Equation 5-11

$$\frac{d[C_{14}H_{12}O_2]}{dt} = k_3[C_7H_8O][C_8H_8O_2]$$

Where C_7H_8O is the chemical formula of benzyl alcohol, C_7H_6O is the chemical formula of benzaldehyde, $C_8H_8O_2$ is the chemical formula of methyl benzoate, and $C_{14}H_{12}O_2$ is the chemical formula of benzyl benzoate.

5.3.1.1 Determining reaction order

In order to determine the reaction order, a set of experiments within the oxidative esterification of benzyl alcohols using a Co-N-C/AL with varying initial concentration was conducted. The results can be seen in Figure 5-13.

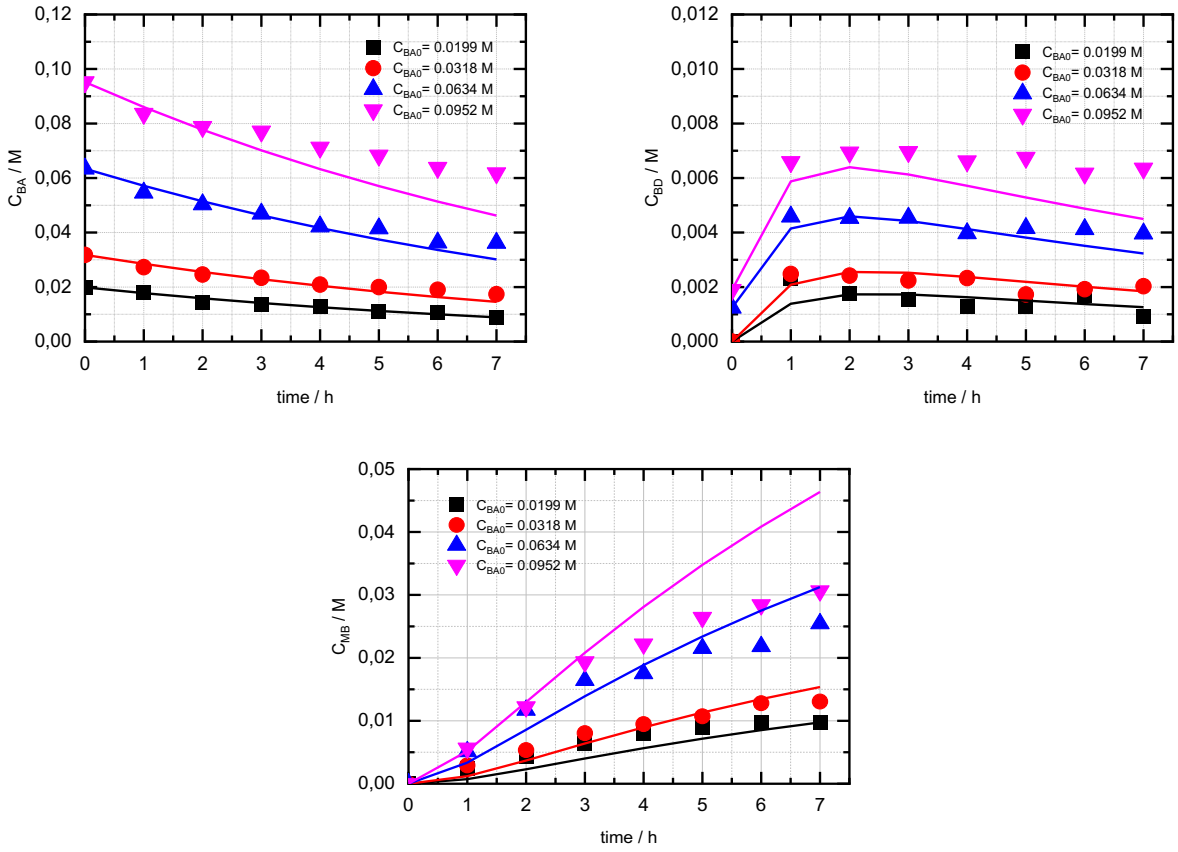

Figure 5-13 Concentration-time profile of oxidative esterification of benzyl alcohol over Co-N-C/AL catalyst with variation of initial alcohol substrate concentration. BA: Benzyl alcohol, BD: benzaldehyde, and MB: Methyl benzoate. Reaction conditions: 0.0199 - 0.0952 M Benzyl alcohol, 2 mmol K_2CO_3, 80 mL methanol, 150 mg Co-N-C/AL catalyst, F_{air}: 20 mL min^{-1}, T: 60°C, speed of stirring: 700 rpm.

The parameter estimation was done in Presto Kinetics to determine the rate constant and reaction order simultaneously using experimental data of the concentration-time profile from various initial concentrations of benzyl alcohols. The calculated reaction order of the first step of the consecutive reaction is 0.93 and the reaction order of the 2nd step of reaction is 1.18. The confidence interval of the

fitting is 0.032 for both parameters with residual 0,169. From Figure 5-13, it shows that the estimated reaction order fits under certain limiting conditions, i.e., in $C_{BA_0} = 0.0199; 0.0318;$ and $0.0634\ M$. While at the highest initial concentration of alcohol substrate ($C_{BA_0} = 0.0952\ M$), it is not well fitted. However, the reason is not well understood which possibly due to the experimental error.

A simplification of an apparent first order power law model was used for further kinetic evaluation. The reliable approach was made by conducting a set of experiments with various catalyst masses and initial concentrations. The rate constant vs. initial concentration of benzyl alcohol for the reaction using different catalyst loadings is plotted in Figure 5-14.

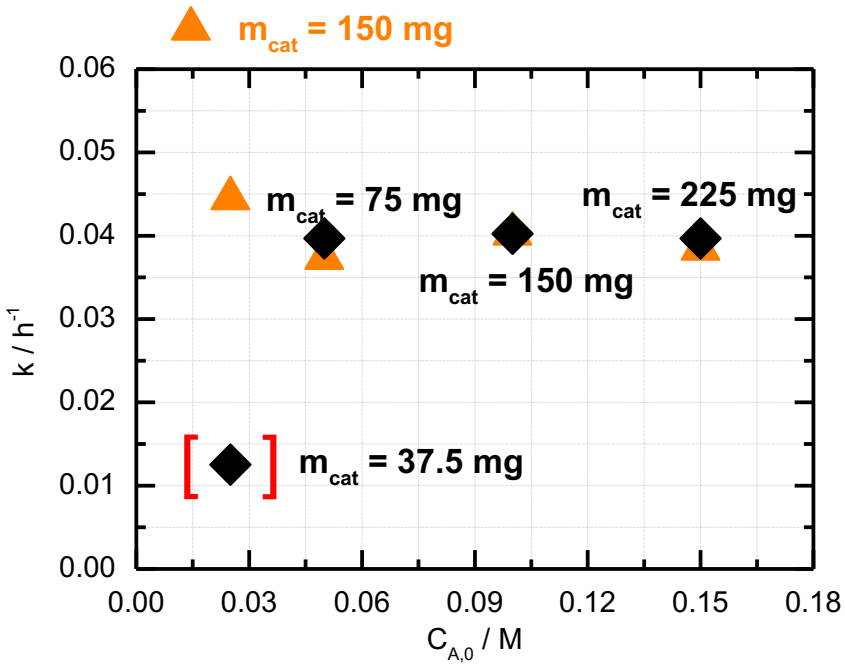

Figure 5-14 Independency of reaction rate towards the catalyst mass and initial concentration of alcohols. Reaction conditions: 0.025 - 0.15 M Benzyl alcohol, 37.5 - 225 mg Co-N-C/AL catalyst, 2 mmol K_2CO_3, 80 mL methanol, F_{air}: 20 mL min^{-1}, T: 60°C, speed of stirring: 700 rpm.

The result shows that the reaction rate constant is independent towards the catalyst mass and initial concentration of alcohols. As the initial concentration of benzyl alcohol is increased with subsequent increase of catalyst loading, the reaction rate keeps constant. This shows that the reaction follows a first order of reaction. However, this approach is not fitted to very low catalyst loadings. As will be seen subsequently, catalyst deactivation could be a reason for this outlier.

Additionally, the experiment with varying catalyst mass was conducted in longer reaction time, inclusively in low loading catalyst mass (i.e., 100, 150, and 250 mg). The time-concentration profile

data was fitted following the first order power law model. The result can be seen in Figure 5-15a and the parity plot of the experiments vs. calculated concentration profile is presented in Figure 5-15b.

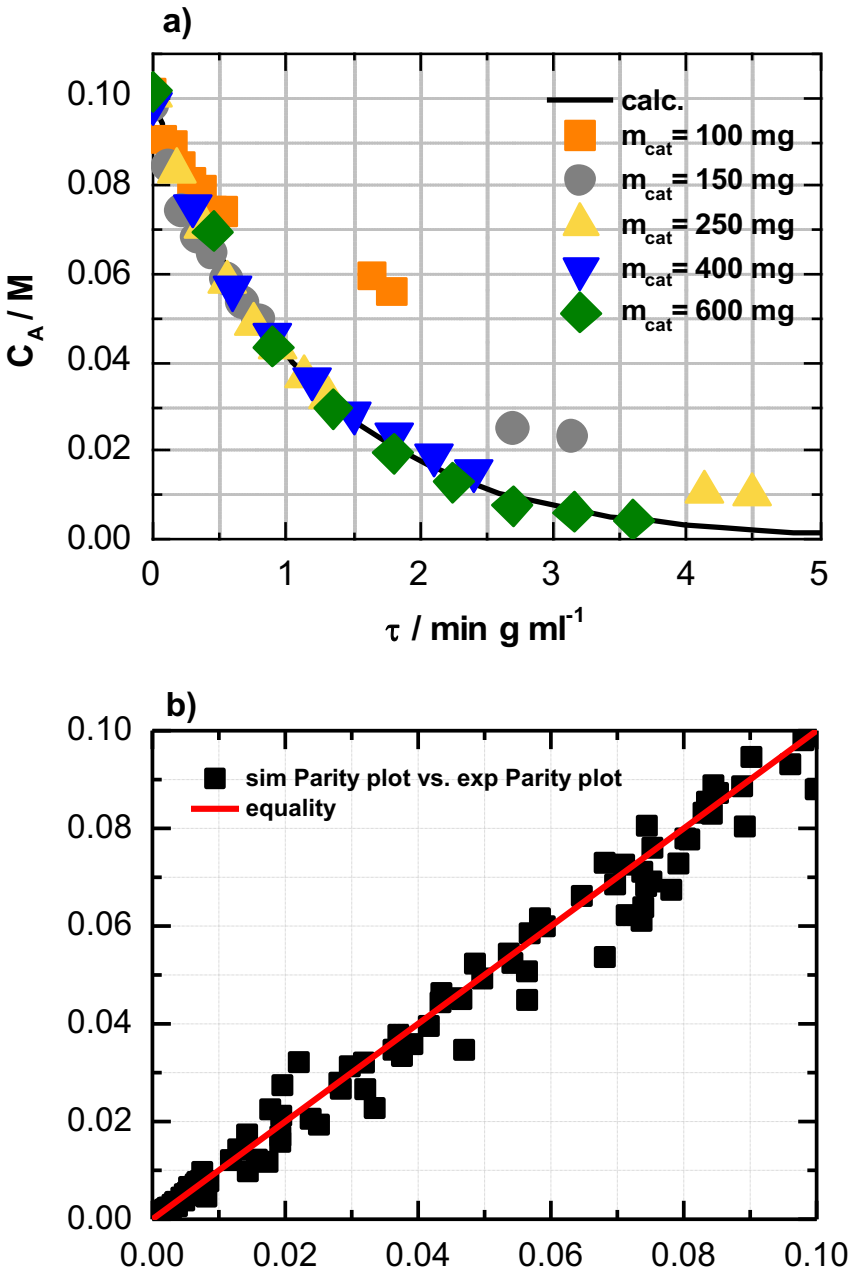

Figure 5-15 (a) concentration profile of benzyl alcohol during reaction with variation of catalyst mass, (b) parity plot of experiment vs simulation. Reaction conditions: 10 mmol Benzyl alcohol, 2 mmol K_2CO_3, 80 mL methanol, 100-600 mg Co-N-C/AL catalyst, T: 60°C, F_{air}: 20 ml min^{-1}, speed of stirring: 300 rpm.

Further investigation showed that the catalyst suffered from deactivation with longer time on stream. To get insights on the deactivation, using a time modified concept, the kinetic analysis was conducted according to the first order power law model and the constant parameter were estimated to be

k_1 = 8.74 x 10^{-1} ml g_{cat}^{-1} min^{-1} and k_2 = 87.63 x 10^{-1} ml g_{cat}^{-1} min^{-1} which fits to all experimental data of the catalyst mass variation. From the plot (Figure 5-15a), deactivation of the catalyst is likely to occur after longer reaction times at low catalyst loadings. This is in agreement with the practical method described by *Ma et al.* [102] in assessing the catalyst activity in a batch reactor, where the curves overlap only in the absence of catalyst deactivation. Further assessment of catalyst instability will be discussed later.

5.3.1.2 Arrhenius Plot

The Arrhenius parameters can be calculated using Equation 4-10 and the plot as shown in Figure 5-16.

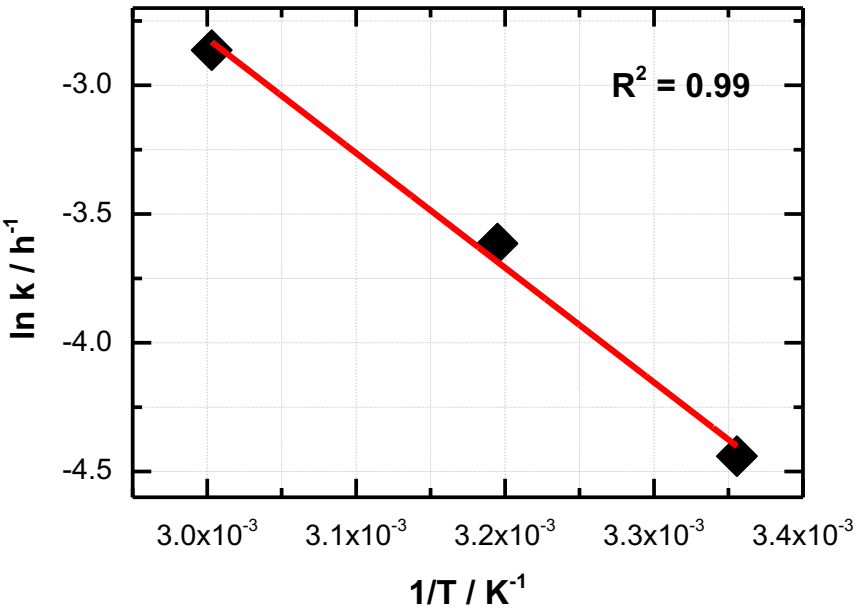

Figure 5-16 Arrhenius plot calculated from different temperatures of 25, 40, and 60 °C. Reaction conditions: 10 mmol Benzyl Alcohol, 2 mmol K_2CO_3, 150 mg Co-N-C/AL catalyst, 80 ml methanol, F_{air}: 20 ml min^{-1}, speed of stirring: 700 rpm.

From the linear regression, the activation energy and pre-exponential factor can be deduced as follow: $E = 37\ kJ\ mol^{-1}$ and $A = 3.78 \times 10^4\ h^{-1}$. Measuring the rate of catalytic reactions at different temperatures and determining the activation energy via Arrhenius plots can reveal mass transfer problems. In general, an activation energy of less than 5 kcal mol^{-1} (20.92 $kJ\ mol^{-1}$) is strong evidence of diffusion control, whether gas-liquid, liquid-solid, or both. On the other hand, an actual activation energy of more than 10 kcal mol^{-1} (41.84 $kJ\ mol^{-1}$) could be an evidence of no mass transfer limitation, while pore diffusion limitation can still not be ruled out [103]. From the determined activation energy, no conclusion about a pore diffusion limitation can be deduced, but the very small particle sizes and determined Weisz-Prater criterion make it likely that no pore diffusion limitation is observed.

5.3.2 Comparison of different kinetic data of Co-N-C catalysts

The kinetic model deduced in section 5.3.1 for Co-N-C/AL reaction rate constants were deduced for all of the investigated catalysts through fitting to experimental data from experiment at temperature of 60 °C. The resulting simulated concentration profiles are compared to the experimental results in Figure 5-17 and show a good agreement. The estimated rate parameters are presented in Table 5-5.

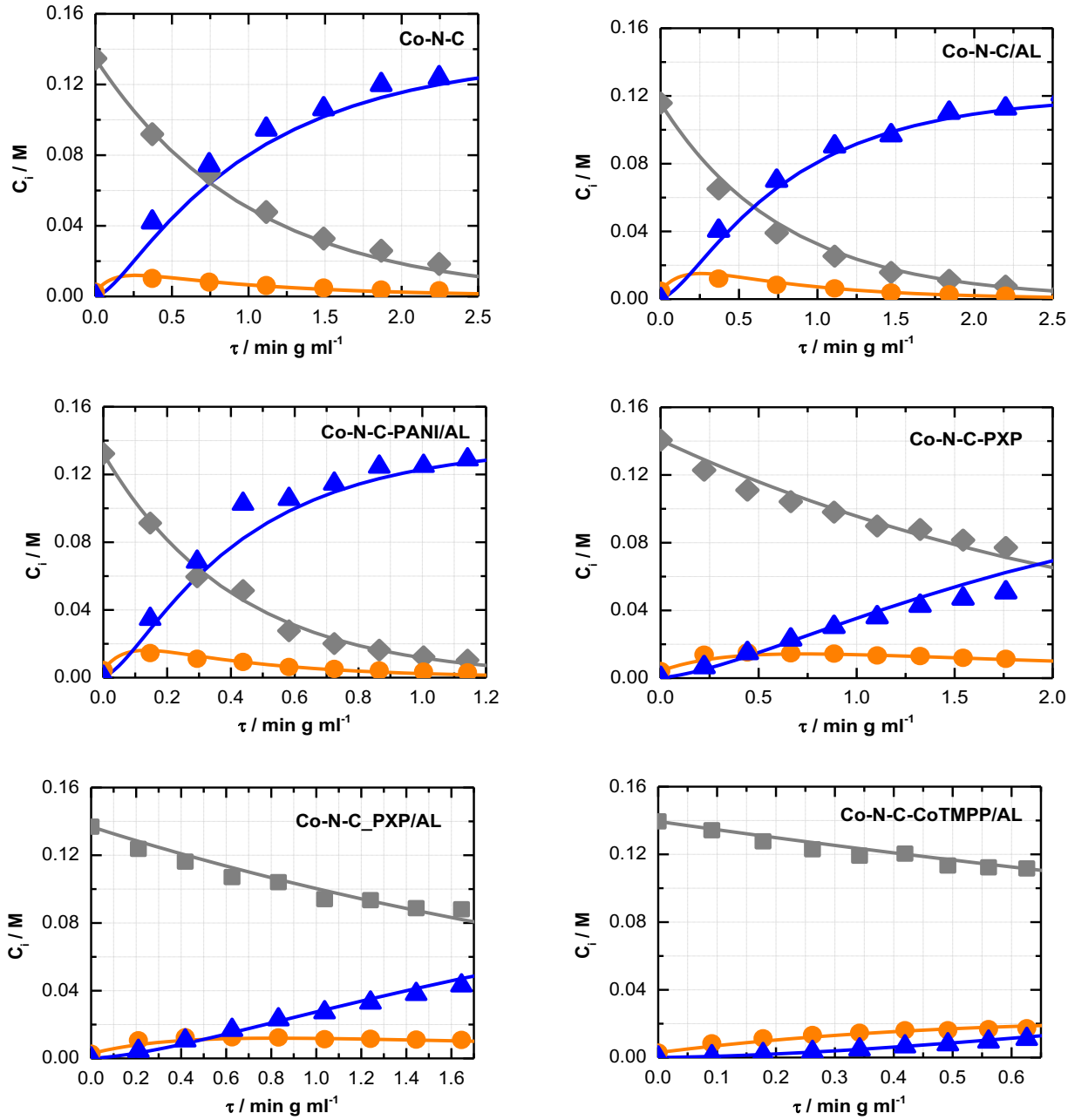

Figure 5-17 Concentration profile of benzyl alcohol (grey line), benzaldehyde (orange line), and methyl benzoate (blue line) calculated based on first order power law model. Reaction conditions: 10 mmol Benzyl alcohol, 2 mmol K_2CO_3, 80 mL methanol, specified amount of Co-N-C type catalyst, T: 60°C, F_{air}: 20 mL min^{-1}, speed of stirring: 300 rpm.

Table 5-5 Rate constant parameters

Catalysts	Catalyst mass (g)	Rate constant (min^{-1} mL g_{cat}^{-1})			Residual
		k_1	k_2	k_3	
Co-N-C	0.500	9.87E-01	85.1E-01	0.963E-01	2.38E-01
Co-N-C/AL	0.500	12.7E-01	68.3E-01	0.645E-01	3.10E-01
Co-N-C-PANI/AL	0.200	24.8E-01	141.0E-01	0.750E-01	2.44E-01
Co-N-C-PXP	0.302	3.84E-01	28.6E-01	0.417E-01	1.99E-01
Co-N-C-PXP/AL	0.284	3.28E-01	28.0E-01	0.495E-01	1.95E-01
Co-N-C-CoTMPP/AL	0.125	3.66E-01	15.3E-01	0.359E-01	0.62E-01

Reaction conditions: 10 mmol benzyl alcohol, 2 mmol K_2CO_3, 80 ml methanol, gas flowrate of 20 mL/min, 60°C (1 bar), 300 rpm of stirring, 8-24 h

The study shows that for all catalysts the rate constant of the first step is at least one magnitude slower than the subsequent reaction towards benzaldehyde. Strong activity differences of almost one order of magnitude can be observed for the studied catalysts, while a polyaniline derived catalyst employing additional acid leaching (Co-N-C-PANI/AL), shows the highest activity. Also, the Co-N-C/AL catalyst shows remarkable activity, although it has a low cobalt content. Comparison of the different Co-N-C catalysts activity can be seen in Figure 5-18.

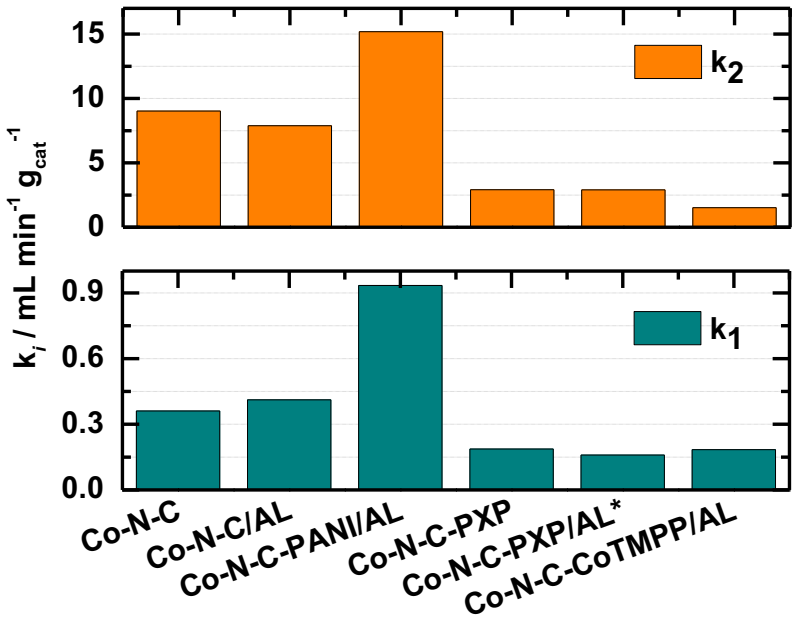

Figure 5-18 Comparison of the calculated rate constants for different Co-N-C catalysts.

The activity of the Co-N-C/AL catalyst has been increased by employing acid leaching to remove inactive phase, i.e., metallic cobalt core, as described earlier by *Liu et al.* [95]. The presence of cobalt nanoparticles in this catalyst is possibly associated with the active sites. In accordance to *Beller et al.* [3], the activity of the catalyst in various alcohol oxidations, such as in benzyl alcohol oxidation, are attributed to Co_3O_4 nanoparticles (with size 2-10 nm) on carbon-nitrogen-based materials. As being

found in the Co-N-C catalyst, Co_3O_4 nanoparticles are also present in the Co-N-C-PANI/AL catalyst with a low amount of 7.43 % based on XPS result. Worth noting that Co-N_x sites are present in Co-N-C-PANI/AL catalyst in large amount up to 92.57 % of the total cobalt present on the surface. These sites have been previously known as active sites for ORR reaction, but at some extent also involve in oxidation reactions of alcohols as investigated in the present study. Previously suggested by *Zhigang et al.* [61] according to their analysis that Co-N_x sites are closely related to the performance of the catalyst. The synergistic effect between cobalt and pyridinic N tune the spin density, charge density, and π state density of C atoms, resulting in more C atoms being activated and more active sites being generated, which further promotes the adsorption/desorption of intermediates for enhancing the catalytic performance. However, it is still hard to correlate the activity based on the number of active sites, since other factors are also involved. The physical and chemical properties of the investigated catalysts are summarized in Table 5-6.

Table 5-6 Physical and chemical properties of the investigated Co-N-C catalysts

Catalyst	**TEM result and XPS-detected Cobalt species**	**XRD-crystallinity analysis**	**BET surface area (m^2 g^{-1})**	**ICP-cobalt content (wt %)**	**Reaction rate, evaluated at 1 h (mol g_{cat}^{-1} min^{-1})**	**Ref.**
Co-N-C	Co_3O_4 nanoparticles (with size 2-10 nm) and Co-N_x	Minor crystallinity	92	3.09	1.25E-04	[3]
Co-N-C/AL	Co_3O_4 and $Co(OH)_2$ with larger particle size (100-200 nm) due to removing N-content by acid leaching which leads to agglomeration	Minor crystallinity	116	1.53	1.36E-04	This work
Co-N-C-PANI/AL	Small fraction around 7 % of Co_3O_4 and 93 % of Co-Nx sites from total of cobalt present in the catalyst	The highest crystallinity compared to other catalysts	288	31.86	2.83E-04	This work
Co-N-C-PXP	Smaller cobalt particle (with size 20-50 nm)	amorphous	351	2.86	5.27E-05	This work
Co-N-C-PXP/AL	undefined	amorphous	346	2.26	4.40E-05	This work
Co-N-C-CoTMPP/AL	Smaller cobalt particle (with size <<20 nm)	amorphous	280	22.73	4.99E-05	This work

In every characterization conducted previously, the Co-N-C-PANI/AL catalyst showed superior physical properties by having a high surface area, a high crystallinity, a high percentage of Co-N-C phase (92.57 %), and the presence of the Co_3O_4 phase despite in small amount (7.43 %). Compared with Co-

N-C-CoTMPP and Co-N-C-PXP, these two catalysts are less active due to an amorphous surface structure and absence of the intended active sites.

The conversion of benzyl alcohol and the selectivity to methyl benzoate of the investigated catalysts in the oxidative esterification of benzyl alcohol are presented in Figure 5-19.

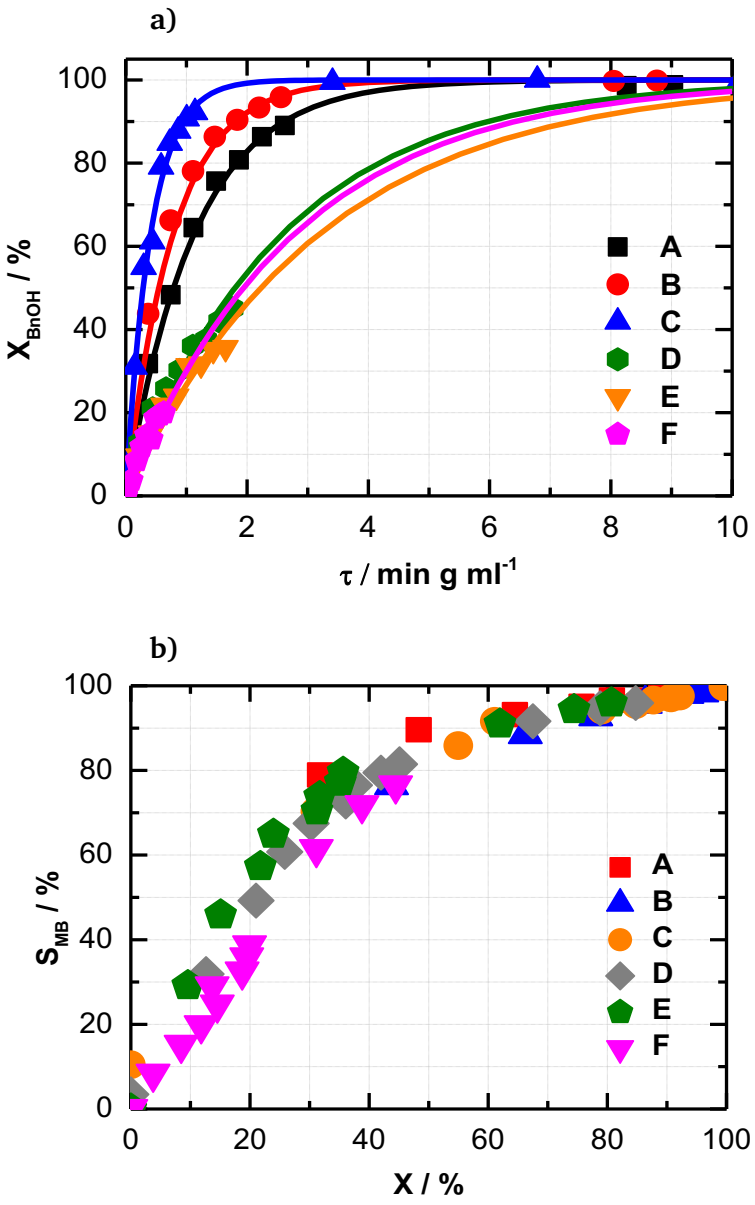

Figure 5-19 (a) Conversion and (b) selectivity of the investigated Co-N-C catalysts at degree of conversion: (A) Co-N-C, (B) Co-N-C/AL, (C) Co-N-C-PANI/AL, (D) Co-N-C-PXP, (E) Co-N-C-PXP/AL, (F) Co-N-C-CoTMPP/AL. Reaction conditions: 10 mmol Benzyl alcohol, 2 mmol K_2CO_3, 80 mL methanol, specified amount of Co-N-C type catalyst, T: 60°C, F_{air}: 20 mL min^{-1}, speed of stirring: 300 rpm.

The different ratio of k_1/k_2 for the catalysts results in slight selectivity differences of the consecutive reaction and for degrees conversion around 40 %. The very low-rate constants of k_3 result in negligible

benzyl benzoate production and thus nearly 100 % methyl benzoate yield. Thus, it shows Co-N-C catalyst is generally active for oxidation reactions, despite requiring optimization of the cobalt content and/or the morphology of the catalyst to enhance their activity further.

5.3.3 Role of basicity

In order to get insights on the function of the base in the model reaction of the oxidative esterification of benzyl alcohol to methyl benzoate, several experiments were conducted with additional base or without it. The results of these experiments are presented in Figure 5-20.

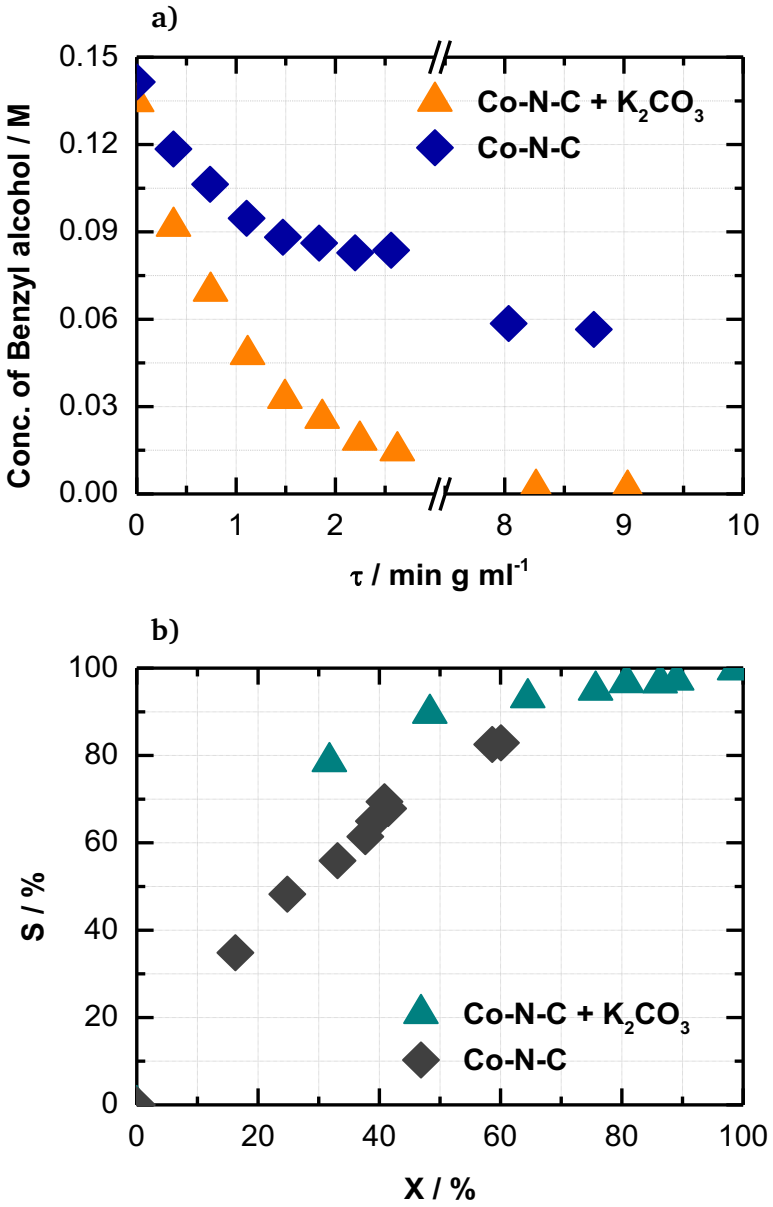

Figure 5-20 (a) concentration profile and (b) selectivity vs conversion of oxidative esterification of benzyl alcohol using Co-N-C catalyst. Reaction conditions: 10 mmol Benzyl alcohol, 2 mmol K_2CO_3 or base-free, 500 mg Co-N-C catalyst, 80 mL methanol, F_{air}: 20 mL min-1, T: 60°C, speed of stirring: 300 rpm.

Initial investigation using benchmark Co-N-C catalyst shows that the base significantly increases the reaction rate (Figure 5-20a). Moreover, as can be seen in Figure 5-20b, the addition of K_2CO_3 increases the selectivity towards the 2nd step of the reaction which results in higher ester production below 70 % conversion. As previously described, direct oxidative esterification of benzyl alcohol constitutes a consecutive reaction. The aldehyde, which is the intermediate product is dissolved in methanol and can undergo a further reaction to form hemiacetals. Most hemiacetals are unstable and decompose to the alcohol and its initial aldehyde. Thus it is not facile to isolate the hemiacetal as by removing methanol it decomposes with the constantly changing equilibrium [104].

Hemiacetals are unstable because they are essentially tetrahedral intermediates containing leaving groups. The formation of hemiacetals is reversible and can be catalyzed by acids or bases, which also catalyze their decomposition back to the initial aldehyde and alcohol. Acid or base catalysts increase the rate of reaching the equilibrium of hemiacetal with its aldehyde and alcohol components.

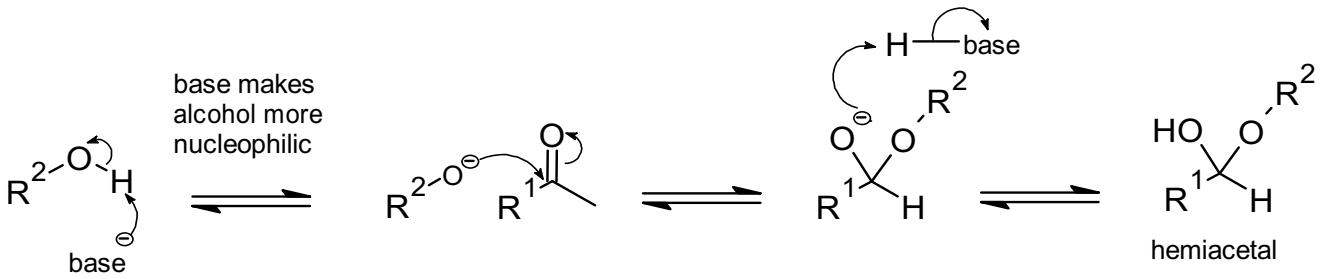

Scheme 5-2 Base-catalyzed hemiacetal formation

Shortly as depicted by Scheme 5-2, the base increases the nucleophilicity of methanol by removing the OH proton before it attacks the C=O group on benzaldehyde to form a hemiacetal [104]. The hemiacetal is an unstable tetrahedral intermediate containing a leaving group, thus it is easily to form the corresponding ester. The experimental results show that the reaction without the base in the presence of Co-N-C catalyst still occur with slower conversion rate, while in the absence of catalyst the reaction did not occur. The influence of base concentrations on the reaction rate of oxidative esterification of benzyl alcohols was investigated earlier by *Astrakova et al.* [25] and the results showed that the reaction rate increases with an increase of base concentration. Another report by *Leng et al.* [88] showed that N-doped carbon could act as built-in and strengthened Lewis base to accelerate the deprotonation process, thus allowing the oxidative esterification reaction occurred in the base additive-free catalytic system. In order to get insights of the influence of the base concentrations on the reaction rate, several experiments by varying the base concentration at different catalyst masses were conducted. The experimental results and simulation following first order power law are presented in Figure 5-21.

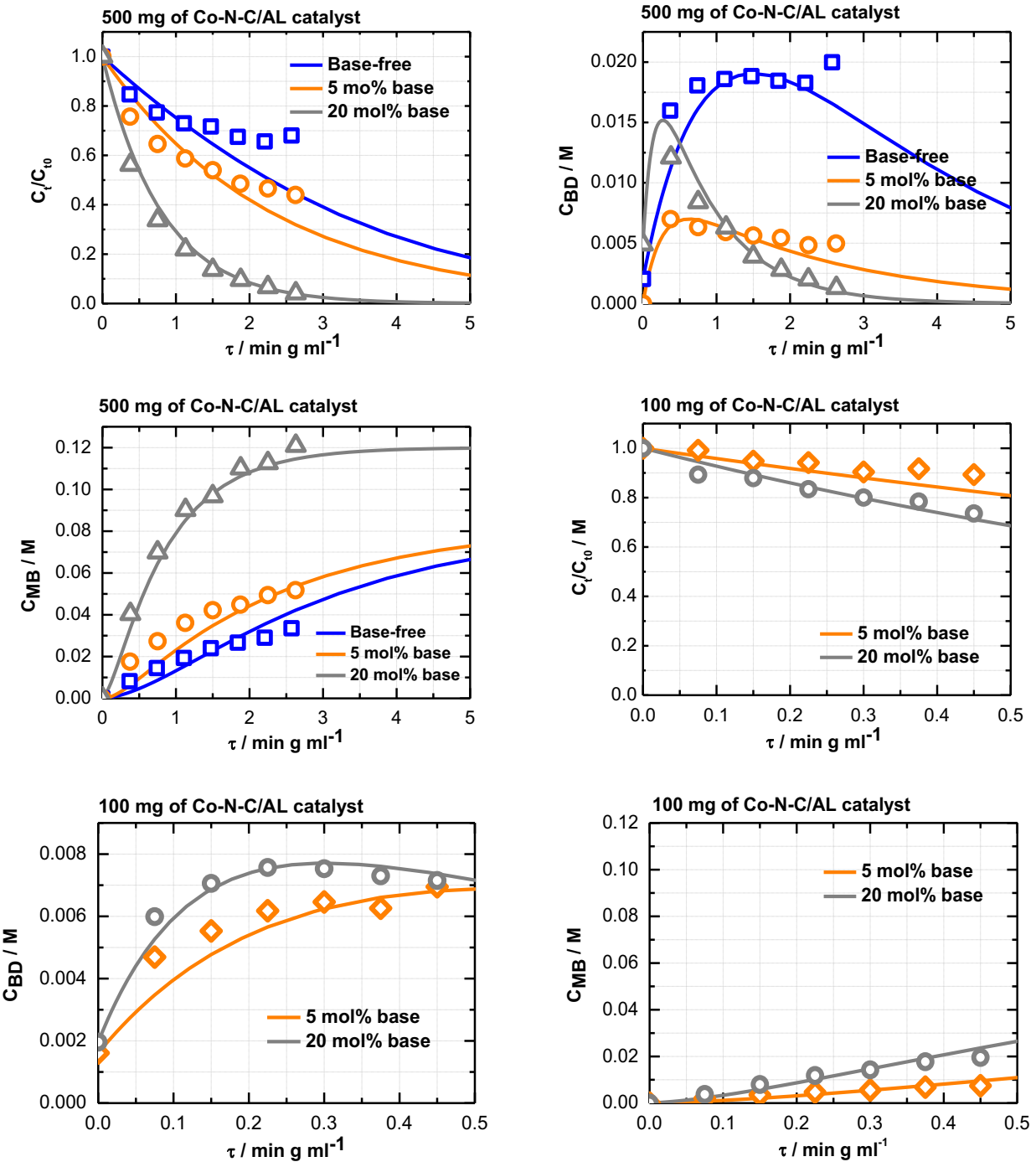

Figure 5-21 Concentration profile of the oxidative esterification of alcohol using Co-N-C/AL catalyst with varying K_2CO_3 concentration at catalyst mass of 500 mg (left figures) and 100 mg (right figures). Reaction conditions: 10 mmol Benzyl alcohol, K_2CO_3: 0.5 mmol (5%) and 2 mmol (20%), 500 mg Co-N-C/AL catalyst, 80 mL methanol, F_{air}: 20 mL min^{-1}, T: 60°C, speed of stirring: 700 rpm.

The result shows the reaction is strongly dependent on the base concentration both with higher (500 mg) and lower catalyst mass (100 mg). However, the applied kinetic model following first order reaction of the consecutive reaction seems less fitted to the experiment data in base-free condition. This is consistent with the previous explanation that the base takes part in speeding up the 2nd step of the reaction. Whereas

in the absence of base, the reaction become slower. The conversion and the selectivity dependency to the base concentration are presented in Figure 5-22.

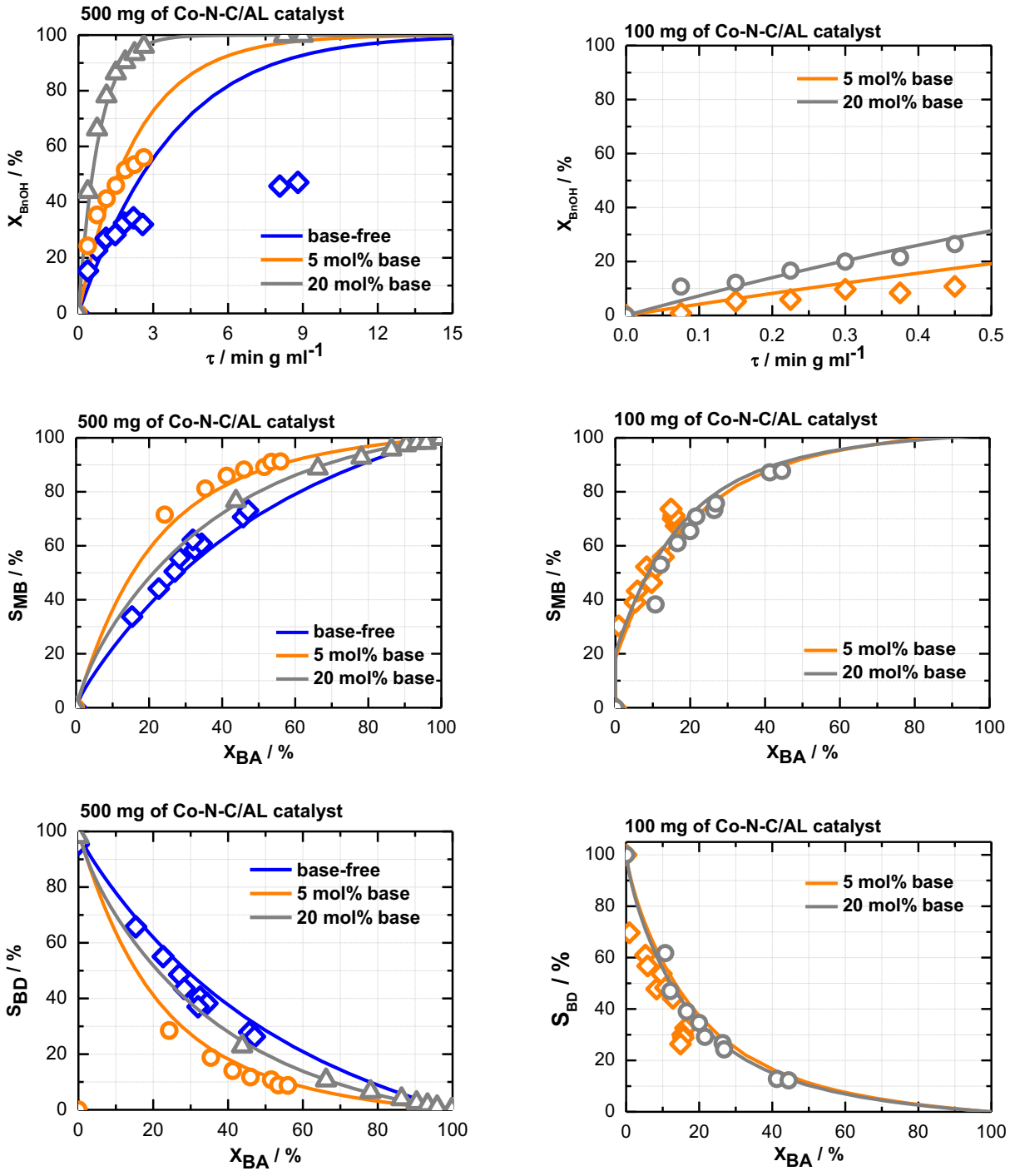

Figure 5-22 Selectivity vs conversion of oxidative esterification of benzyl alcohol with varying base concentration at 500 mg catalyst (left figures) and 100 mg catalyst (right figures). Reaction conditions: 10 mmol Benzyl alcohol, K_2CO_3: 0.5 mmol (5%) and 2 mmol (20%), 100 and 500 mg Co-N-C/AL catalyst, 80 mL methanol, F_{air}: 20 mL min^{-1}, T: 60°C, speed of stirring: 700 rpm.

The conversion of benzyl alcohol is strongly dependent on the base concentration. The selectivity to the expected methyl ester was optimized with 5 mol % base and 500 mg of the catalyst. Benzaldehyde is the intermediate product, which is then converted to the ester by involving the base as the co-catalyst. By using 5 mol % of base concentration, the 2nd step of the consecutive reaction was improved much higher than using 20 mol % base. In line with Scheme 5-2, providing excess of base increases the decomposition of hemiacetal back to benzaldehyde. Whereas, under base-free condition, more benzaldehyde was found in the product. Thus, it supports previous finding that base in some extent improves yield of methyl ester.

However, for low catalyst loading (100 mg), the selectivity seems to be less influenced by the base concentration. Worth noting that the reaction occurred heterogeneously by involving the Co-N-C catalyst and the base as co-catalyst which participates in the 1st and 2nd steps of the consecutive reaction, respectively. Hence, an optimized conditions can be achieved by tuning the "concentration" of active sites as well as adjusting the base concentration as co-catalyst. To conclude, 5 mol % base concentration is sufficient for the oxidative esterification of benzyl alcohol independent of the catalyst mass.

5.4 Stability assessment of catalysts

The stability of the Co-N-C catalysts was initially observed form the reaction with low catalyst mass and longer reaction time as presented in Figure 5-23.

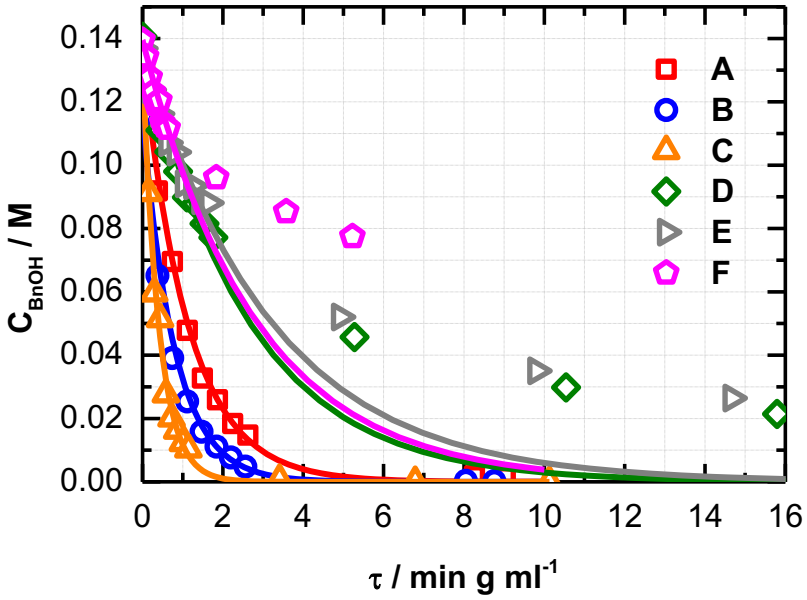

Figure 5-23 Activity and destability of different catalysts: (A) Co-N-C, (B) Co-N-C/AL, (C) Co-N-C-PANI/AL, (D) Co-N-C-PXP, (E) Co-N-C-PXP/AL, (F) Co-N-C-CoTMPP. The symbols are experiment data and solid line is simulation data. Reaction conditions: 10 mmol benzyl alcohol, 2 mmol K_2CO_3, 80 ml methanol, catalyst mass: (A) 500 mg, (B) 500 mg, (C) 200 mg, (D) 302 mg, (E) 284 mg, (F) 125 mg, gas flowrate of 20 mL min^{-1}, 60°C (1 bar), 300 rpm of stirring, 8-72 h

Despite having high activity and selectivity in the investigated model reaction, the stability of the catalysts for long-term reaction is still unknown. Hence, the stability assessment of the catalysts was also conducted in the present study. The simulation is conducted based on the rate constants fitted to the initial activity, which was proven from the mass variation to be valid for the whole regime. When increasing the reaction time by using a lower catalyst mass, as can be seen in Figure 5-23, the experimental results for catalyst Co-N-C-PXP (D), Co-N-C-PXP/AL (E), and Co-N-C-CoTMPP (F) differ from the simulation. This difference is caused by deactivation behavior of the catalysts.

A commonly observed deactivation of the catalyst in such reaction is due to over-oxidation of the active sites. According to literature, the rate of alcohol oxidation enhances on a reduced metal surface rather than on the oxidized surface [23]. In this experiment, the catalytic activity was tested in the kinetic region, however, it seems that the active sites were oxidized, so that their activity declined. While to the best of our knowledge the stability of the Co-N-C catalyst has not been described in partial conversion, especially in the kinetic region where activity is better explained. *Beller et al.* [3] have introduced the Co-N-C catalyst as highly stable and that it can be reused several times. The present study shows that a more detailed evaluation within the kinetic regime is needed to give insights to the deactivation behavior of the catalyst.

To understand the stability of the catalyst, the used-catalysts were characterized using N_2 sorption and compared to the pristine ones. The catalyst was filtered from the mixture after 24 h reaction at typical operation conditions. The washing was applied using methanol and subsequently water for several times before drying and performing the analysis. The results are presented in Figure 5-24.

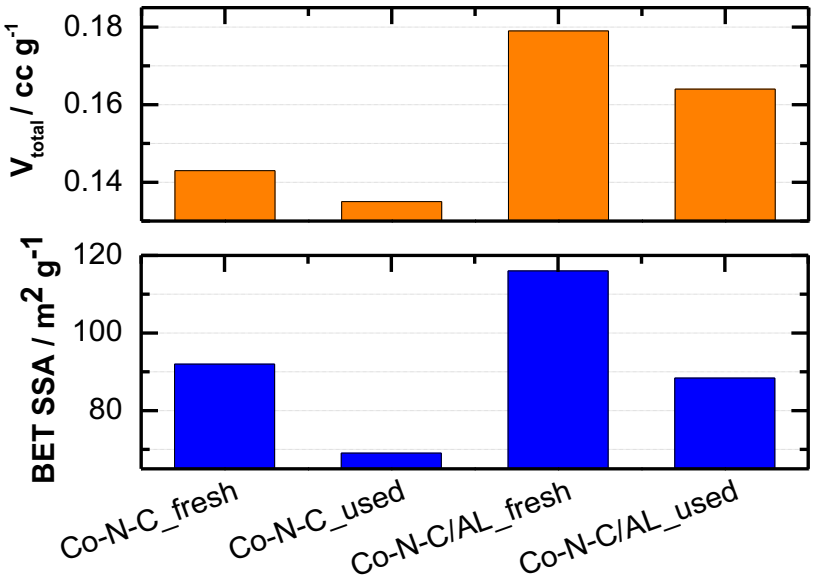

Figure 5-24 Comparison of N_2 sorption measurement between pristine and the used catalysts.

Characterization of the surface properties of the used Co-N-C/AL catalysts using nitrogen sorption measurement shows a decreased of catalysts surface area to around 20-25% of the initial value after being used for 24 h reaction. A significant decrease of total pore volume was also detected from the used- Co-N-C and Co-N-C/AL catalysts. This finding gave an overview that initial investigation regarding catalyst deactivation can be confirmed.

Further analysis using XPS and TEM of the pristine and used Co-N-C catalysts were also conducted. The atomic percentage of elemental surface composition of the investigated Co-N-C catalysts are presented in Table 5-7.

Table 5-7 Atomic percentage of elemental surface composition on the Co-N-C catalysts.

Catalyst	Element composition (at %)				
	C 1s	O 1s	N 1s	Co 2p	S 2p
Co-N-C-PANI/AL	73.0	11.6	11.1	3.1	1.2
Co-N-C-PANI/AL_used	72.8	11.0	11.9	3.8	0.5
Co-N-C-CoTMPP/AL	68.0	19.8	4.8	4.1	3.4
Co-N-C-CoTMPP/AL_used	42.0	41.4	1.2	13.4	2.1

Due to limitations, the analysis was conducted only for several representative catalysts. The result shows that Co-N-C-PANI/AL catalyst which has not suffered from deactivation shows no significant changes in the elemental surface composition after being used under oxidation reaction condition. As a comparison, for the Co-N-C-CoTMPP/AL catalyst, that showed a deactivation during the reaction, a decreased number of Nitrogen in the used catalyst can be observed, thus possibly reducing the number of available Co-N_x site. In addition, the used catalyst shows a higher amount of cobalt on the surface which is possibly due to displacement of cobalt from the bulk phase to the surface. Worth noting that the average depth of analysis for an XPS measurement is approximately 5 nm. As suggested by *Zhigang et al.* [61], the pyridinic N is most likely to form coordination structures with cobalt (Co-N_x) which stabilizes Co nanoparticles and prevents them from agglomerating, and thus facilitates the dispersion of Co nanoparticle.

Additionally, analysis using High Resolution Transmission Electron Microscopy (HR-TEM) was conducted to identify the change of surface morphology of the Co-N-C catalyst caused by deactivation. In the present study, only the used Co-N-C/AL sample was analyzed and the measurement result is presented in Figure 5-25.

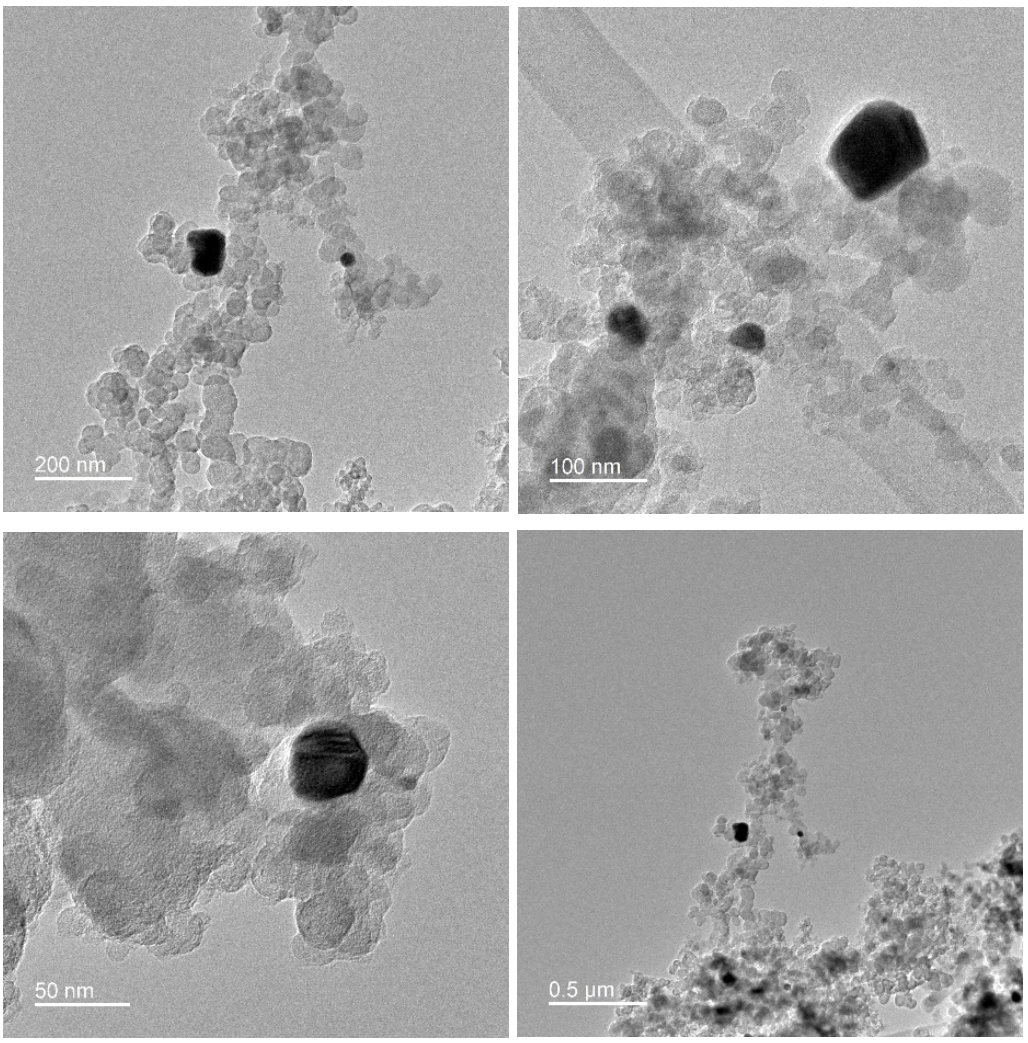

Figure 5-25 TEM image of Co-N-C/AL catalyst after used in oxidative esterification of benzyl alcohol at typical reaction conditions (T: 60 °C, P: 1 bar, F_{air}: 20 ml min^{-1}). The black dot is an enlargement image of cobalt.

The results show there is no obvious change of the catalyst due to formation of cobalt clusters or agglomeration. The cobalt is identified as nanoparticle with size ranging from 50 to 200 nm, which is relatively unchanged during the course of reaction.

Further assessment of catalysts deactivation was carried out experimentally to determine the cause of deactivation due to the base and/or oxygen. The catalyst was pre-treated under reaction conditions in the presence and absence of oxygen and base for 3 hours, while the alcohol substrate was introduced later. A set of experiments was conducted as follows: 1st experiment (exp. 1) is a general reaction system using catalyst without pre-treatment, 2nd experiment (exp. 2) is the catalytic reaction with oxygen and base pre-treatment, and the 3rd experiment (exp. 3) is the catalytic reaction in the presence of base without oxygen pre-treatment. The experimental results and simulations are presented in Figure 5-26.

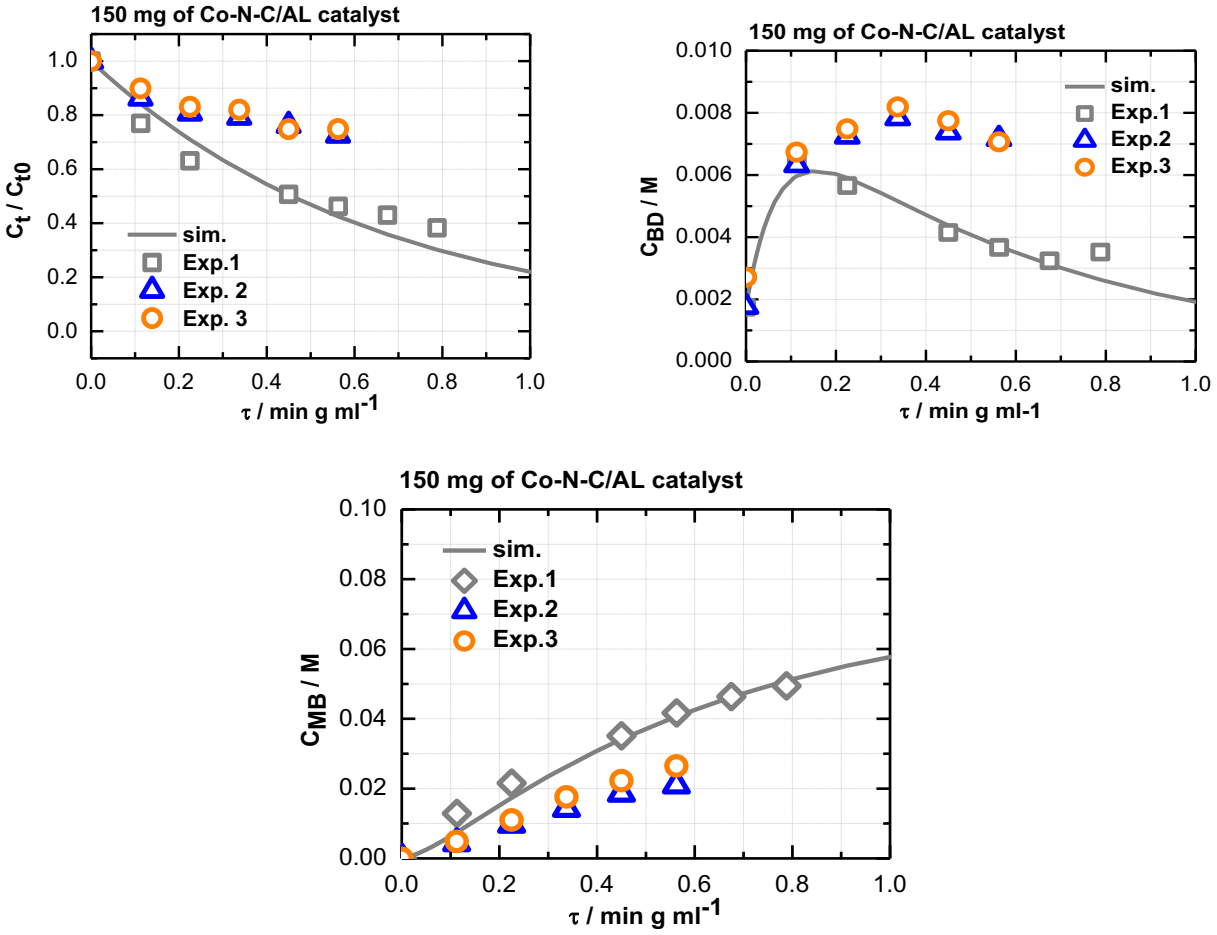

Figure 5-26 Concentration profile of benzyl alcohol, benzaldehyde, and methyl benzoate in the oxidative reaction using pristine and aged-Co-N-C/Al catalyst. The symbols are experimental data and solid lines are simulation data. Reaction conditions: 10 mmol Benzyl alcohol, 2 mmol K_2CO_3, 150 mg Co-N-C/AL catalyst, 80 mL methanol, F_{air}: 20 mL min^{-1}, T: 60°C, speed of stirring: 700 rpm.

The catalysts undergo deactivation after being treated with oxygen and base. As can be seen in Figure 5-26, the 1st experiment with typical reaction conditions fits properly with the simulation according to the approached model. In contrast, the 2nd and 3rd experiment which were pre-treated either with oxygen or base showed lower activity. However, the result is not significantly different between the reaction in the presence and absence of oxygen, thus giving insight that oxygen is less responsible for the deactivation. This finding is in agreement with the previously study by *Astrakova et al.* [25], although the reaction rate is strongly dependent on the K_2CO_3 concentration, but its increasing concentration also leads to catalyst decaying behavior. They identified that an equimolar ratio between benzyl alcohol and K_2CO_3 is inappropriate and less base concentration of an order of magnitude can be used. Also, their study showed that 5 mol % K_2CO_3 relative to benzyl alcohol was sufficient to obtain a strong catalytic effect. While in the present study, typical reaction conditions with 20 mol % K_2CO_3 relative to benzyl alcohol were applied.

To further investigate the dependency of the deactivation to the base, a set of experiments was conducted by varying the base concentration in different catalyst masses. The experimental results and simulations are presented in Figure 5-27.

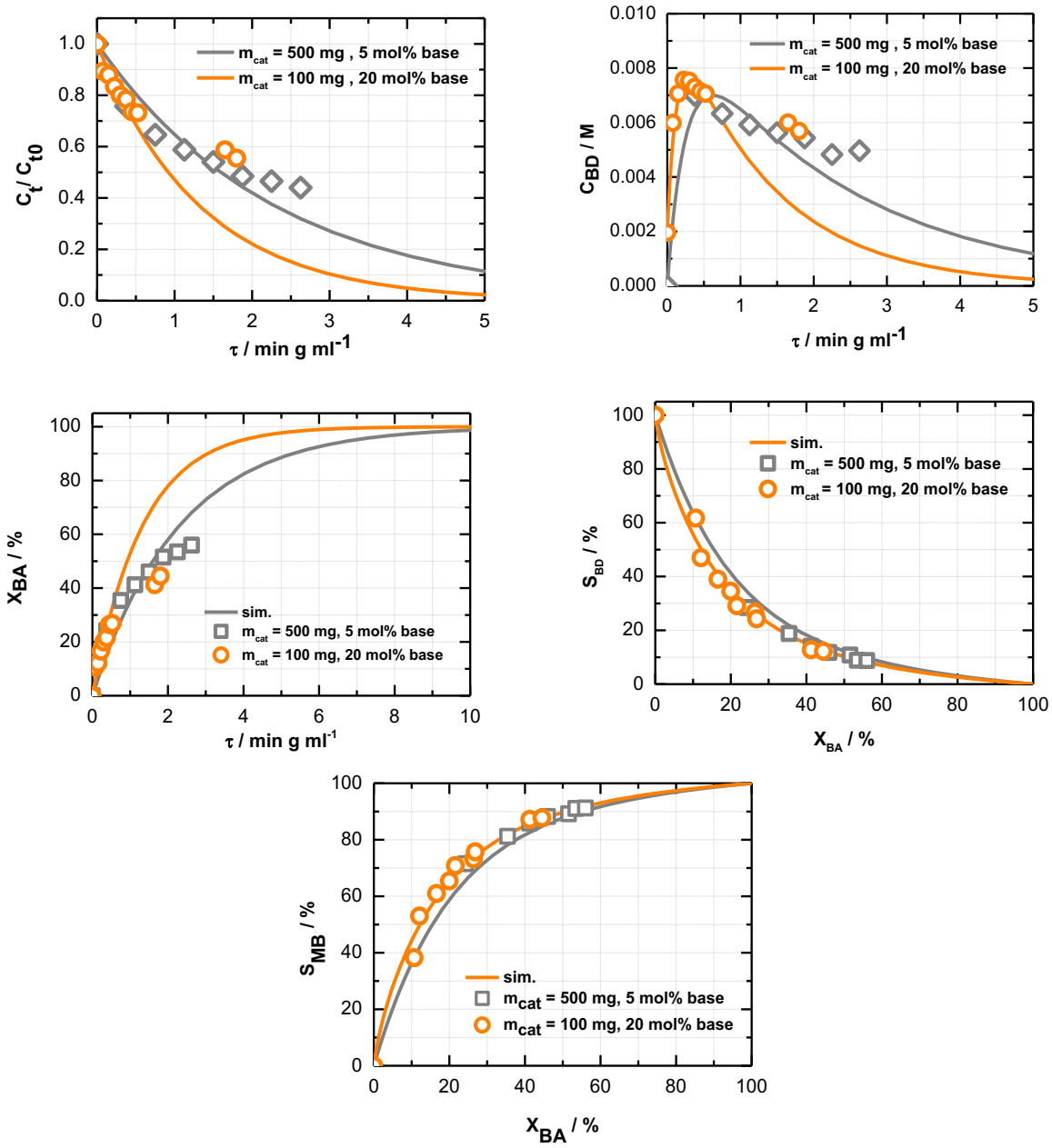

Figure 5-27 Concentration profile of oxidative esterification of benzyl alcohol using Co-N-C/AL catalyst by varying catalyst mass and base concentration. Reaction conditions: 10 mmol Benzyl alcohol, K_2CO_3: 0.5 mmol (5%) and 2 mmol (20%), 100 and 500 mg Co-N-C/AL catalyst, 80 mL methanol, F_{air}: 20 mL min^{-1}, T: 60°C, speed of stirring: 700 rpm.

From the experiment using different catalyst masses and different base concentrations, deactivation behavior may still appear, but the deviation is more pronounced with the higher base concentration (20 mol %) and lower catalyst mass (100 mg). A slight selectivity differences towards the ester product

can be seen in the degree of conversion below 60 %, in which higher base concentration (20 mol %) resulted in higher selectivity to the ester product. However, no selectivity differences can be observed at full degree of conversion in both of the base concentrations and catalyst masses variation.

To get an idea of the correlation between the catalytic activity and the base concentration which is associated with the deactivation behavior, the concentration profile of the reaction using different catalyst mass at the same base concentration was fitted as presented in Figure 5-28.

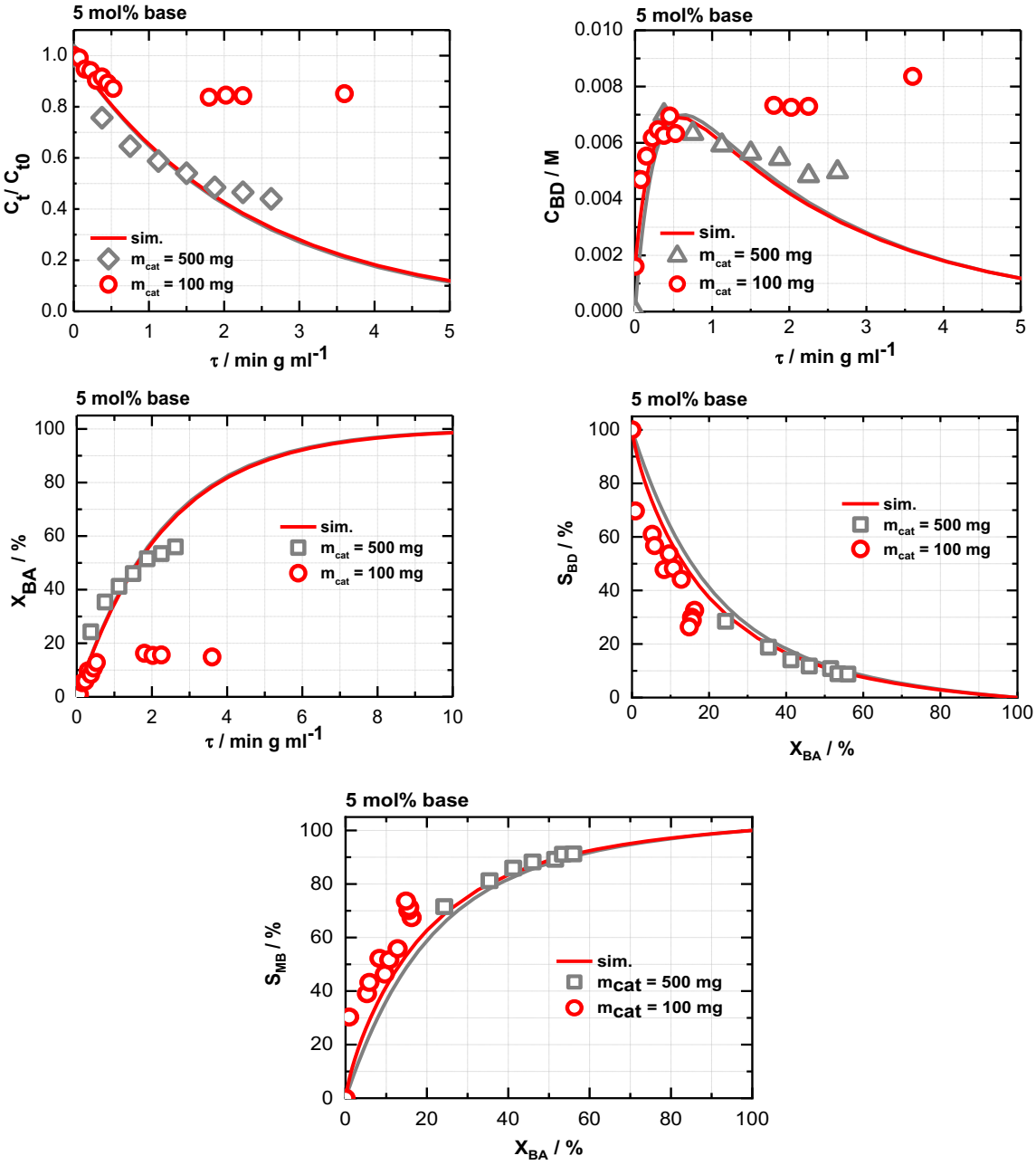

Figure 5-28 Concentration profile of oxidative esterification of benzyl alcohol using Co-N-C/AL catalyst by varying catalyst mass at 5 mol% base concentration. Reaction conditions: 10 mmol Benzyl alcohol, K_2CO_3: 0.5 mmol (5%), 100 and 500 mg Co-N-C/AL catalyst, 80 mL methanol, F_{air}: 20 mL min^{-1}, T: 60°C, speed of stirring: 700 rpm.

In a pseudo homogeneous approach under kinetic region, the reaction rate is not dependent to the catalyst mass as described earlier in section 5.3.1.1. From Figure 5-28, deactivation may still appear in the concentration profile of the reaction using a low amount of Co-N-C/AL catalyst (100 mg) under typical reaction conditions with 5 mol% base addition. The selectivity differences towards the ester product can also be seen in the degree of conversion below 60 %. The reaction using lower catalyst mass (100 mg) and base concentration of 5 mol %, thus higher ratio between base concentration and catalyst mass, results in higher selectivity to the ester product. This is in agreement with the previous finding regarding the strong dependency of the reaction rate to the base concentration. Nevertheless, the higher ratio between base concentration and catalyst mass has caused the deactivation behavior. This study gives an insight that to assess the reliable kinetic data should be done in the overlapped area where there is no influence of deactivation. To conclude, reaction using 500 mg catalyst and 5 mol % base concentration was likely to be the optimized condition with less influence of deactivation behavior and is thus suitable for kinetic studies.

6 Conclusion

Non-noble metal catalysts based on cobalt for the oxidation reaction of alcohols were investigated. A variety of catalysts were employed in the study stemming from literature routes and external collaboations. The investigated catalysts in the present study, i.e., Co-N-C, Co-N-C-PANI, Co-N-C-PXP, and Co-N-C-CoTMPP, have been prepared using different precursor materials to produce porous carbon with the attached cobalt to enhance its activity. Different synthesis parameters have shown significant influence on the catalyst properties and activity.

The physical characterization conducted using N_2 sorption has shown that the Co-N-C-PXP catalyst, which was prepared through one pot pyrolysis of a mixtured of CoTMPP and PXP ligand, has the highest BET specific surface area. Carbon-based and polymer derived carbon-based support material have a large surface area due to their microporous structure. The combination of micro-and mesoporous structure was identified only in the Co-N-C-CoTMPP/AL catalyst. Further analysis using ICP-AES showed that the Co-N-C-PANI/AL and Co-N-C-CoTMPP catalysts possess a relatively higher cobalt loading (~20-30 wt%) compared to the other Co-N-C catalysts (only ~1-3 wt%). The XRD analysis showed that Co-N-C, Co-N-C/AL, Co-N-C-PANI/AL catalysts contained crystalline cobalt, while its carbon support is amorphous. The other catalysts, i.e., Co-N-C-PXP and Co-N-C-CoTMPP, are amorphous even though its cobalt content is relatively high. From the XRD measurements, only metallic cobalt was identified in all the investigated catalysts samples. The XPS analysis has shown the atomic percentage of cobalt on the surface in the investigated Co-N-C catalysts samples is ~9-20% from its total cobalt content. The deconvoluted spectra of the Co-N-C catalyst showed formation of Co-Nx and cobalt oxide nanoparticles, while acid leaching has removed ~30% of the nitrogen content which means less Co-Nx in the Co-N-C/AL catalyst. Also, the formation of cobalt oxide can be identified in the acid-leached catalyst. Additionally, the cobalt content in the Co-N-C-PANI/AL catalyst is clearly distinguished by formation of Co-N-C (92.57 at%) and Co_3O_4 nanoparticles (7.43 at%). The TEM analysis has proven the existence of nanoparticles in all the investigated catalysts, where large particles about 100-200 nm were identified in the Co-N-C/AL catalyst. In this catalyst sample, the attached cobalt tends to form cobalt cluster, leading to the formation of large nanoparticles. Whereas in Co-N-C-PXP catalyst sample, smaller particles of ~20-50 nm are present and well dispersed on the carbon framework. Well dispersed nanoparticles with size of 20 nm were also identified in Co-N-C-CoTMPP catalyst.

The prepared Co-N-C catalyst has been tested in the oxidative esterification of benzyl alcohols using oxygen as oxidant under relatively mild conditions. A proper experimental procedure was developed to deduce kinetic data for this material. As kinetic description, a consecutive reaction from benzyl alcohol

to benzaldehyde and then methyl benzoate described with an apparent first order power law kinetics proofed to be sufficient. The kinetic data were measured in the kinetic region, where the influence of diffusion limitation can be neglected. The first reaction step was one order of magnitude slower than the subsequent reaction step to the final product. Kinetic differences of the investigated catalysts were observed, in which the polyaniline derived catalyst (Co-N-C-PANI/AL) shows the highest activity. Worth noting that Co-N-C-PANI/AL possesses the highest cobalt content which can be distinguished by formation of Co-Nx and Co_3O_4. These two forms are also present in other Co-N-C and Co-N-C/AL catalyst sample which contributes to the catalytic activity. The concentration of the active phases has a strong influence on the rate of reaction, but does not affect to the product selectivity. This was proven that all the catalyst showed more than 99 % selectivity to the ester product at full conversion.

Additionally, investigations were done to study the role of the basicity in the reaction which occurred consecutively involving K_2CO_3 as co-catalyst for the second step of the reaction. The presence of the base has catalyzed the formation of the hemiacetal from the aldehyde which is then faster converted into the ester. However, with increasing the concentration of the base leads to a faster reaction, but its increased concentration also led to deactivation behavior of the catalyst. This was confirmed by kinetic deduced from the time dependent concentration profiles which showed continuous deactivation of the catalysts used in the oxidation reaction in the kinetic region. Further investigation has been conducted which showed 5 mol % base concentration was sufficient for the reaction.

To study the catalyst deactivation behavior, initially characterization was conducted for the pristine and the used catalyst sample. The N_2 sorption measurement of Co-N-C/AL catalyst showed that the specific surface area decreases to 20 % after used. While TEM analysis of this sample shows no changes in the cobalt particle size and distribution. Further XPS measurements were conducted to analyze Co-N-C-PANI/AL and Co-N-C-CoTMPP/AL catalysts, both pristine and used samples, which shows that the polyaniline derived catalyst is more stable without any changes in the elemental surface composition. Whereas the Co-N-C-CoTMPP/AL catalyst is less stable, identified by less atomic concentration of nitrogen and a higher atomic concentration of cobalt on the surface after used, indicating a disposition of cobalt to the surface. This also proofs the importance of nitrogen content in the catalyst, which may facilitate the binding of the metal, leading to higher metal dispersion and preventing the formation of metal clusters or agglomeration.

Additionally, a low amount of base (5 mol %) was used in the reaction with different amount of catalyst loading (i.e., 100 and 500 mg). However, the kinetic results showed that catalyst deactivation still occurred in the reaction using lower catalyst mass (100 mg). It is not in agreement that the reaction rate

is independently influenced by the catalyst mass in the kinetic region. In this case, it seems that the catalyst mass was not sufficient to drive the reaction fast enough to compete with the deactivation rate. Hence, in future studies, an optimization of the base concentration needs to be done for each catalyst mass in the kinetic region. A reliable kinetic data deduced from the reaction profile in this case can be still used in the kinetic region where the reaction rate is less influenced by the deactivation rate.

7 References

[1] X. Cheng *et al.*, "Tuning metal catalysts via nitrogen-doped nanocarbons for energy chemistry: from metal nanoparticles to single metal sites," *EnergyChem*, p. 100066, 2021, doi: https://doi.org/10.1016/j.enchem.2021.100066.

[2] M. Song, Y. Song, W. Sha, B. Xu, J. Guo, and Y. Wu, "Recent Advances in Non-Precious Transition Metal/Nitrogen-doped Carbon for Oxygen Reduction Electrocatalysts in PEMFCs," *Catalysts*, vol. 10, no. 1. 2020, doi: 10.3390/catal10010141.

[3] R. V Jagadeesh, H. Junge, M.-M. Pohl, J. Radnik, A. Brückner, and M. Beller, "Selective Oxidation of Alcohols to Esters Using Heterogeneous Co3O4–N@C Catalysts under Mild Conditions," *J. Am. Chem. Soc.*, vol. 135, no. 29, pp. 10776–10782, Jul. 2013, doi: 10.1021/ja403615c.

[4] R. V Jagadeesh *et al.*, "Corrigendum: Cobalt-based nanocatalysts for green oxidation and hydrogenation processes," *Nat. Protoc.*, vol. 11, p. 192, Dec. 2015.

[5] V. Panwar, S. S. Ray, and S. L. Jain, "Highly efficient (CoOx-N@C, PANI) nanopowder derived from pyrolysis of polyaniline grafted cobalt acetate for oxidative methyl esterification of benzyl alcohols," *Mol. Catal.*, vol. 427, pp. 31–38, Feb. 2017, doi: 10.1016/J.MOLCATA.2016.11.027.

[6] Z.-Y. Wu *et al.*, "Switching Co/N/C Catalysts for Heterogeneous Catalysis and Electrocatalysis by Controllable Pyrolysis of Cobalt Porphyrin," *iScience*, vol. 15, pp. 282–290, 2019, doi: https://doi.org/10.1016/j.isci.2019.04.032.

[7] R. Sibul *et al.*, "Iron- and Nitrogen-Doped Graphene-Based Catalysts for Fuel Cell Applications," *ChemElectroChem*, vol. 7, no. 7, pp. 1739–1747, Apr. 2020, doi: https://doi.org/10.1002/celc.202000011.

[8] K. Mamtani, D. Jain, A. C. Co, and U. S. Ozkan, "Nitrogen-Coordinated Iron−Carbon as Efficient Bifunctional Electrocatalysts for the Oxygen Reduction and Oxygen Evolution Reactions in Acidic Media," *Energy & Fuels*, vol. 31, no. 6, pp. 6541–6547, Jun. 2017, doi: 10.1021/acs.energyfuels.7b00242.

[9] A. Morozan, V. Goellner, Y. Nedellec, J. Hannauer, and F. Jaouen, "Effect of the Transition Metal on Metal–Nitrogen–Carbon Catalysts for the Hydrogen Evolution Reaction," *J. Electrochem. Soc.*, vol. 162, no. 9, pp. H719–H726, 2015, doi: 10.1149/2.0051511jes.

[10] D. Karapinar *et al.*, “FeNC catalysts for CO2 electroreduction to CO: effect of nanostructured carbon supports,” *Sustain. Energy Fuels*, vol. 3, no. 7, pp. 1833–1840, 2019, doi: 10.1039/C9SE00214F.

[11] Y. Wang *et al.*, “Rational Design of Fe–N/C Hybrid for Enhanced Nitrogen Reduction Electrocatalysis under Ambient Conditions in Aqueous Solution,” *ACS Catal.*, vol. 9, no. 1, pp. 336–344, Jan. 2019, doi: 10.1021/acscatal.8b03802.

[12] S. G. Peera, J. Balamurugan, N. H. Kim, and J. H. Lee, “Sustainable Synthesis of Co@NC Core Shell Nanostructures from Metal Organic Frameworks via Mechanochemical Coordination Self-Assembly: An Efficient Electrocatalyst for Oxygen Reduction Reaction,” *Small*, vol. 14, no. 19, p. 1800441, May 2018, doi: https://doi.org/10.1002/smll.201800441.

[13] D. Yu *et al.*, “Metal-organic framework derived Co@NC/CNT hybrid as a multifunctional electrocatalyst for hydrogen and oxygen evolution reaction and oxygen reduction reaction,” *Int. J. Hydrogen Energy*, vol. 44, no. 60, pp. 32054–32065, 2019, doi: https://doi.org/10.1016/j.ijhydene.2019.10.149.

[14] F. Mao, D. Sui, Z. Qi, H. Fan, R. Chen, and J. Huang, “Heterogeneous cobalt catalysts for reductive amination with H2: general synthesis of secondary and tertiary amines,” *RSC Adv.*, vol. 6, no. 96, pp. 94068–94073, 2016, doi: 10.1039/C6RA21415K.

[15] L. Zhang *et al.*, “Co–N–C Catalyst for C–C Coupling Reactions: On the Catalytic Performance and Active Sites,” *ACS Catal.*, vol. 5, no. 11, pp. 6563–6572, Nov. 2015, doi: 10.1021/acscatal.5b01223.

[16] N. Dimitratos, J. A. Lopez-Sanchez, D. Morgan, A. Carley, L. Prati, and G. J. Hutchings, “Solvent free liquid phase oxidation of benzyl alcohol using Au supported catalysts prepared using a sol immobilization technique,” *Catal. Today*, vol. 122, no. 3, pp. 317–324, 2007, doi: 10.1016/j.cattod.2007.01.002.

[17] J. Sun *et al.*, “Mesoporous silica-based nanotubes loaded Pd nanoparticles: Effect of framework compositions on the performance in heterogeneous catalysis,” *Microporous Mesoporous Mater.*, vol. 247, pp. 1–8, 2017, doi: https://doi.org/10.1016/j.micromeso.2017.03.040.

[18] A. Villa, N. Janjic, P. Spontoni, D. Wang, D. S. Su, and L. Prati, “Au–Pd/AC as catalysts for alcohol oxidation: Effect of reaction parameters on catalytic activity and selectivity,” *Appl. Catal. A Gen.*,

vol. 364, no. 1, pp. 221–228, 2009, doi: 10.1016/j.apcata.2009.05.059.

[19] J. Hu, L. Chen, K. Zhu, A. Suchopar, and R. Richards, “Aerobic oxidation of alcohols catalyzed by gold nano-particles confined in the walls of mesoporous silica,” *Catal. Today*, vol. 122, no. 3, pp. 277–283, 2007, doi: 10.1016/j.cattod.2007.01.012.

[20] S. Tang, J. Yuan, C. Liu, and A. Lei, “Direct oxidative esterification of alcohols,” *Dalt. Trans.*, vol. 43, no. 36, pp. 13460–13470, 2014, doi: 10.1039/C4DT01133C.

[21] F. Wang, Q. Xiao, P. Han, S. Sarina, and H. Zhu, “Highly efficient self-esterification of aliphatic alcohols using supported gold nanoparticles under mild conditions,” *J. Mol. Catal. A Chem.*, 2016, doi: 10.1016/j.molcata.2016.06.010.

[22] S. Wang, Y. Yoshikawa, Z. Wang, H. Tanaka, and K. Kaneko, “Highly oxidation-resistant graphene-based porous carbon as a metal catalyst support,” *Carbon Trends*, vol. 3, p. 100029, 2021, doi: https://doi.org/10.1016/j.cartre.2021.100029.

[23] T. Mallat and A. Baiker, “Oxidation of Alcohols with Molecular Oxygen on Solid Catalysts,” *Chem. Rev.*, vol. 104, no. 6, pp. 3037–3058, Jun. 2004, doi: 10.1021/cr0200116.

[24] W. Zhong, H. Liu, C. Bai, S. Liao, and Y. Li, “Base-Free Oxidation of Alcohols to Esters at Room Temperature and Atmospheric Conditions using Nanoscale Co-Based Catalysts,” *ACS Catal.*, vol. 5, no. 3, pp. 1850–1856, Mar. 2015, doi: 10.1021/cs502101c.

[25] T. V Astrakova, A. N. Chernov, V. I. Sobiolev, and K. Y. Koltunov, “Effect of Bases on Catalytic Properties of Cobalt-Nitrogen-Carbon Composites in Oxidative Esterification of Benzyl Alcohol with Methanol,” *Russ. J. Appl. Chem.*, vol. 92, no. 2, pp. 295–299, 2019, doi: 10.1134/S1070427219020198.

[26] X. Zhao, Y. Zhou, A.-L. Jin, K. Huang, F. Liu, and D.-J. Tao, “Co-N-C catalysts synthesized by pyrolysis of Co-based deep eutectic solvents for aerobic oxidation of alcohols,” *New J. Chem.*, vol. 42, no. 19, pp. 15871–15878, 2018, doi: 10.1039/C8NJ03446J.

[27] M. Li *et al.*, “Highly efficient single atom cobalt catalyst for selective oxidation of alcohols,” *Appl. Catal. A Gen.*, vol. 543, pp. 61–66, Aug. 2017, doi: 10.1016/J.APCATA.2017.06.018.

[28] H. Su *et al.*, “Activating Cobalt Nanoparticles via the Mott–Schottky Effect in Nitrogen-Rich Carbon Shells for Base-Free Aerobic Oxidation of Alcohols to Esters,” *J. Am. Chem. Soc.*, vol. 139,

no. 2, pp. 811–818, Jan. 2017, doi: 10.1021/jacs.6b10710.

[29] Z. Shi, W. Yang, Y. Gu, T. Liao, and Z. Sun, “Metal-Nitrogen-Doped Carbon Materials as Highly Efficient Catalysts: Progress and Rational Design,” *Adv. Sci.*, vol. 7, no. 15, p. 2001069, Aug. 2020, doi: https://doi.org/10.1002/advs.202001069.

[30] F.-L. Meng, Z.-L. Wang, H.-X. Zhong, J. Wang, J.-M. Yan, and X.-B. Zhang, “Reactive Multifunctional Template-Induced Preparation of Fe-N-Doped Mesoporous Carbon Microspheres Towards Highly Efficient Electrocatalysts for Oxygen Reduction,” *Adv. Mater.*, vol. 28, no. 36, pp. 7948–7955, Sep. 2016, doi: https://doi.org/10.1002/adma.201602490.

[31] Y. Cheng *et al.*, “Atomically Dispersed Transition Metals on Carbon Nanotubes with Ultrahigh Loading for Selective Electrochemical Carbon Dioxide Reduction,” *Adv. Mater.*, vol. 30, no. 13, p. 1706287, Mar. 2018, doi: https://doi.org/10.1002/adma.201706287.

[32] X. Chen *et al.*, “Atomic Structure Modification for Electrochemical Nitrogen Reduction to Ammonia,” *Adv. Energy Mater.*, vol. 10, no. 3, p. 1903172, Jan. 2020, doi: https://doi.org/10.1002/aenm.201903172.

[33] W. Liu *et al.*, “Discriminating Catalytically Active FeNx Species of Atomically Dispersed Fe–N–C Catalyst for Selective Oxidation of the C–H Bond,” *J. Am. Chem. Soc.*, vol. 139, no. 31, pp. 10790–10798, Aug. 2017, doi: 10.1021/jacs.7b05130.

[34] Y. Han *et al.*, “Hollow N-Doped Carbon Spheres with Isolated Cobalt Single Atomic Sites: Superior Electrocatalysts for Oxygen Reduction,” *J. Am. Chem. Soc.*, vol. 139, no. 48, pp. 17269–17272, Dec. 2017, doi: 10.1021/jacs.7b10194.

[35] L. Tao *et al.*, “Charge Transfer Modulated Activity of Carbon-Based Electrocatalysts,” *Adv. Energy Mater.*, vol. 10, no. 11, p. 1901227, Mar. 2020, doi: https://doi.org/10.1002/aenm.201901227.

[36] H. Fei *et al.*, “General synthesis and definitive structural identification of MN4C4 single-atom catalysts with tunable electrocatalytic activities,” *Nat. Catal.*, vol. 1, no. 1, pp. 63–72, 2018, doi: 10.1038/s41929-017-0008-y.

[37] Z. Wang *et al.*, “Fe, Cu-Coordinated ZIF-Derived Carbon Framework for Efficient Oxygen Reduction Reaction and Zinc–Air Batteries,” *Adv. Funct. Mater.*, vol. 28, no. 39, p. 1802596, Sep. 2018, doi: https://doi.org/10.1002/adfm.201802596.

[38] C. Tang, B. Wang, H.-F. Wang, and Q. Zhang, “Defect Engineering toward Atomic Co–Nx–C in Hierarchical Graphene for Rechargeable Flexible Solid Zn-Air Batteries,” *Adv. Mater.*, vol. 29, no. 37, p. 1703185, Oct. 2017, doi: https://doi.org/10.1002/adma.201703185.

[39] Y. Pan *et al.*, “Design of Single-Atom Co–N5 Catalytic Site: A Robust Electrocatalyst for CO2 Reduction with Nearly 100% CO Selectivity and Remarkable Stability,” *J. Am. Chem. Soc.*, vol. 140, no. 12, pp. 4218–4221, Mar. 2018, doi: 10.1021/jacs.8b00814.

[40] X. Cui *et al.*, “Pyridinic-Nitrogen-Dominated Graphene Aerogels with Fe–N–C Coordination for Highly Efficient Oxygen Reduction Reaction,” *Adv. Funct. Mater.*, vol. 26, no. 31, pp. 5708–5717, Aug. 2016, doi: https://doi.org/10.1002/adfm.201601492.

[41] S. Yasuda, A. Furuya, Y. Uchibori, J. Kim, and K. Murakoshi, “Iron–Nitrogen-Doped Vertically Aligned Carbon Nanotube Electrocatalyst for the Oxygen Reduction Reaction,” *Adv. Funct. Mater.*, vol. 26, no. 5, pp. 738–744, Feb. 2016, doi: https://doi.org/10.1002/adfm.201503613.

[42] G. Wu, K. L. More, C. M. Johnston, and P. Zelenay, “High-Performance Electrocatalysts for Oxygen Reduction Derived from Polyaniline, Iron, and Cobalt,” *Science (80-.).*, vol. 332, no. 6028, pp. 443 LP – 447, Apr. 2011, doi: 10.1126/science.1200832.

[43] L. Lin, Q. Zhu, and A.-W. Xu, “Noble-Metal-Free Fe–N/C Catalyst for Highly Efficient Oxygen Reduction Reaction under Both Alkaline and Acidic Conditions,” *J. Am. Chem. Soc.*, vol. 136, no. 31, pp. 11027–11033, Aug. 2014, doi: 10.1021/ja504696r.

[44] R. Sibul *et al.*, “Iron- and Nitrogen-Doped Graphene-Based Catalysts for Fuel Cell Applications,” *ChemElectroChem*, vol. 7, no. 7, pp. 1739–1747, Apr. 2020, doi: https://doi.org/10.1002/celc.202000011.

[45] H. Zhang *et al.*, “High-performance fuel cell cathodes exclusively containing atomically dispersed iron active sites,” *Energy Environ. Sci.*, vol. 12, no. 8, pp. 2548–2558, 2019, doi: 10.1039/C9EE00877B.

[46] S. Gonen and L. Elbaz, “Comparison of new metal organic framework-based catalysts for oxygen reduction reaction,” *Data Br.*, vol. 19, pp. 281–287, 2018, doi: https://doi.org/10.1016/j.dib.2018.05.011.

[47] P. Su *et al.*, “Nitrogen-doped carbon nanotubes derived from Zn–Fe-ZIF nanospheres and their

application as efficient oxygen reduction electrocatalysts with in situ generated iron species," *Chem. Sci.*, vol. 4, no. 7, pp. 2941–2946, 2013, doi: 10.1039/C3SC51052B.

[48] S. Rösler, J. Obenauf, and R. Kempe, "A Highly Active and Easily Accessible Cobalt Catalyst for Selective Hydrogenation of C═O Bonds," *J. Am. Chem. Soc.*, vol. 137, no. 25, pp. 7998–8001, Jul. 2015, doi: 10.1021/jacs.5b04349.

[49] T. Stemmler *et al.*, "Design of N-doped graphene-coated cobalt-based nanoparticles supported on ceria," *J. Mater. Chem. A*, vol. 3, no. 34, pp. 17728–17737, 2015, doi: 10.1039/C5TA02745D.

[50] L. Fu, Y. Chen, and Z. Liu, "Cobalt catalysts embedded in N-doped carbon derived from cobalt porphyrin via a one-pot method for ethylbenzene oxidation," *J. Mol. Catal. A Chem.*, vol. 408, Jul. 2015, doi: 10.1016/j.molcata.2015.07.011.

[51] R. Nie, J. Shi, W. Du, W. Ning, Z. Hou, and F.-S. Xiao, "A sandwich N-doped graphene/Co3O4 hybrid: an efficient catalyst for selective oxidation of olefins and alcohols," *J. Mater. Chem. A*, vol. 1, no. 32, pp. 9037–9045, 2013, doi: 10.1039/C3TA11672G.

[52] S. Pisiewicz, T. Stemmler, A.-E. Surkus, K. Junge, and M. Beller, "Synthesis of Amines by Reductive Amination of Aldehydes and Ketones using Co3O4/NGr@C Catalyst," *ChemCatChem*, vol. 7, no. 1, pp. 62–64, Jan. 2015, doi: https://doi.org/10.1002/cctc.201402527.

[53] T. Stemmler, F. A. Westerhaus, A.-E. Surkus, M.-M. Pohl, K. Junge, and M. Beller, "General and selective reductive amination of carbonyl compounds using a core–shell structured Co3O4/NGr@C catalyst," *Green Chem.*, vol. 16, no. 10, pp. 4535–4540, 2014, doi: 10.1039/C4GC00536H.

[54] Y. Chen, S. Jie, C. Yang, and Z. Liu, "Active and efficient Co-N/C catalysts derived from cobalt porphyrin for selective oxidation of alkylaromatics," *Appl. Surf. Sci.*, vol. 419, pp. 98–106, Oct. 2017, doi: 10.1016/J.APSUSC.2017.04.246.

[55] J. Zhu, K. Kailasam, A. Fischer, and A. Thomas, "Supported Cobalt Oxide Nanoparticles As Catalyst for Aerobic Oxidation of Alcohols in Liquid Phase," *ACS Catal.*, vol. 1, no. 4, pp. 342–347, Apr. 2011, doi: 10.1021/cs100153a.

[56] T. Cheng, H. Yu, F. Peng, H. Wang, B. Zhang, and D. Su, "Identifying active sites of CoNC/CNT from pyrolysis of molecularly defined complexes for oxidative esterification and hydrogenation

reactions," *Catal. Sci. Technol.*, vol. 6, no. 4, pp. 1007–1015, 2016, doi: 10.1039/C5CY01349F.

[57] Y. Fu, W. Zhan, Y. Guo, Y. Guo, Y. Wang, and G. Lu, "Highly efficient cobalt-doped carbon nitride polymers for solvent-free selective oxidation of cyclohexane," *Green Energy Environ.*, vol. 2, no. 2, pp. 142–150, 2017, doi: https://doi.org/10.1016/j.gee.2017.01.006.

[58] X. Li, C. Zeng, J. Jiang, and L. Ai, "Magnetic cobalt nanoparticles embedded in hierarchically porous nitrogen-doped carbon frameworks for highly efficient and well-recyclable catalysis," *J. Mater. Chem. A*, vol. 4, no. 19, pp. 7476–7482, 2016, doi: 10.1039/C6TA01054G.

[59] J. Zhu, J. L. Faria, J. L. Figueiredo, and A. Thomas, "Reaction Mechanism of Aerobic Oxidation of Alcohols Conducted on Activated-Carbon-Supported Cobalt Oxide Catalysts," *Chem. – A Eur. J.*, vol. 17, no. 25, pp. 7112–7117, Jun. 2011, doi: https://doi.org/10.1002/chem.201003025.

[60] C. Bai, A. Li, X. Yao, H. Liu, and Y. Li, "Efficient and selective aerobic oxidation of alcohols catalysed by MOF-derived Co catalysts," *Green Chem.*, vol. 18, no. 4, pp. 1061–1069, 2016, doi: 10.1039/C5GC02082D.

[61] G. Xiang, X. Wang, L. Zhang, and Z. Liu, "Influence of doping nitrogen on the catalytic performance of carbon nanotubes encapsulating cobalt for selective oxidation of arylalkanes," *Particuology*, vol. 58, pp. 85–91, 2021, doi: https://doi.org/10.1016/j.partic.2021.02.002.

[62] R. JASINSKI, "A New Fuel Cell Cathode Catalyst," *Nature*, vol. 201, no. 4925, pp. 1212–1213, 1964, doi: 10.1038/2011212a0.

[63] B. Chi, X. Zhang, M. Liu, S. Jiang, and S. Liao, "Applications of M/N/C analogue catalysts in PEM fuel cells and metal-air/oxygen batteries: Status quo, challenges and perspectives," *Prog. Nat. Sci. Mater. Int.*, vol. 30, no. 6, pp. 807–814, 2020, doi: https://doi.org/10.1016/j.pnsc.2020.10.014.

[64] M. Liu, Z. Zhao, X. Duan, and Y. Huang, "Nanoscale Structure Design for High-Performance Pt-Based ORR Catalysts," *Adv. Mater.*, vol. 31, no. 6, p. 1802234, Feb. 2019, doi: https://doi.org/10.1002/adma.201802234.

[65] Z. W. Seh, J. Kibsgaard, C. F. Dickens, I. Chorkendorff, J. K. Nørskov, and T. F. Jaramillo, "Combining theory and experiment in electrocatalysis: Insights into materials design," *Science (80-.).*, vol. 355, no. 6321, p. eaad4998, Jan. 2017, doi: 10.1126/science.aad4998.

[66] X. Zou and Y. Zhang, "Noble metal-free hydrogen evolution catalysts for water splitting," *Chem.*

Soc. Rev., vol. 44, no. 15, pp. 5148–5180, 2015, doi: 10.1039/C4CS00448E.

[67] K. Singh, F. Razmjooei, and J.-S. Yu, "Active sites and factors influencing them for efficient oxygen reduction reaction in metal-N coordinated pyrolyzed and non-pyrolyzed catalysts: a review," *J. Mater. Chem. A*, vol. 5, no. 38, pp. 20095–20119, 2017, doi: 10.1039/C7TA05222G.

[68] S. Xu, Y. Kim, D. Higgins, M. Yusuf, T. F. Jaramillo, and F. B. Prinz, "Building upon the Koutecky-Levich Equation for Evaluation of Next-Generation Oxygen Reduction Reaction Catalysts," *Electrochim. Acta*, vol. 255, pp. 99–108, 2017, doi: https://doi.org/10.1016/j.electacta.2017.09.145.

[69] X. Yan *et al.*, "Large specific surface area S-doped Fe–N–C electrocatalysts derived from Metal–Organic frameworks for oxygen reduction reaction," *Prog. Nat. Sci. Mater. Int.*, vol. 30, no. 6, pp. 896–904, 2020, doi: https://doi.org/10.1016/j.pnsc.2020.10.018.

[70] Y. Ma *et al.*, "Cobalt based non-precious electrocatalysts for oxygen reduction reaction in proton exchange membrane fuel cells," *Electrochim. Acta*, vol. 55, no. 27, pp. 7945–7950, 2010, doi: https://doi.org/10.1016/j.electacta.2010.03.087.

[71] H.-W. Liang, W. Wei, Z.-S. Wu, X. Feng, and K. Müllen, "Mesoporous Metal–Nitrogen-Doped Carbon Electrocatalysts for Highly Efficient Oxygen Reduction Reaction," *J. Am. Chem. Soc.*, vol. 135, no. 43, pp. 16002–16005, Oct. 2013, doi: 10.1021/ja407552k.

[72] B. You, N. Jiang, M. Sheng, W. S. Drisdell, J. Yano, and Y. Sun, "Bimetal–Organic Framework Self-Adjusted Synthesis of Support-Free Nonprecious Electrocatalysts for Efficient Oxygen Reduction," *ACS Catal.*, vol. 5, no. 12, pp. 7068–7076, Dec. 2015, doi: 10.1021/acscatal.5b02325.

[73] J. Meng, H. Lei, X. Li, J. Qi, W. Zhang, and R. Cao, "Attaching Cobalt Corroles onto Carbon Nanotubes: Verification of Four-Electron Oxygen Reduction by Mononuclear Cobalt Complexes with Significantly Improved Efficiency," *ACS Catal.*, vol. 9, no. 5, pp. 4551–4560, May 2019, doi: 10.1021/acscatal.9b00213.

[74] X. X. Wang *et al.*, "Nitrogen-Coordinated Single Cobalt Atom Catalysts for Oxygen Reduction in Proton Exchange Membrane Fuel Cells," *Adv. Mater.*, vol. 30, no. 11, p. 1706758, Mar. 2018, doi: https://doi.org/10.1002/adma.201706758.

[75] Y. He *et al.*, "Highly active atomically dispersed CoN4 fuel cell cathode catalysts derived from

surfactant-assisted MOFs: carbon-shell confinement strategy," *Energy Environ. Sci.*, vol. 12, no. 1, pp. 250–260, 2019, doi: 10.1039/C8EE02694G.

[76] Q. Cheng *et al.*, "Single Cobalt Atom and N Codoped Carbon Nanofibers as Highly Durable Electrocatalyst for Oxygen Reduction Reaction," *ACS Catal.*, vol. 7, no. 10, pp. 6864–6871, Oct. 2017, doi: 10.1021/acscatal.7b02326.

[77] R. Wang *et al.*, "MOF@Cellulose Derived Co–N–C Nanowire Network as an Advanced Reversible Oxygen Electrocatalyst for Rechargeable Zinc–Air Batteries," *ACS Appl. Energy Mater.*, vol. 1, no. 3, pp. 1060–1068, Mar. 2018, doi: 10.1021/acsaem.7b00204.

[78] Y. Zheng *et al.*, "Molecule-Level g-C3N4 Coordinated Transition Metals as a New Class of Electrocatalysts for Oxygen Electrode Reactions," *J. Am. Chem. Soc.*, vol. 139, no. 9, pp. 3336–3339, Mar. 2017, doi: 10.1021/jacs.6b13100.

[79] B. Ni, C. Ouyang, X. Xu, J. Zhuang, and X. Wang, "Modifying Commercial Carbon with Trace Amounts of ZIF to Prepare Derivatives with Superior ORR Activities," *Adv. Mater.*, vol. 29, no. 27, p. 1701354, Jul. 2017, doi: https://doi.org/10.1002/adma.201701354.

[80] B. Y. Guan, L. Yu, and X. W. (David) Lou, "Formation of Single-Holed Cobalt/N-Doped Carbon Hollow Particles with Enhanced Electrocatalytic Activity toward Oxygen Reduction Reaction in Alkaline Media," *Adv. Sci.*, vol. 4, no. 10, p. 1700247, Oct. 2017, doi: https://doi.org/10.1002/advs.201700247.

[81] T. Wang *et al.*, "2D Dual-Metal Zeolitic-Imidazolate-Framework-(ZIF)-Derived Bifunctional Air Electrodes with Ultrahigh Electrochemical Properties for Rechargeable Zinc–Air Batteries," *Adv. Funct. Mater.*, vol. 28, no. 5, p. 1705048, Jan. 2018, doi: https://doi.org/10.1002/adfm.201705048.

[82] X. Zhu *et al.*, "N,P co-coordinated Fe species embedded in carbon hollow spheres for oxygen electrocatalysis," *J. Mater. Chem. A*, vol. 7, no. 24, pp. 14732–14742, 2019, doi: 10.1039/C9TA03011E.

[83] Y.-W. Yang and B.-Y. Song, "Integrated Three-Dimensional Carbon Nanopolyhedron/Metal Sulfides: An Efficient Electrocatalyst Toward Oxygen Reduction Reaction," *Frontiers in Energy Research*, vol. 9. 2021.

[84] Y.-X. Zhou, Y.-Z. Chen, L. Cao, J. Lu, and H.-L. Jiang, “Conversion of a metal–organic framework to N-doped porous carbon incorporating Co and CoO nanoparticles: direct oxidation of alcohols to esters,” *Chem. Commun.*, vol. 51, no. 39, pp. 8292–8295, 2015, doi: 10.1039/C5CC01588J.

[85] M. Cordoba *et al.*, “Catalytic Performance of Co3O4 on Different Activated Carbon Supports in the Benzyl Alcohol Oxidation,” *Catalysts*, vol. 7, no. 12. 2017, doi: 10.3390/catal7120384.

[86] S. Gowrisankar, H. Neumann, and M. Beller, “General and Selective Palladium-Catalyzed Oxidative Esterification of Alcohols,” *Angew. Chemie Int. Ed.*, vol. 50, no. 22, pp. 5139–5143, May 2011, doi: https://doi.org/10.1002/anie.201008035.

[87] S. E. Davis, M. S. Ide, and R. J. Davis, “Selective oxidation of alcohols and aldehydes over supported metal nanoparticles,” *Green Chem.*, vol. 15, no. 1, pp. 17–45, 2013, doi: 10.1039/C2GC36441G.

[88] J. Jiang *et al.*, “Facile synthesis of a highly efficient Co/Cu@NC catalyst for base-free oxidation of alcohols to esters,” *New J. Chem.*, vol. 44, no. 19, pp. 7780–7785, 2020, doi: 10.1039/D0NJ00172D.

[89] X. Liu, S. Cheng, J. Long, W. Zhang, X. Liu, and D. Wei, “MOFs-Derived Co@CN bi-functional catalysts for selective transfer hydrogenation of α,β-unsaturated aldehydes without use of base additives,” *Mater. Chem. Front.*, vol. 1, no. 10, pp. 2005–2012, 2017, doi: 10.1039/C7QM00189D.

[90] J. Long, K. Shen, L. Chen, and Y. Li, “Multimetal-MOF-derived transition metal alloy NPs embedded in an N-doped carbon matrix: highly active catalysts for hydrogenation reactions,” *J. Mater. Chem. A*, vol. 4, no. 26, pp. 10254–10262, 2016, doi: 10.1039/C6TA00157B.

[91] D. Liu *et al.*, “Direct reductive coupling of nitroarenes and alcohols catalysed by Co–N–C/CNT@AC,” *Green Chem.*, vol. 21, no. 8, pp. 2129–2137, 2019, doi: 10.1039/C8GC03818J.

[92] C. R. Wilke and P. Chang, “Correlation of diffusion coefficients in dilute solutions,” *AIChE J.*, vol. 1, no. 2, pp. 264–270, Jun. 1955, doi: https://doi.org/10.1002/aic.690010222.

[93] K. A. Cychosz and M. Thommes, “Progress in the Physisorption Characterization of Nanoporous Gas Storage Materials,” *Engineering*, vol. 4, no. 4, pp. 559–566, 2018, doi: https://doi.org/10.1016/j.eng.2018.06.001.

[94] M. Thommes *et al.*, “Physisorption of gases, with special reference to the evaluation of surface

area and pore size distribution (IUPAC Technical Report)," *Pure Appl. Chem.*, vol. 87, no. 9–10, pp. 1051–1069, 2015, doi: doi:10.1515/pac-2014-1117.

[95] H. Liu, M.-Q. Wang, Z.-Y. Chen, H. Chen, M.-W. Xu, and S.-J. Bao, "Design and synthesis of Co–N–C porous catalyst derived from metal organic complexes for highly effective ORR," *Dalt. Trans.*, vol. 46, no. 45, pp. 15646–15650, 2017, doi: 10.1039/C7DT03279J.

[96] Y. Li, S. Jie, K. Li, and Z. Liu, "Synthesis of efficient Co and N co-doped carbon catalysts with high surface areas for selective oxidation of ethylbenzene," *New J. Chem.*, vol. 42, no. 15, pp. 12677–12683, 2018, doi: 10.1039/C8NJ01402G.

[97] J. Zhang *et al.*, "Nitrogen-self-doped carbon with a porous graphene-like structure as a highly efficient catalyst for oxygen reduction," *J. Mater. Chem. A*, vol. 3, no. 20, pp. 10851–10857, 2015, doi: 10.1039/C5TA00547G.

[98] J. Li *et al.*, "Cobalt Single Atoms Embedded in Nitrogen-Doped Graphene for Selective Oxidation of Benzyl Alcohol by Activated Peroxymonosulfate," *Small*, vol. 17, no. 16, p. 2004579, Apr. 2021, doi: https://doi.org/10.1002/smll.202004579.

[99] A. V Naumkin, A. Kraust-Vass, S. W. Gaarenstroom, and C. J. Powell, "NIST X-ray Photoelectron Spectroscopy Database, National Institute of Standards and Technology," *NIST Standard Reference Database Number 20*, 2000. .

[100] H. S. Fogler, "Elements of Chemical Reaction Engineering Third Edition," *Elem. Chem. React. Eng.*, 1999, doi: 10.1016/0009-2509(87)80130-6.

[101] F. Brühne and E. Wright, "Benzyl Alcohol," *Ullmann's Encyclopedia of Industrial Chemistry*. Jun. 15, 2000, doi: https://doi.org/10.1002/14356007.a04_001.

[102] M. Zhang, M. Wang, B. Xu, and D. Ma, "How to Measure the Reaction Performance of Heterogeneous Catalytic Reactions Reliably," *Joule*, vol. 3, no. 12, pp. 2876–2883, 2019, doi: https://doi.org/10.1016/j.joule.2019.11.005.

[103] G. V. Smith and F. Notheisz, *Heterogeneous Catalysis in Organic Chemistry*. San Diego, CA, U.S.A: Academic Press, 1999.

[104] J. Clayden, N. Geeves, and S. Warren, *Organic Chemistry*. 2012.

8 Appendix

8.1 Calibration of reaction components in the gas chromatography (GC) analysis

8.1.1 Calibration of benzyl alcohol

Compound	Retention time	GC Area					
		Std 1	Std 2	Std 3	Std 4	Std 5	Std 6
MeOH	2.803	28259576	28229877	27781834	27099168	26751770	27027516
Hexadecane	10.098	514870	534449	487594	486414	556716	515681
Benzyl alcohol	13.602	961130	1919373	2902277	3848671	4840335	5558691

Standard	C_{BA} (mg/ml)	C_{BA} (mmol/ml)	C_{IS} (mg/ml)	C_{IS} (mmol/ml)	Cx/Cis	Ax	Ais	Ax/Ais
1	10	0.0925	5	0.0221	4.1881	961130	514870	1.8667
2	20	0.1849	5	0.0221	8.3762	1919373	534449	3.5913
3	30	0.2774	5	0.0221	12.5643	2902277	487594	5.9522
4	40	0.3699	5	0.0221	16.7524	3848671	486414	7.9123
5	50	0.4624	5	0.0221	20.9404	4840335	556716	8.6944
6	60	0.5548	5	0.0221	25.1285	5558691	515681	10.7793

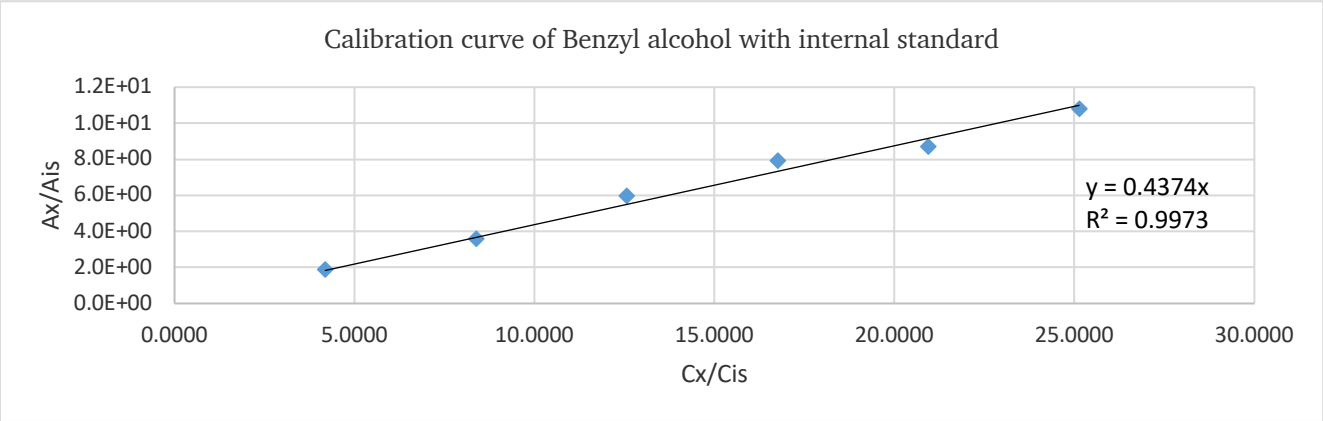

8.1.2 Calibration of benzaldehyde

Compound	RT	GC Area				
		Std 1	Std 2	Std 3	Std 4	Std 5
MeOH	2.803	27274916	28315420	27266491	26848348	26875534
Hexadecane	10.097	619952	561904	503911	556236	527839
Benzaldehyde	9.56	798922	1618111	2279407	2914611	3419165

Standard	C_{BD} (mg/ml)	C_{BD} (mmol/ml)	C_{IS} (mg/ml)	C_{IS} (mmol/ml)	Cx/Cis	Ax	Ais	Ax/Ais
1	10	0.0942	5	0.0221	4.2678	798922	619952	1.2887
2	20	0.1885	5	0.0221	8.5355	1618111	561904	2.8797
3	30	0.2827	5	0.0221	12.8033	2279407	503911	4.5234
4	40	0.3769	5	0.0221	17.0711	2914611	556236	5.2399
5	50	0.4712	5	0.0221	21.3388	3419165	527839	6.4777

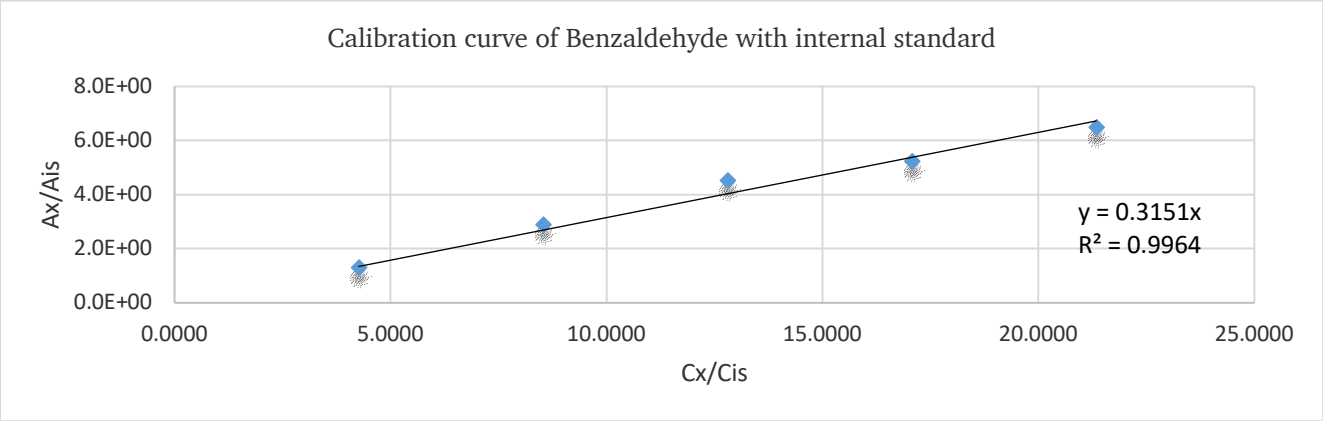

8.1.3 Calibration of methyl benzoate

Compound	RT	GC Area					
		Std 1	Std 2	Std 3	Std 4	Std 5	Std 6
MeOH	2.803	28465379	27898266	27844253	27557882	27189463	26635431
Hexadecane	10.109	602567	565716	561218	584983	589387	557653
Methyl benzoate	10.752	763268	1586007	2412846	3209187	3939598	4712635

Standard	C_{MB} (mg/ml)	C_{MB} (mmol/ml)	C_{IS} (mg/ml)	C_{IS} (mmol/ml)	Cx/Cis	Ax	Ais	Ax/Ais
1	10	0.0734	5	0.0221	3.3265	763268	602567	1.2667
2	20	0.1469	5	0.0221	6.6530	1586007	565716	2.8035
3	30	0.2203	5	0.0221	9.9794	2412846	561218	4.2993
4	40	0.2938	5	0.0221	13.3059	3209187	584983	5.4859
5	50	0.3672	5	0.0221	16.6324	3939598	589387	6.6842
6	60	0.4407	5	0.0221	19.9589	4712635	557653	8.4508

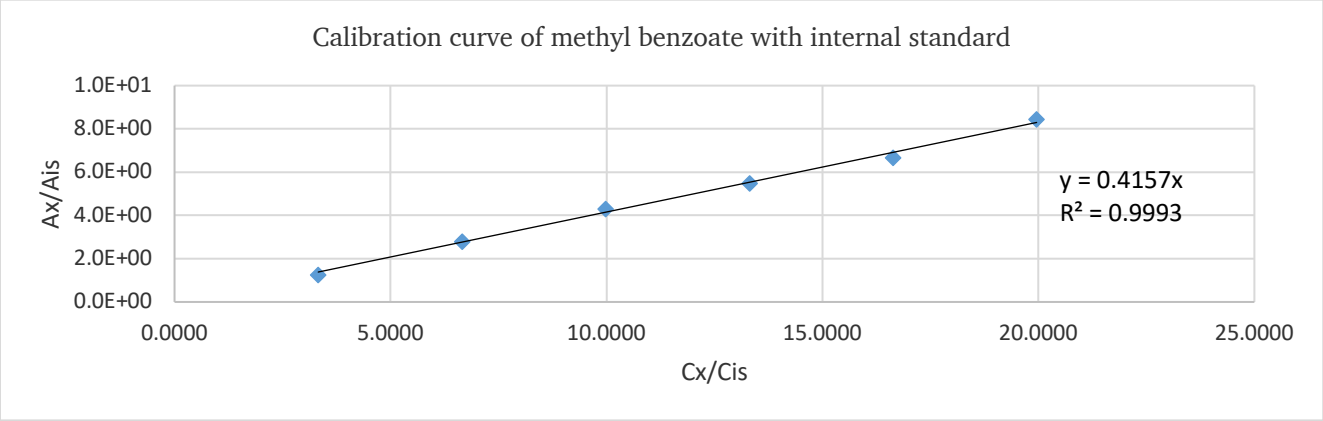

8.1.4 Calibration of benzyl benzoate

Compound	RT	GC Area					
		Std 1	Std 2	Std 3	Std 4	Std 5	Std 6
MeOH	2.802	28624261	28490144	28030802	27695024	27469714	36325702
Hexadecane	10.101	587034	489884	501344	476196	501344	665870
Benzyl benzoate	21.71	837204	1762950	2754744	3482004	4527745	6888409

Standard	C_{BB} (mg/ml)	C_{BB} (mmol/ml)	C_{IS} (mg/ml)	C_{IS} (mmol/ml)	Cx/Cis	Ax	Ais	Ax/Ais
1	10	0.0471	5	0.0221	2.1338	837204	587034	1.4262
2	20	0.0942	5	0.0221	4.2676	1762950	489884	3.5987
3	30	0.1413	5	0.0221	6.4014	2754744	501344	5.4947
4	40	0.1885	5	0.0221	8.5352	3482004	476196	7.3121
5	50	0.2356	5	0.0221	10.6690	4527745	501344	9.0312
6	60	0.2827	5	0.0221	12.8028	6888409	665870	10.3450

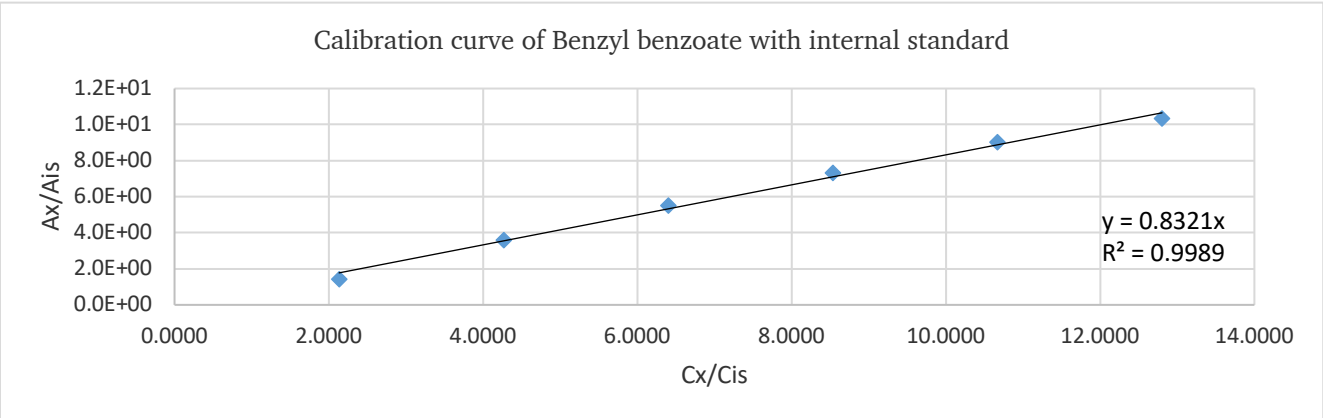

8.2 The XPS wide spectrum of the investigated catalysts

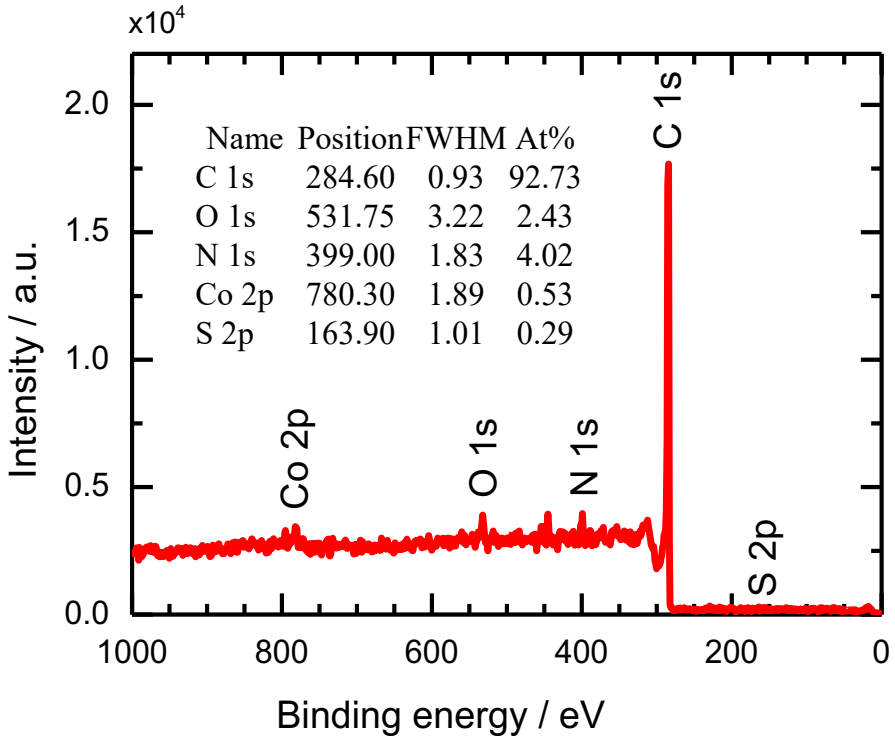

Figure 8-1 XPS spectra of Co-N-C catalyst

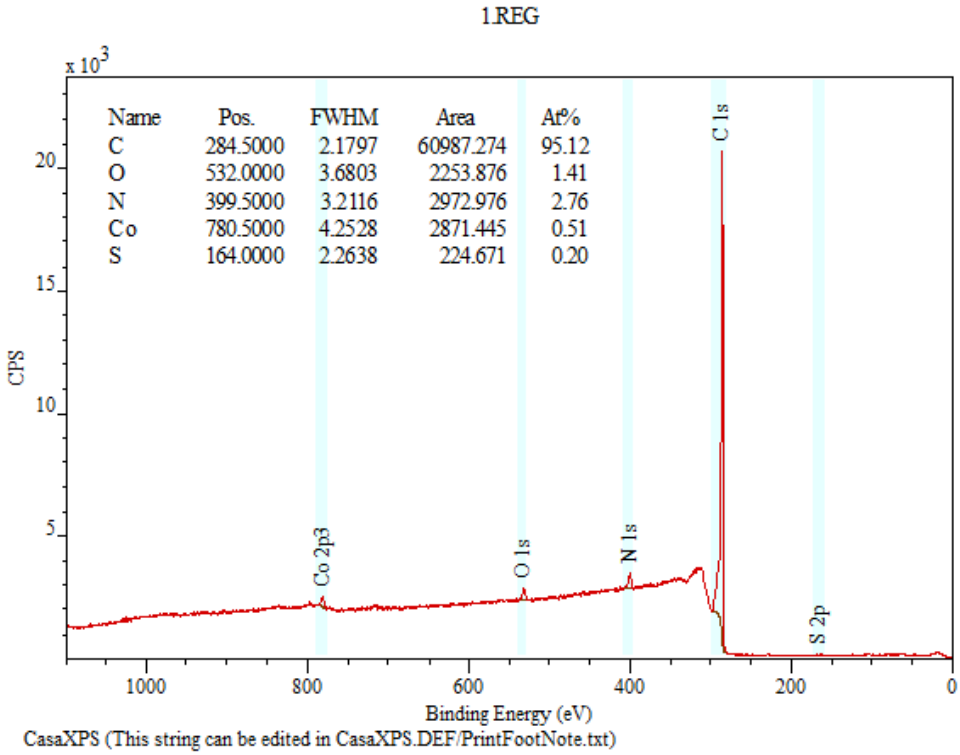

Figure 8-2 XPS spectra of Co-N-C/AL catalyst

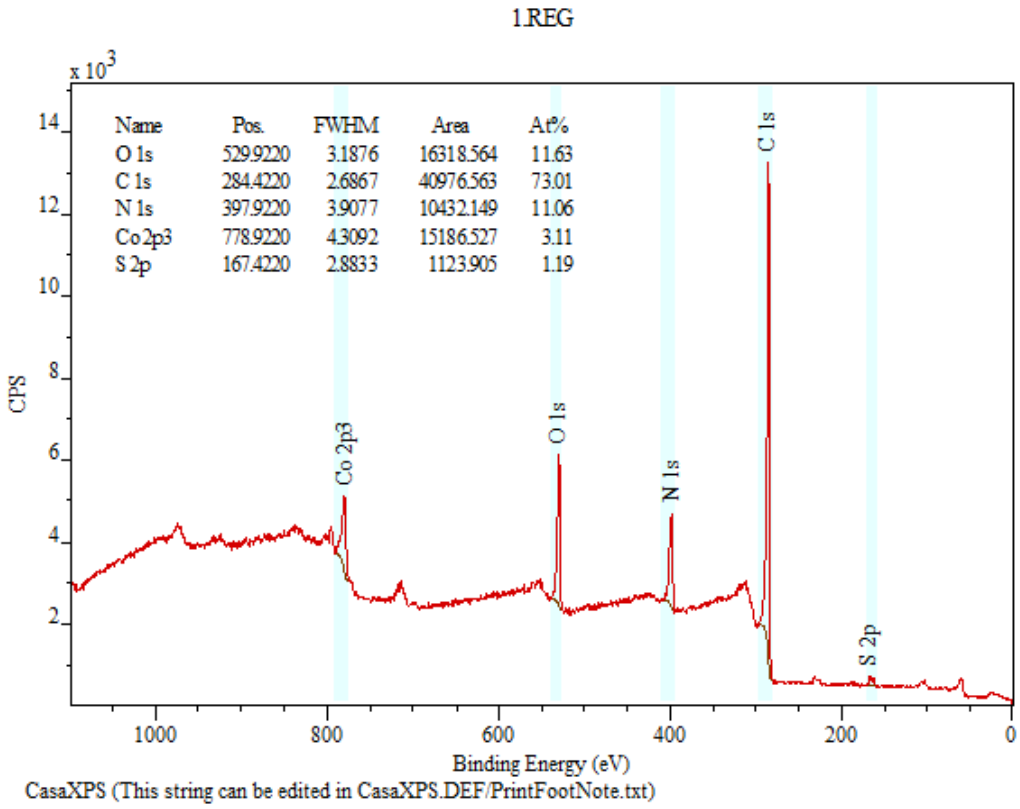

Figure 8-3 XPS spectra of Co-N-C-PANI/AL catalyst

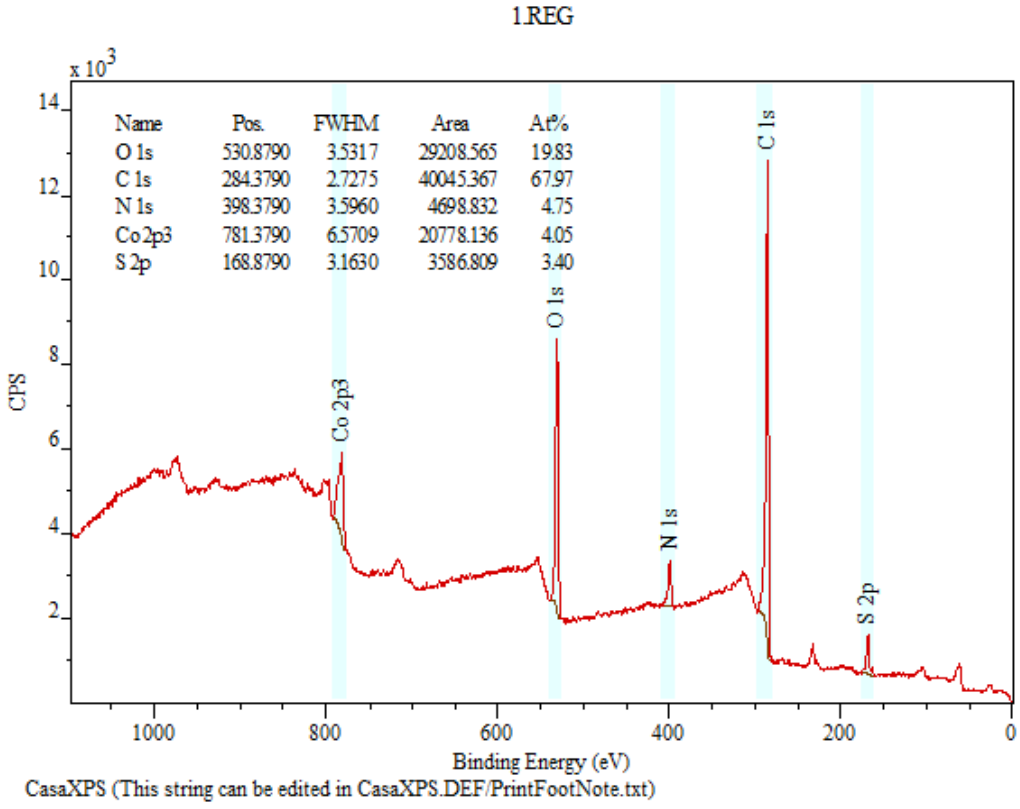

Figure 8-4 XPS spectra of Co-N-C-CoTMPP/AL catalyst

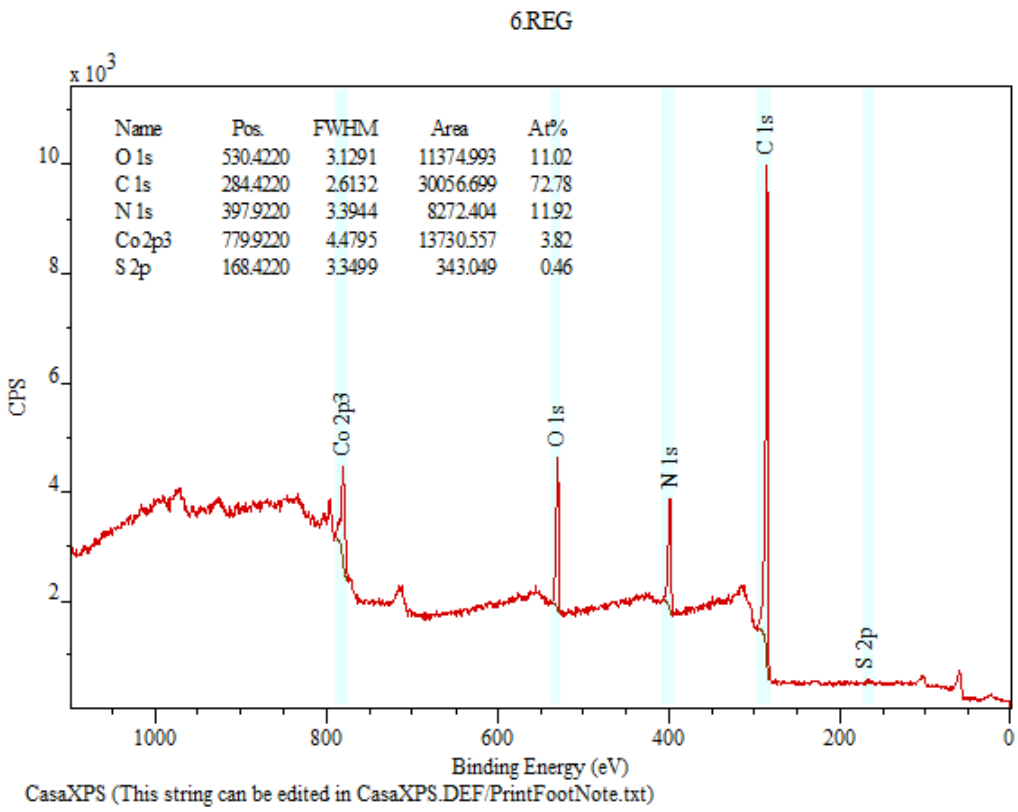

Figure 8-5 XPS spectra of Co-N-C-PANI/AL used catalyst

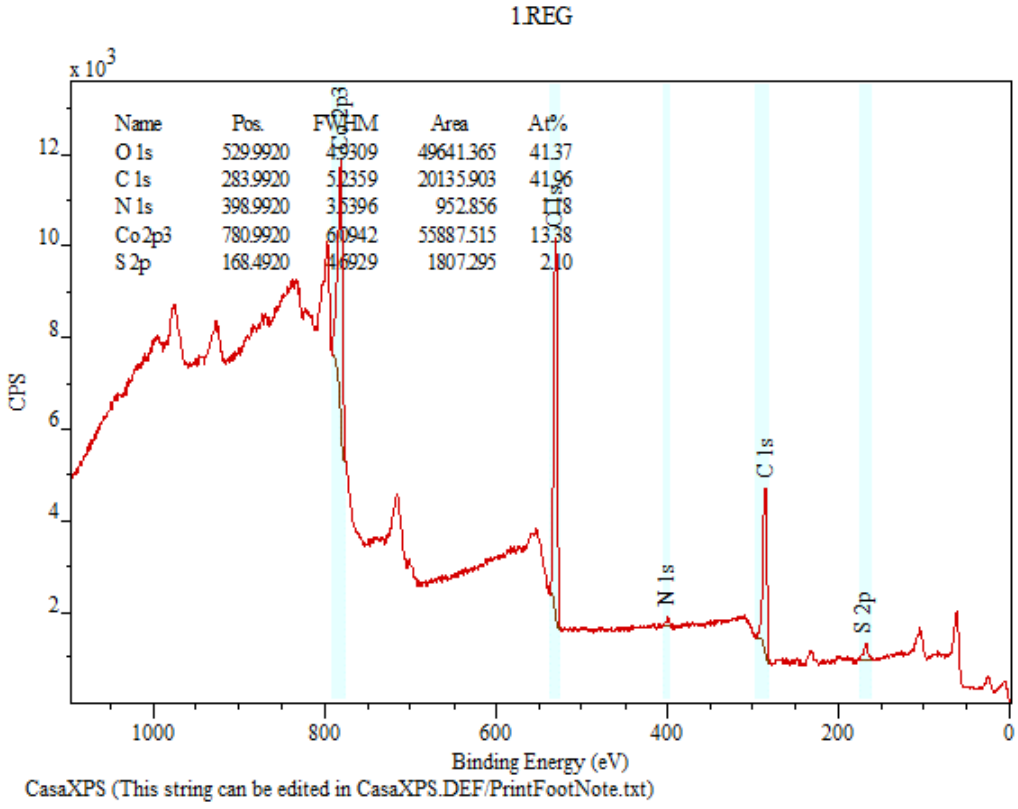

Figure 8-6 XPS spectra of Co-N-C-CoTMPP used catalyst

8.3 Deconvolution XPS spectra of Co-N-C/AL

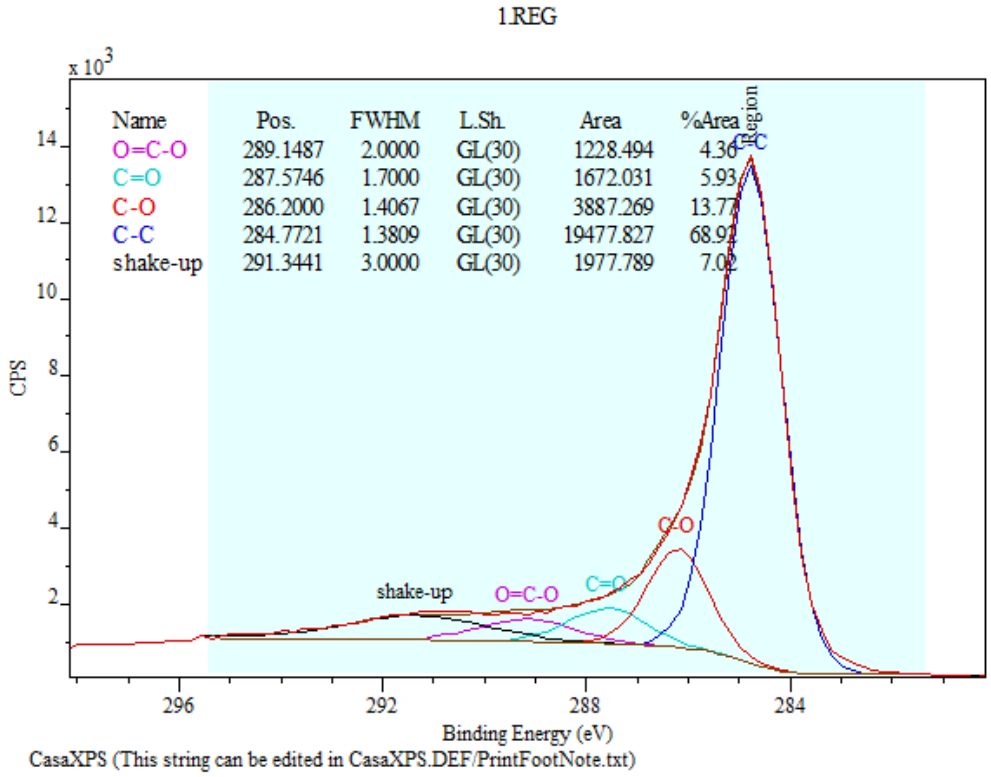

Figure 8-7 Deconvolution spectra of C 1s (Co-N-C/AL)

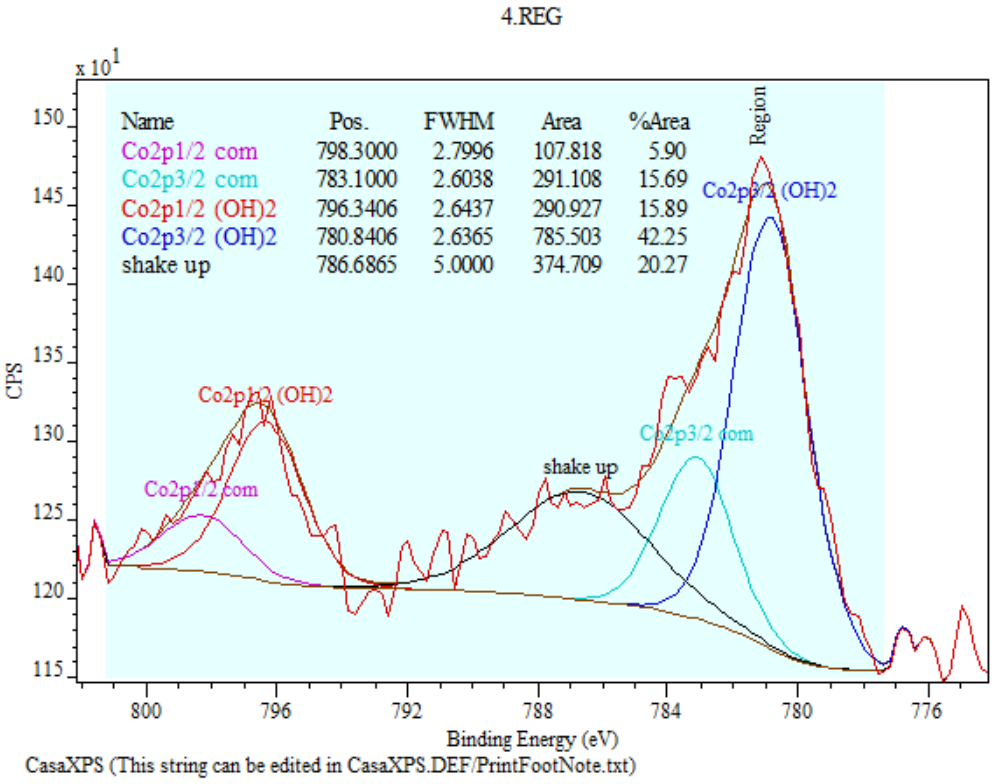

Figure 8-8 Deconvolution spectra of Co 2p (Co-N-C/AL)

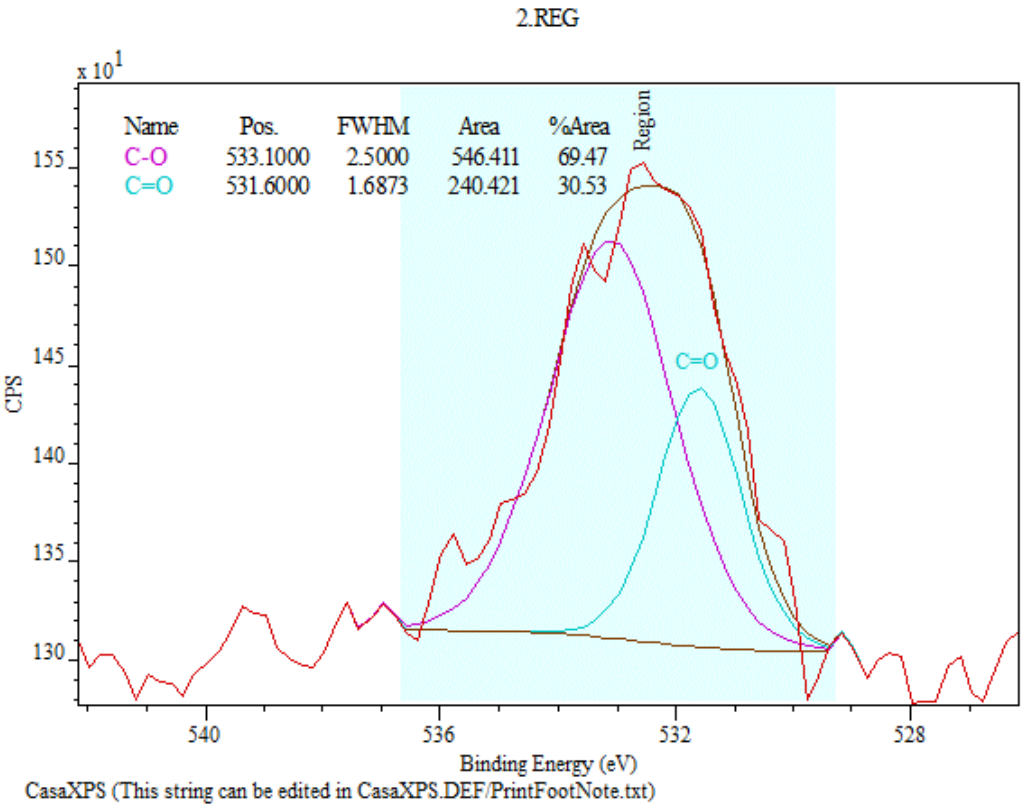

Figure 8-9 Deconvolution spectra of O 1s (Co-N-C/AL)

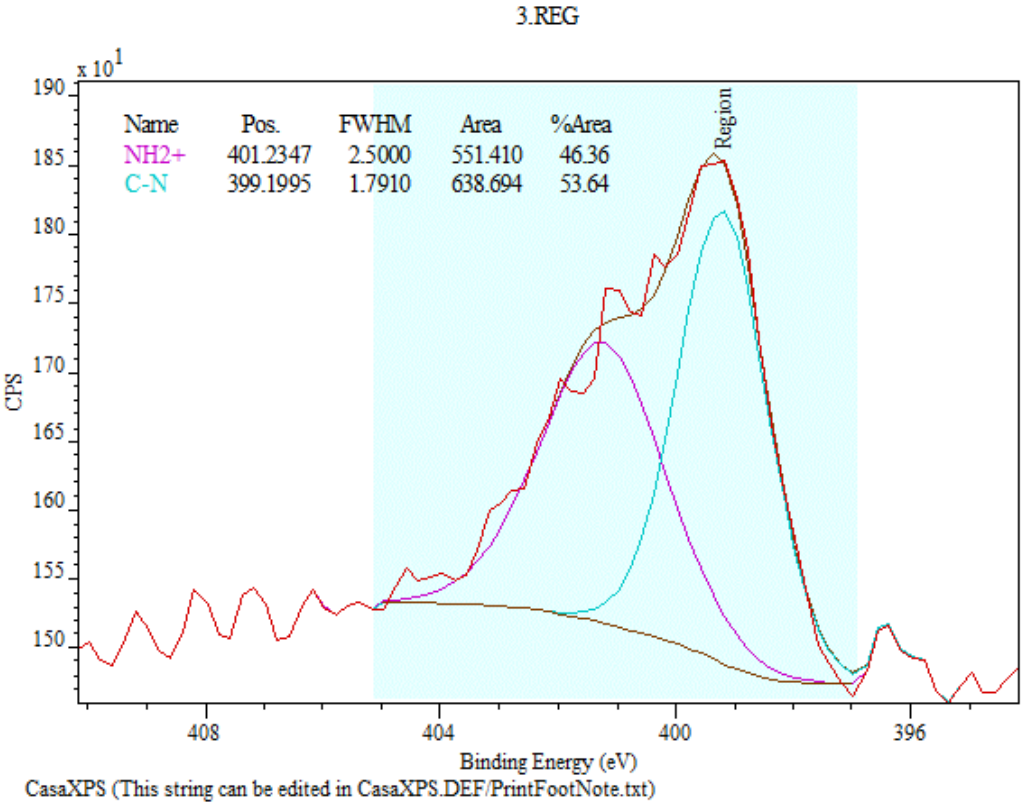

Figure 8-10 Deconvolution spectra of N 1s (Co-N-C/AL)

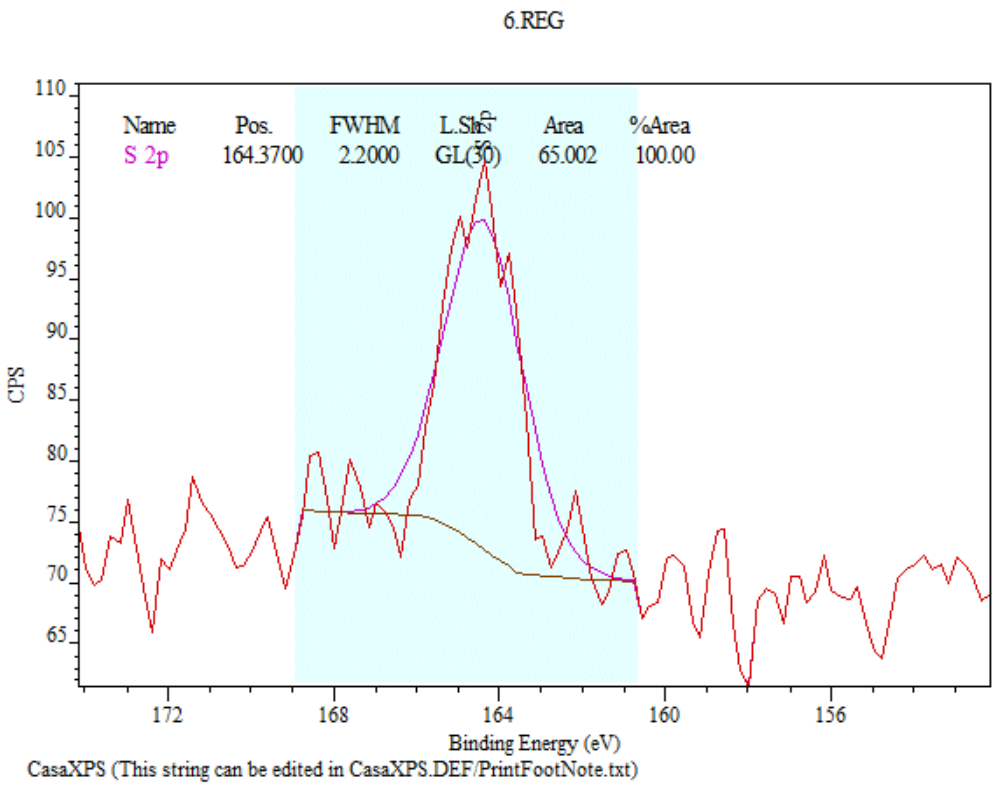

Figure 8-11 Deconvolution spectra of S 2p (Co-N-C/AL)

8.4 Deconvolution XPS spectra of Co-N-C-PANI/AL

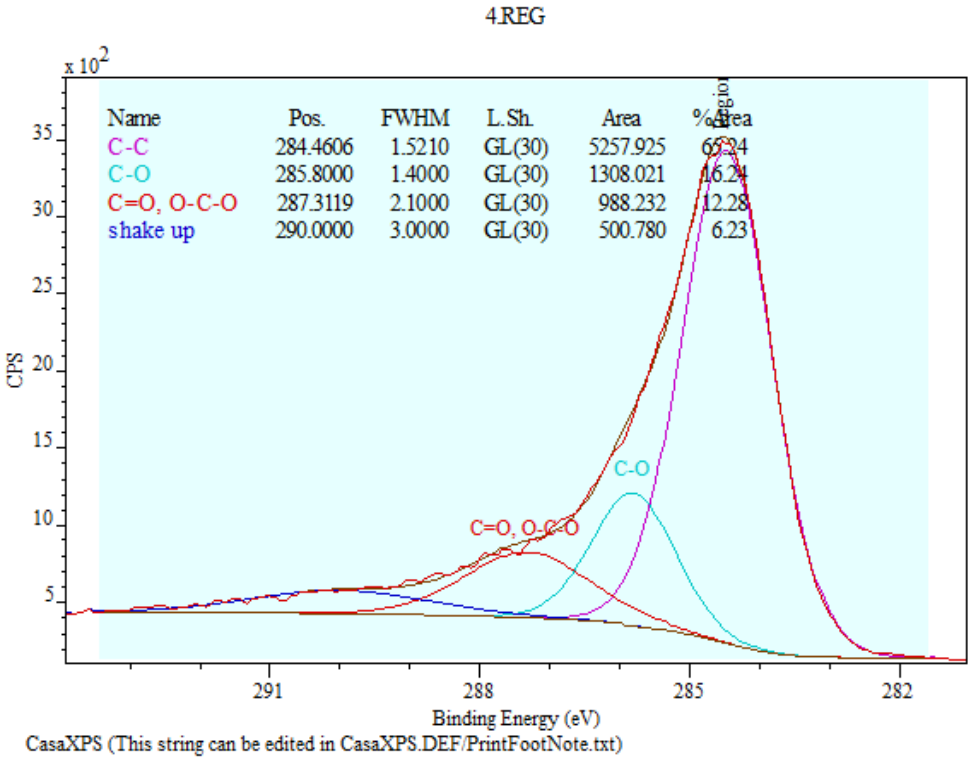

Figure 8-12 Deconvolution spectra of C 1s (Co-N-C-PANI/AL)

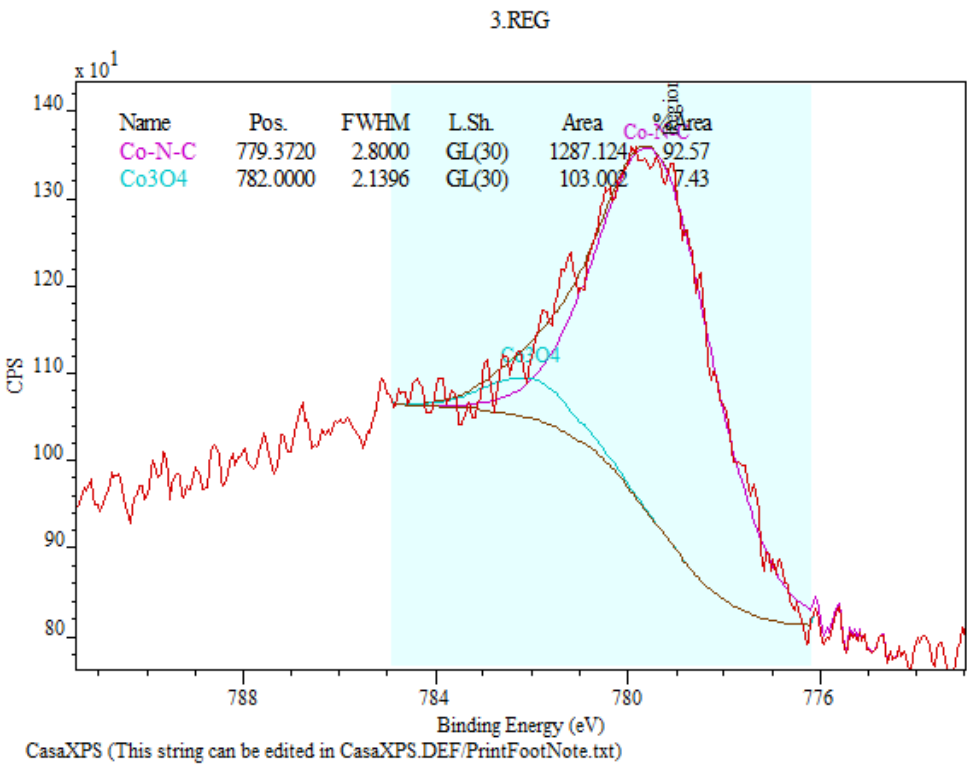

Figure 8-13 Deconvolution spectra of Co 2p (Co-N-C-PANI/AL)

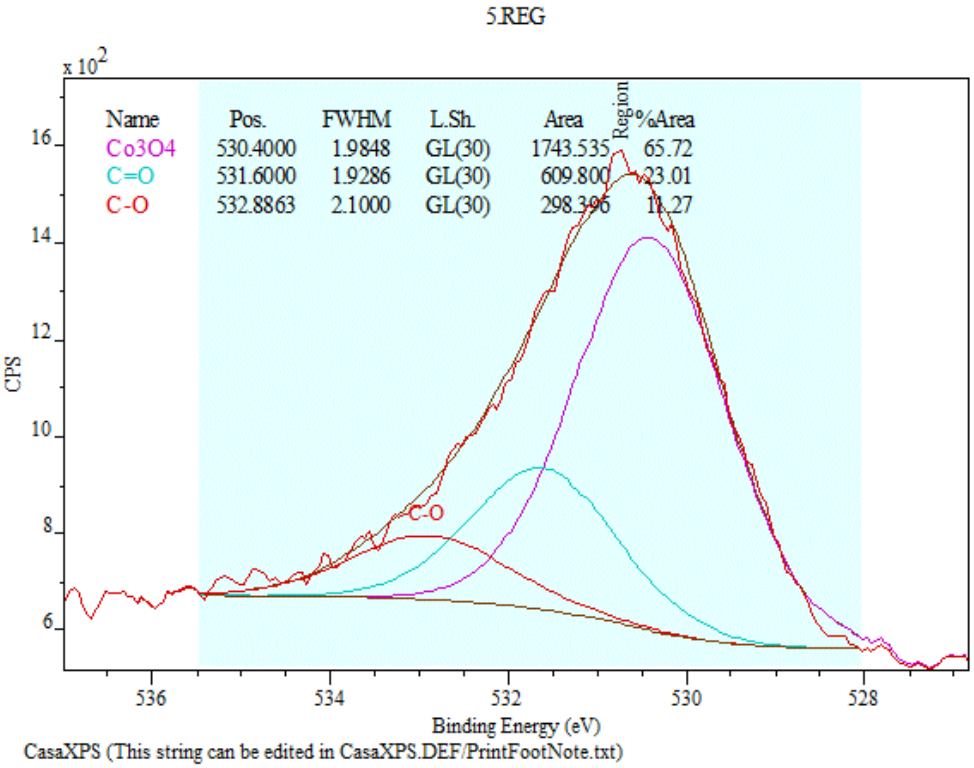

Figure 8-14 Deconvolution spectra of O 1s (Co-N-C-PANI/AL)

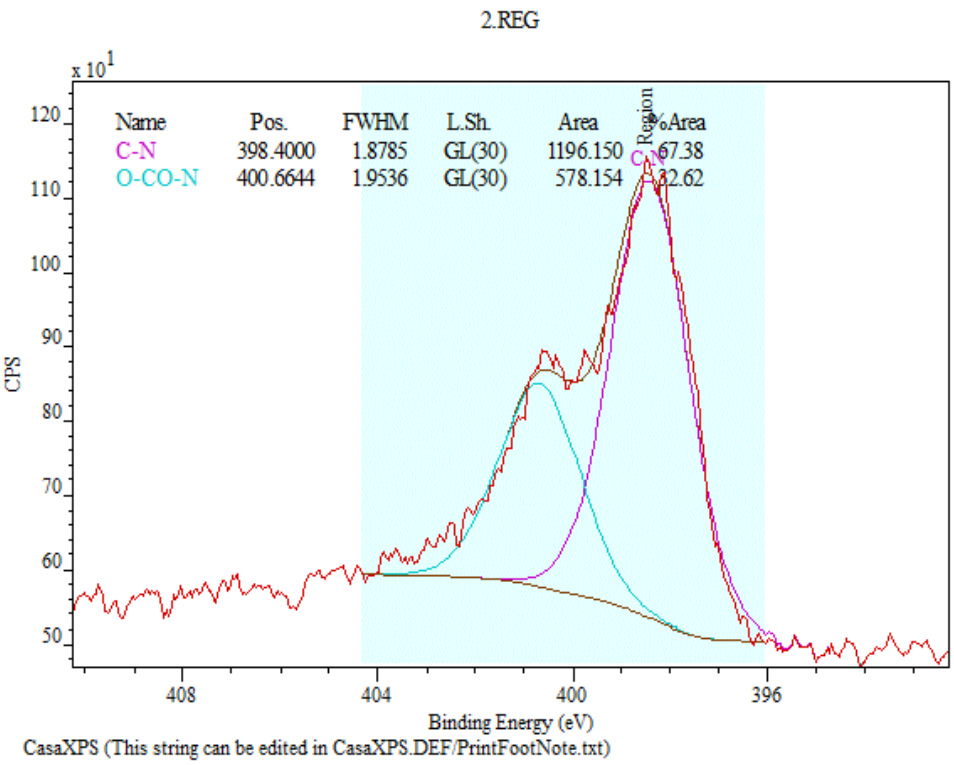

Figure 8-15 Deconvolution spectra of N 1s (Co-N-C-PANI/AL)

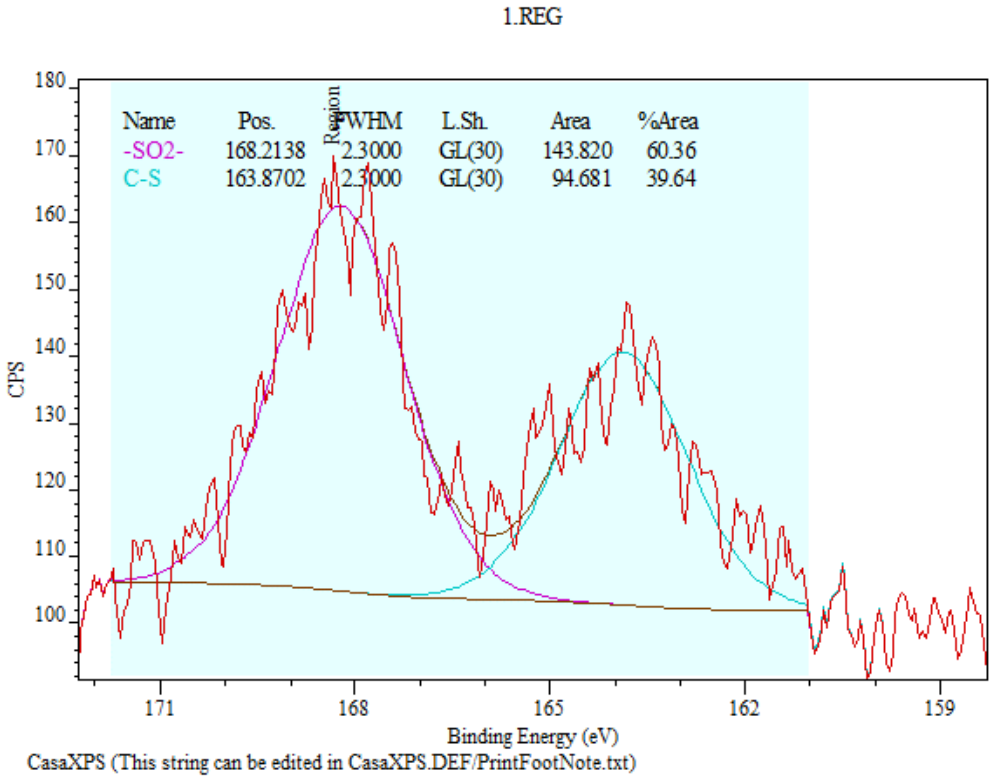

Figure 8-16 Deconvolution spectra of S 2p (Co-N-C-PANI/AL)

8.5 ICP-AES analysis of different Co-N-C catalysts

Mikroanalytisches Laboratorium KOLBE(Nachf.)

Höhenweg 17
D-45470 Mülheim an der Ruhr

Catur Rini Widyastuti
Technische Universität Darmstadt
Ernst-Berl-Institut für Technische und Makromolekulare Chemie
Arbeitsgruppe Prof. Dr. Bastian J.M. Etzold
64287 Darmstadt

Telefon : +49 - (0)208 - 32502
Telefax : +49 - (0)208 - 382314
www.mikro-lab.de
Datum : 31.01.2018

Probenbezeichnung	% Co	% Dry								
Co - N - CB/AL	1,53	0,86								
Co - N - PXP - 750	2,86	1,53								
Co - N - PXP - 750HCL	2,26	2,11								
Co - N - C_HZB	22,73	0,85								

Mit freundlichen Grüssen

Patrick Springer

H. KOLBE
Mikroanalytisches Laboratorium
Höhenweg 17
D-45470 Mülheim a. d. Ruhr

MIKROLAB
Mikroanalytisches Laboratorium Kolbe

Catur Rini Widyastuti
Technische Universität Darmstadt
Ernst-Berl-Institut für Technische und
Makromolekulare Chemie
Arbeitsgruppe Prof. Dr. Bastian J.M. Etzold
64287 Darmstadt

Anschrift : Osterfelder Str. 3
D-46047 Oberhausen
Telefon : +49 - (0)208 - 32502
Telefax : +49 - (0)208 - 382314
Email : info@mikro-lab.de
Webseite : www.mikro-lab.de

Datum : 26.10.2018

Probenbezeichnung	% Co	% Dry										
Co - N - C - PANI	31,86	3,62										

Mit freundlichen Grüssen

Patrick Springer

8.6 Evaluation of internal mass transfer

The Weisz-Prater Criterion is calculated by using equation as follow:

$$C_{WP} = \frac{-r'\rho_s R^2}{D_e C_{AS}}$$

$-r'$ is the observed reaction rate. In this calculation, the rate is evaluated at 1 hour reaction time from experiment using Co-N-C/AL catalyst, where $-r' = kC_A$, $k = 8.74 \times 10^{-4}\ L\ g_{cat}^{-1}\ min^{-1}$, and $C_A \approx 0.09\ M$ (observed at 1 h) Hence, the calculated $-r' = 0{,}7866 \times 10^{-4} mol\ g_{cat}^{-1}\ min^{-1}$.

ρ_s is solid catalyst density, which can be measured from $\rho_s = \frac{m_{cat.}}{V_{cat.}}$. The observed mass of catalyst is 0.12 g and the volume of solid catalyst is 0.2 ml.

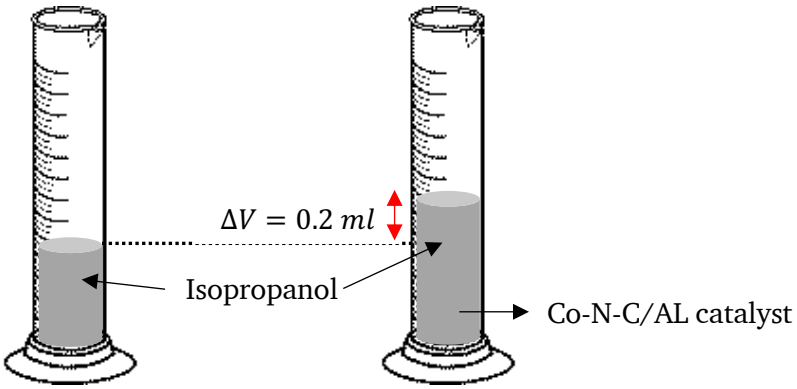

Hence, the density of solid catalyst is $\rho_s = \frac{0.12\ g}{0.2\ ml} = 0.6\ g\ ml^{-1} = 0.6\ g\ cm^{-3}$

R is average catalyst particle radius, which can be described with catalyst mesh size in this study. The average catalyst mesh is $\ll 500\ \mu m = 0.05\ cm$, R = 0.025 cm.

C_{AS} is the reactant concentration at the catalyst surface, which in this study, when the diffusion layer is minimized, the concentration is equal to concentration at bulk liquid. Thus, $C_{AS} = C_A \approx 0{,}09\ M$ (evaluated at 1 hour reaction)

The effective diffusivity, D_e, can be calculated following this formula:

$$D_e = \frac{D_{AB}\emptyset\sigma}{\tau}$$

D_{AB} is the diffusion coefficient which can be calculated using the Wilke-Chang equation as follow:

$$D_{AB} = 7.4 \times 10^{-8} \frac{(\varphi M_B)^{1/2} T}{\eta V_m^{0.6}}$$

Where φ is the association parameter of solvent ($\varphi_{methanol} = 1.9$), M_B is molecular weight of solvent ($M_{methanol} = 32.04\ g\ mol^{-1}$), T is temperature ($T = 333K$), η is viscosity of solution ($\eta_{MeOH\ at\ 60°C} = 0.3528\ cP$), V_m is molar volume of solute (Benzyl alcohol) at normal boiling point. The molar volume of substance i is defined as its molar mass divided by its density ρ_i^0 as follow:

Equation 8-1

$$V_{m,i} = \frac{M_i}{\rho_i^0}$$

Hence, molar volume of benzyl alcohol is $V_{m,i} = \frac{108.14\ g/mol}{1.04\ g/cm^3} = 103.98\ cm^3/mol$

Calculation of D_{AB} is as follow:

$$D_{AB} = 7.4 \times 10^{-8} \frac{(1.9 \times 32.04)^{1/2} \times 333}{0.3528 \times 103.98^{0.6}} = 3.36 \times 10^{-5}$$

Calculation of D_e is as follow:

$$D_e = \frac{3.36 \times 10^{-5} \times 0.4 \times 0.8}{3} = 3.58 \times 10^{-6}$$

Then, all parameters are known to calculate effective diffusivity, D_e, and thus the Weisz-Prater Criterion as listed in Table 8-1.

Table 8-1 Parameter values for calculating the Weisz-Prater Criterion

Parameter	Description	Value	Unit
$-r'$	Observed reaction rate	0.7866×10^{-4}	$mol\ g_{cat}^{-1}\ min^{-1}$
ρ_s	Solid catalyst density	0.6	$g\ cm^{-3}$
R	Average catalyst particle radius	0.025	cm
C_{AS}	Concentration of A (benzyl alcohol) at catalyst surface	0.09	$mol\ cm^{-3}$
D_e	Effective diffusivity of solute into solvent at 333 K (60 °C)	3.58×10^{-6}	$cm^2\ min^{-1}$
∅	Catalyst porosity	0.4[1]	unitless
σ	Constriction factor	0.8[1]	unitless
τ	Tortuosity	3.0[1]	unitless

[1] typical value for the porous catalyst pellet [100].

The Weisz-Prater Criterion can be calculated as follow:

$$C_{WP} = \frac{0.7866 \times 10^{-4} \times 0.6 \times 0.025^2}{3.58 \times 10^{-6} \times 0.09} = 0.0916$$

$C_{WP} \ll 1$

8.7 Presto Kinetics

8.7.1 Determining the reaction order

Variation of initial concentration of benzyl alcohol

Measured data file (.mdf)

$[A]_0 = 0.02\ M$				
Times (h)	[A], M	[B], M	[C], M	[D], M
1	0,0199	0,00000	0,00000	0,0000
2	0,0179	0,00233	0,00247	0,0000
3	0,0144	0,00177	0,00426	0,0000
4	0,0137	0,00156	0,00645	0,0000
5	0,0127	0,00129	0,00795	0,0000
6	0,0110	0,00127	0,00892	0,0000
7	0,0106	0,00169	0,00972	0,0000

Concentration of benzyl alcohol, benzaldehyde, methyl benzoate, and benzyl benzoate are denoted as [A], [B], [C], and [D], respectively.

Calculated concentration

$[A]_0 = 0.02\ M$				
Times (h)	[A], M	[B], M	[C], M	[D], M
1	0,0199	0,000000	0.000000	0,0000
2	0,017782	0,001389	0,000729	0,0000
3	0,015876	0,001732	0,002292	0,0000
4	0,014162	0,001729	0,004009	0,0000
5	0,012623	0,001627	0,00565	0,0000
6	0,011241	0,001503	0,007156	0,0000
7	0,010001	0,001378	0,008521	0,0000

Concentration of benzyl alcohol, benzaldehyde, methyl benzoate, and benzyl benzoate are denoted as [A], [B], [C], and [D], respectively.

Measured data file (.mdf)

$[A]_0 = 0.03\ M$				
Times (h)	[A], M	[B], M	[C], M	[D], M
1	0,0318	0,00000	0,00000	0,0000
2	0,0273	0,00248	0,00292	0,0000
3	0,0246	0,00242	0,00534	0,0000
4	0,0234	0,00224	0,00803	0,0000
5	0,0209	0,00233	0,00947	0,0000
6	0,0200	0,00173	0,01071	0,0000
7	0,0190	0,00192	0,01280	0,0000

Concentration of benzyl alcohol, benzaldehyde, methyl benzoate, and benzyl benzoate are denoted as [A], [B], [C], and [D], respectively.

Calculated concentration

$[A]_0 = 0.03\ M$				
Times (h)	[A], M	[B], M	[C], M	[D], M
1	0,031800	0,000000	0,000000	0,0000
2	0,028517	0,002088	0,001196	0,0000
3	0,025552	0,002554	0,003695	0,0000
4	0,022877	0,002526	0,006397	0,0000
5	0,020466	0,002371	0,008962	0,0000
6	0,018295	0,002190	0,011315	0,0000
7	0,016339	0,002012	0,013448	0,0000

Concentration of benzyl alcohol, benzaldehyde, methyl benzoate, and benzyl benzoate are denoted as [A], [B], [C], and [D], respectively.

Measured data file (.mdf)

$[A]_0 = 0.06\ M$				
Times (h)	[A], M	[B], M	[C], M	[D], M
1	0,0634	0,00124	0,00000	0,0000
2	0,0546	0,00458	0,00511	0,0000
3	0,0503	0,00453	0,01170	0,0000
4	0,0469	0,00454	0,01642	0,0000
5	0,0422	0,00397	0,01750	0,0000
6	0,0415	0,00416	0,02152	0,0000
7	0,0363	0,00412	0,02181	0,0000

Calculated concentration

$[A]_0 = 0.06\ M$				
Times (h)	[A], M	[B], M	[C], M	[D], M
1	0,063400	0,001240	0,000000	0,0000
2	0,057140	0,004147	0,003353	0,0000
3	0,051461	0,004595	0,008584	0,0000
4	0,046313	0,004427	0,013899	0,0000
5	0,041652	0,004129	0,018860	0,0000
6	0,037430	0,003814	0,023396	0,0000
7	0,033610	0,003513	0,027517	0,0000

Concentration of benzyl alcohol, benzaldehyde, methyl benzoate, and benzyl benzoate are denoted as [A], [B], [C], and [D], respectively.

Measured data file (.mdf)

$[A]_0 = 0.1\ M$				
Times (h)	[A], M	[B], M	[C], M	[D], M
1	0,0952	0,00190	0,00000	0,0000
2	0,0836	0,00659	0,00565	0,0000
3	0,0788	0,00694	0,01220	0,0000
4	0,0771	0,00696	0,01936	0,0000
5	0,0712	0,00662	0,02219	0,0000
6	0,0683	0,00675	0,02642	0,0000
7	0,0638	0,00617	0,02843	0,0000

Concentration of benzyl alcohol, benzaldehyde, methyl benzoate, and benzyl benzoate are denoted as [A], [B], [C], and [D], respectively.

Calculated concentration

$[A]_0 = 0.1\ M$				
Times (h)	[A], M	[B], M	[C], M	[D], M
1	0,095200	0,001900	0,000000	0,0000
2	0,086046	0,005876	0,005179	0,0000
3	0,077718	0,006398	0,012984	0,0000
4	0,070149	0,006132	0,020819	0,0000
5	0,063276	0,005714	0,028110	0,0000
6	0,057034	0,005285	0,034780	0,0000
7	0,051370	0,004877	0,040852	0,0000

ODE solver/ syntax

Arguments 3
A value
B value
C value

A = arg1
B = arg2
C = arg3

k1 = getkp("k1")
k2 = getkp("k2")

x = getkp("x")
y = getkp("y")

result1 = -k1*A^x
result2 = k1*A^x-k2*B^y
result3 = k2*B^y

Result overview:

Coefficient's name	Value	95% confidence interval	Residual
x	0.9318	+/- 0.0328	0.1691
y	1.1845	+/- 0.0325	
k1	0.0858	+/- 0.0081	
k2	3.1729	+/- 0.8692	

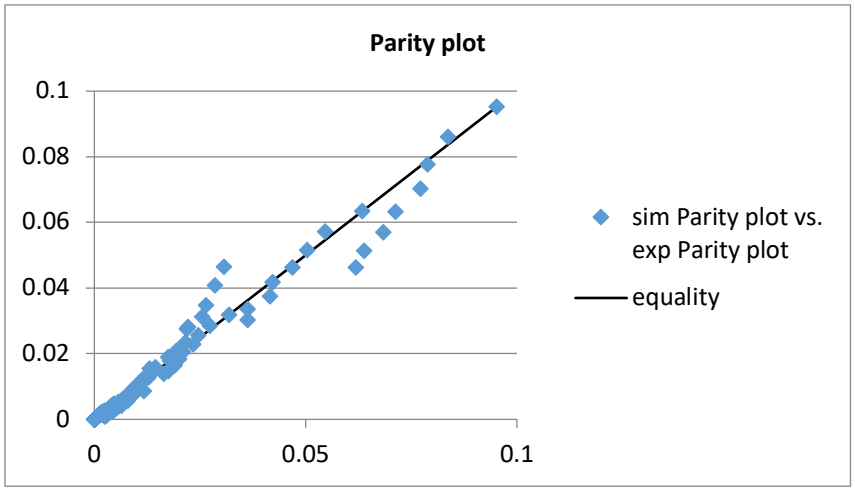

Figure 8-17 Parity plot from parameter estimation (PE) for experiment with variation of initial concentration of benzyl alcohol. Reaction conditions: 0.0199 - 0.0952 M Benzyl alcohol, 2 mmol K_2CO_3, 80 mL methanol, 150 mg Co-N-C/AL catalyst, F_{air}: 20 mL min^{-1}, T: 60°C, speed of stirring: 700 rpm.

8.7.2 Evaluation of the independency of reaction rate to the catalyst mass

Parameter estimation was done using the measured data from t_0 to t_{7h} (t=0.53 min g ml^{-1})

Experiment using catalyst mass of 100 mg

Experimental data

$m_{catalyst} = 100\ mg$				
Times (min g ml^{-1})	[A], M	[B], M	[C], M	[D], M
0,00	0,1010	0,0020	0,0000	0,0000
0,08	0,0902	0,0060	0,0037	0,0000
0,15	0,0888	0,0071	0,0080	0,0000
0,23	0,0842	0,0076	0,0118	0,0000
0,30	0,0808	0,0075	0,0143	0,0000
0,38	0,0792	0,0073	0,0178	0,0000
0,45	0,0743	0,0072	0,0196	0,0000
0,53	0,0739	0,0071	0,0220	0,0000
1,65	0,0593	0,0060	0,0410	0,0000
1,80	0,0561	0,0057	0,0408	0,0000

Concentration of benzyl alcohol, benzaldehyde, methyl benzoate, and benzyl benzoate are denoted as [A], [B], [C], and [D], respectively.

Calculated concentration

$m_{catalyst} = 100\ mg$				
Times (min g ml^{-1})	[A], M	[B], M	[C], M	[D], M
0,00	0,1010	0,0020	0,0000	0,0000
0,08	0,0945	0,0057	0,0027	0,0000
0,15	0,0884	0,0074	0,0072	0,0000
0,23	0,0828	0,0079	0,0123	0,0000
0,30	0,0774	0,0079	0,0176	0,0000
0,38	0,0725	0,0077	0,0228	0,0000
0,45	0,0678	0,0073	0,0278	0,0000
0,53	0,0635	0,0069	0,0326	0,0000

Concentration of benzyl alcohol, benzaldehyde, methyl benzoate, and benzyl benzoate are denoted as [A], [B], [C], and [D], respectively

Experiment using catalyst mass of 150 mg

Experimental data

$m_{catalyst} = 150\ mg$				
Times (min g ml^{-1})	[A], M	[B], M	[C], M	[D], M
0,00	0,0980	0,0019	0,0000	0,0000
0,11	0,0845	0,0071	0,0081	0,0000
0,23	0,0744	0,0071	0,0173	0,0000
0,34	0,0681	0,0068	0,0251	0,0000
0,45	0,0647	0,0065	0,0321	0,0000
0,56	0,0591	0,0055	0,0376	0,0000
0,68	0,0537	0,0059	0,0416	0,0000
0,79	0,0497	0,0053	0,0454	0,0000
2,70	0,0250	0,0038	0,0713	0,0000
3,15	0,0232	0,0032	0,0745	0,0000

Concentration of benzyl alcohol, benzaldehyde, methyl benzoate, and benzyl benzoate are denoted as [A], [B], [C], and [D], respectively.

Calculated concentration

$m_{catalyst} = 150\ mg$				
Times (min g ml^{-1})	[A], M	[B], M	[C], M	[D], M
0,00	0,0980	0,0019	0,0000	0,0000
0,11	0,0887	0,0065	0,0047	0,0000
0,23	0,0803	0,0077	0,0119	0,0000
0,34	0,0727	0,0076	0,0197	0,0000
0,45	0,0658	0,0071	0,0270	0,0000
0,56	0,0596	0,0065	0,0338	0,0000
0,68	0,0539	0,0060	0,0400	0,0000
0,79	0,0488	0,0054	0,0457	0,0000

Concentration of benzyl alcohol, benzaldehyde, methyl benzoate, and benzyl benzoate are denoted as [A], [B], [C], and [D], respectively

Experiment using catalyst mass of 250 mg

Experimental data

$m_{catalyst} = 250\,mg$				
Times (min g ml^{-1})	[A], M	[B], M	[C], M	[D], M
0,00	0,1007	0,0023	0,0000	0,0000
0,19	0,0835	0,0084	0,0144	0,0000
0,38	0,0710	0,0082	0,0335	0,0000
0,56	0,0584	0,0064	0,0469	0,0000
0,75	0,0486	0,0057	0,0564	0,0000
0,94	0,0434	0,0054	0,0681	0,0000
1,13	0,0370	0,0046	0,0736	0,0000
1,31	0,0319	0,0035	0,0781	0,0000
4,13	0,0107	0,0017	0,1123	0,0000
4,50	0,0100	0,0020	0,1142	0,0000

Concentration of benzyl alcohol, benzaldehyde, methyl benzoate, and benzyl benzoate are denoted as [A], [B], [C], and [D], respectively.

Calculated concentration

$m_{catalyst} = 250\,mg$				
Times (min g ml^{-1})	[A], M	[B], M	[C], M	[D], M
0,00	0,1007	0,0023	0,0000	0,0000
0,19	0,0853	0,0078	0,0100	0,0000
0,38	0,0722	0,0077	0,0231	0,0000
0,56	0,0612	0,0067	0,0351	0,0000
0,75	0,0519	0,0057	0,0454	0,0000
0,94	0,0439	0,0049	0,0542	0,0000
1,13	0,0372	0,0041	0,0616	0,0000
1,31	0,0315	0,0035	0,0680	0,0000

Concentration of benzyl alcohol, benzaldehyde, methyl benzoate, and benzyl benzoate are denoted as [A], [B], [C], and [D], respectively

Experiment using catalyst mass of 400 mg

Experimental data

$m_{catalyst} = 400\ mg$				
Times (min g ml^{-1})	[A], M	[B], M	[C], M	[D], M
0,00	0,0988	0,0020	0,0000	0,0000
0,30	0,0753	0,0072	0,0193	0,0000
0,60	0,0568	0,0059	0,0391	0,0000
0,90	0,0465	0,0052	0,0564	0,0000
1,20	0,0363	0,0048	0,0714	0,0000
1,50	0,0284	0,0030	0,0738	0,0000
1,80	0,0238	0,0028	0,0802	0,0000
2,10	0,0193	0,0024	0,0830	0,0000
2,40	0,0157	0,0024	0,0852	0,0000

Concentration of benzyl alcohol, benzaldehyde, methyl benzoate, and benzyl benzoate are denoted as [A], [B], [C], and [D], respectively.

Calculated concentration

$m_{catalyst} = 400\ mg$				
Times (min g ml^{-1})	[A], M	[B], M	[C], M	[D], M
0,00	0,0988	0,0020	0,0000	0,0000
0,30	0,0758	0,0078	0,0173	0,0000
0,60	0,0581	0,0064	0,0363	0,0000
0,90	0,0446	0,0049	0,0513	0,0000
1,20	0,0342	0,0038	0,0628	0,0000
1,50	0,0262	0,0029	0,0716	0,0000
1,80	0,0201	0,0022	0,0784	0,0000
2,10	0,0154	0,0017	0,0836	0,0000

Concentration of benzyl alcohol, benzaldehyde, methyl benzoate, and benzyl benzoate are denoted as [A], [B], [C], and [D], respectively

Experiment using catalyst mass of 600 mg

Experimental data

$m_{catalyst} = 600\ mg$				
Times (min g ml^{-1})	[A], M	[B], M	[C], M	[D], M
0,00	0,1015	0,0023	0,0000	0,0000
0,45	0,0697	0,0072	0,0282	0,0000
0,90	0,0435	0,0049	0,0542	0,0000
1,35	0,0297	0,0034	0,0751	0,0000
1,80	0,0194	0,0026	0,0892	0,0000
2,25	0,0129	0,0019	0,0999	0,0000
2,70	0,0075	0,0000	0,0960	0,0000
3,15	0,0063	0,0000	0,1028	0,0000

Concentration of benzyl alcohol, benzaldehyde, methyl benzoate, and benzyl benzoate are denoted as [A], [B], [C], and [D], respectively.

Calculated concentration

$m_{catalyst} = 600\ mg$				
Times (min g ml^{-1})	[A], M	[B], M	[C], M	[D], M
0,00	0,1015	0,0023	0,0000	0,0000
0,45	0,0682	0,0074	0,0283	0,0000
0,90	0,0458	0,0051	0,0530	0,0000
1,35	0,0308	0,0034	0,0697	0,0000
1,80	0,0207	0,0023	0,0809	0,0000
2,25	0,0139	0,0015	0,0884	0,0000
2,70	0,0094	0,0010	0,0935	0,0000
3,15	0,0063	0,0007	0,0969	0,0000

Concentration of benzyl alcohol, benzaldehyde, methyl benzoate, and benzyl benzoate are denoted as [A], [B], [C], and [D], respectively

ODE solver/ syntax of the first order power law of consecutive reaction for evaluating kinetic of different catalyst mass

```
Arguments      3
A        value
B        value
C        value

A = arg1
B = arg2
C = arg3

k1 = getkp("k1")
k2 = getkp("k2")

result1 = (-k1*A)
result2 = k1*A-k2*B
result3 = k2*B
```

Result overview:

Coefficient's name	Value	95% confidence interval	t-value	Standard error
k1	8.8593e-01	+/- 2.4551e-02	7.0106e+01	1.2526e-02
k2	8.8673e+00	+/- 2.6048e-01	6.6691e+01	1.3290e-01

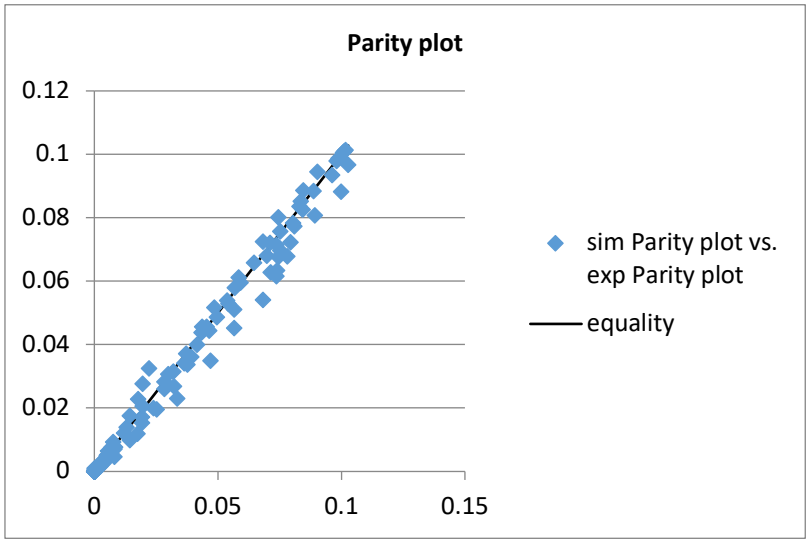

Figure 8-18 Parity plot from parameter estimation (PE) for experiment with variation of catalyst mass. Reaction conditions: 10 mmol Benzyl alcohol, 2 mmol K_2CO_3, 80 mL methanol, 100-600 mg Co-N-C/AL catalyst, T: 60°C, F_{air}: 20 ml min^{-1}, speed of stirring: 300 rpm.

8.7.3 Kinetic differences of various Co-N-C catalysts

Parameter estimation was done using measured data at t_0 to t_{7h}. ODE solver/ syntax of the first order power law of consecutive reaction for evaluating kinetic of different catalyst is as follow:

```
Arguments     4
A         value
B         value
C         value
D         value

A = arg1
B = arg2
C = arg3
D = arg4

k1 = getkp("k1")
k2 = getkp("k2")
k3 = getkp("k3")

result1 = -k1*A-k3*A*C
result2 = k1*A-k2*B
result3 = k2*B-k3*A*C
result4 = k3*A*C
```

Experiment using Co-N-C catalyst

Experimental data

$m_{catalyst} = 500\,mg$				
Times (min g ml^{-1})	[A], M	[B], M	[C], M	[D], M
0,00	0,1347	0,0024	0,0000	0,0003
0,37	0,0919	0,0102	0,0421	0,0010
0,74	0,0696	0,0081	0,0745	0,0006
1,12	0,0478	0,0062	0,0947	0,0007
1,49	0,0328	0,0048	0,1062	0,0006
1,87	0,0259	0,0036	0,1190	0,0005
2,24	0,0184	0,0032	0,1238	0,0011
2,62	0,0148	0,0027	0,1312	0,0011
8,26	0,0019	0,0005	0,1514	0,0001
9,03	0,0016	0,0004	0,1566	0,0001

Concentration of benzyl alcohol, benzaldehyde, methyl benzoate, and benzyl benzoate are denoted as [A], [B], [C], and [D], respectively.

Calculated concentration

$m_{catalyst} = 500\ mg$				
Times (min g ml^{-1})	[A], M	[B], M	[C], M	[D], M
0,00	0,1347	0,0024	0	0,0003
0,37	0,093607	0,011508	0,03188	0,000352
0,74	0,064943	0,008417	0,063369	0,000485
1,12	0,045001	0,005854	0,085585	0,00063
1,49	0,031101	0,004047	0,10104	0,000756
1,87	0,021464	0,002794	0,111733	0,000855
2,25	0,014779	0,001924	0,119139	0,000929
2,62	0,010164	0,001323	0,124247	0,000983

Concentration of benzyl alcohol, benzaldehyde, methyl benzoate, and benzyl benzoate are denoted as [A], [B], [C], and [D], respectively

Result overview:

Coefficient's name	Value	95% confidence interval	t-value	Standard error
k1	9.8000e-01	+/- 1.2453e-01	1.6093e+01	6.0897e-02
k2	8.5200e+00	+/- 1.4614e+00	1.1895e+01	7.1460e-01
k3	9.5000e-02	+/- 2.4740e-02	7.9354e+00	1.2098e-02

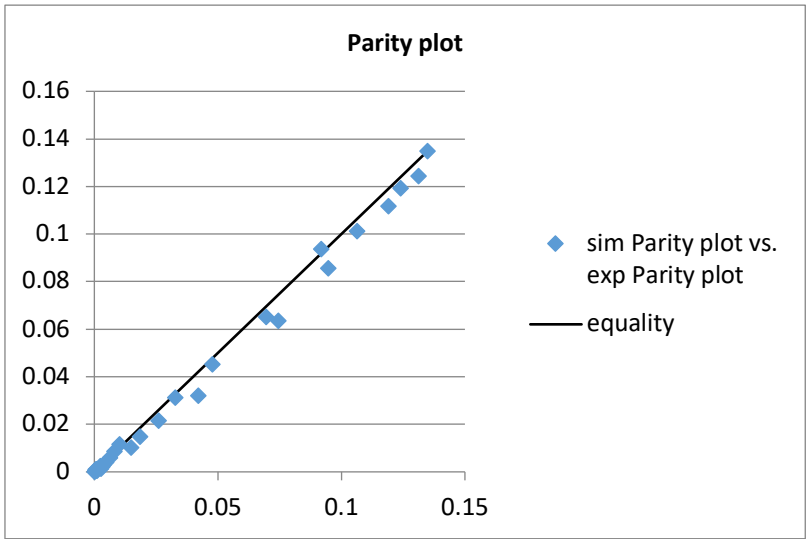

Figure 8-19 Parity plot from parameter estimation (PE) for experiment using Co-N-C catalyst. Reaction conditions: 10 mmol Benzyl alcohol, 2 mmol K_2CO_3, 80 mL methanol, 500 mg Co-N-C catalyst, T: 60°C, F_{air}: 20 mL min^{-1}, speed of stirring: 300 rpm.

Experiment using Co-N-C/AL catalyst

Experimental data

$m_{catalyst} = 500\,mg$				
Times (min g ml^{-1})	[A], M	[B], M	[C], M	[D], M
0,00	0,1158	0,0049	0,0000	0,0000
0,38	0,0651	0,0121	0,0404	0,0003
0,75	0,0391	0,0084	0,0699	0,0006
1,13	0,0254	0,0063	0,0902	0,0007
1,50	0,0158	0,0039	0,0968	0,0004
1,88	0,0111	0,0028	0,1101	0,0002
2,25	0,0077	0,0020	0,1126	0,0002
2,63	0,0048	0,0013	0,1209	0,0006
8,25	0,0003	0,0001	0,1256	0,0000
9,00	0,0002	0,0001	0,1178	0,0000

Concentration of benzyl alcohol, benzaldehyde, methyl benzoate, and benzyl benzoate are denoted as [A], [B], [C], and [D], respectively.

Calculated concentration

$m_{catalyst} = 500\,mg$				
Times (min g ml^{-1})	[A], M	[B], M	[C], M	[D], M
0,00	0,1158	0,0049	0,0000	0,0000
0,38	0,071476	0,014672	0,034488	3,21E-05
0,75	0,044678	0,010049	0,065771	0,000101
1,13	0,027585	0,006279	0,0865	0,000168
1,50	0,017243	0,003931	0,099091	0,000217
1,88	0,01064	0,002427	0,107129	0,000252
2,25	0,006649	0,001517	0,111985	0,000275
2,63	0,004102	0,000936	0,115083	0,000289

Concentration of benzyl alcohol, benzaldehyde, methyl benzoate, and benzyl benzoate are denoted as [A], [B], [C], and [D], respectively

Result overview:

Coefficient's name	Value	95% confidence interval	t-value	Standard error
k1	1.2690e+00	+/- 1.7009e-01	1.5269e+01	8.3176e-02
k2	6.8400+00	+/- 1.2522e+00	1.1106e+01	6.1231e-01
k3	6.5060e-02	+/- 1.7455e-02	7.5572e+00	8.5357e-03

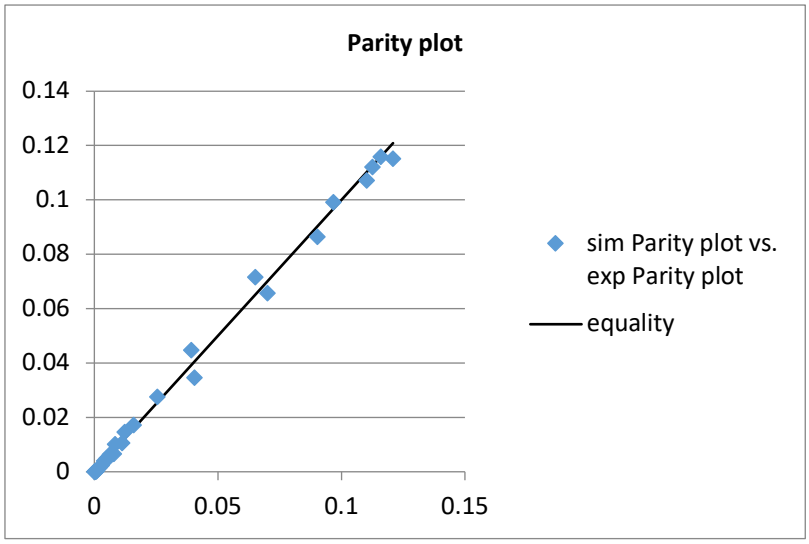

Figure 8-20 Parity plot from parameter estimation (PE) for experiment using Co-N-C/AL catalyst. Reaction conditions: 10 mmol Benzyl alcohol, 2 mmol K_2CO_3, 80 mL methanol, 500 mg Co-N-C/AL catalyst, T: 60°C, F_{air}: 20 mL min^{-1}, speed of stirring: 300 rpm.

Experiment using Co-N-C-PANI/AL catalyst

Experimental data

$m_{catalyst} = 200\ mg$				
Times (min g ml^{-1})	[A], M	[B], M	[C], M	[D], M
0,000	0,13232	0,00445	0,00052	0,00000
0,147	0,09131	0,01450	0,03470	0,00012
0,294	0,05958	0,01114	0,06847	0,00013
0,438	0,05147	0,00927	0,10270	0,00015
0,582	0,02769	0,00628	0,10556	0,00016
0,724	0,02012	0,00514	0,11458	0,00019
0,865	0,01623	0,00424	0,12460	0,00014

Experimental data (continued)

$m_{catalyst} = 200\ mg$				
Times (min g ml^{-1})	[A], M	[B], M	[C], M	[D], M
1,004	0,01233	0,00355	0,12509	0,00015
1,142	0,01033	0,00310	0,12889	0,00012
3,410	0,00069	0,00030	0,14688	0,00000
6,786	0,00003	0,00009	0,15155	0,00000
10,128	0,00000	0,00011	0,15296	0,00000

Concentration of benzyl alcohol, benzaldehyde, methyl benzoate, and benzyl benzoate are denoted as [A], [B], [C], and [D], respectively.

Calculated concentration

$m_{catalyst} = 200\ mg$				
Times (min g ml^{-1})	[A], M	[B], M	[C], M	[D], M
0	0,13232	0,00445	0,00052	0,00000
0,147	0,092309	0,016617	0,028339	1,28E-05
0,294	0,064393	0,013344	0,059461	4,61E-05
0,438	0,045282	0,009616	0,082225	8,35E-05
0,582	0,031837	0,006794	0,098425	0,000117
0,724	0,022491	0,004805	0,109708	0,000143
0,865	0,015926	0,003403	0,117634	0,000164
1,004	0,011331	0,002421	0,123179	0,000179

Concentration of benzyl alcohol, benzaldehyde, methyl benzoate, and benzyl benzoate are denoted as [A], [B], [C], and [D], respectively

Result overview:

Coefficient's name	Value	95% confidence interval	t-value	Standard error
k1	2.4490e+00	+/- 2.7497e-01	1.8072e+01	1.3446e-01
k2	1.3917e+01	+/- 2.5849e+00	1.1392e+01	1.2640e+00
k3	6.6819e-02	+/- 1.5768e-02	8.1707e+00	7.7104e-03

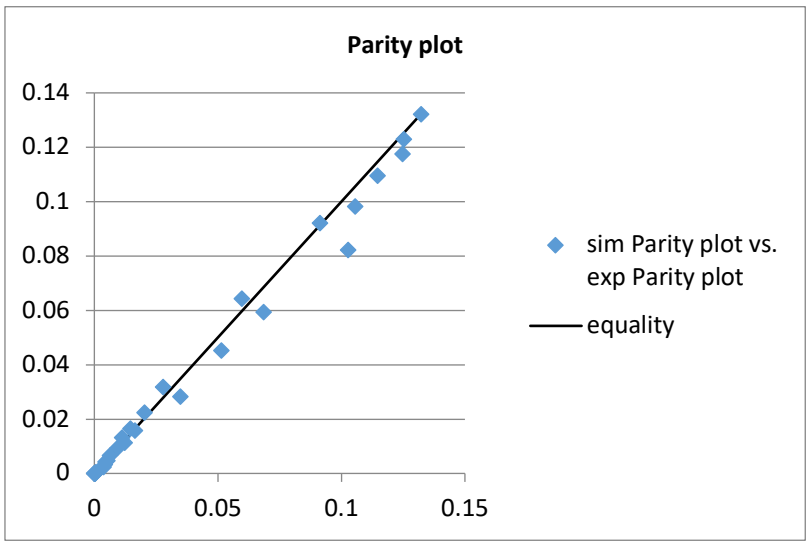

Figure 8-21 Parity plot from parameter estimation (PE) for experiment using Co-N-C-PANI/AL catalyst. Reaction conditions: 10 mmol Benzyl alcohol, 2 mmol K_2CO_3, 80 mL methanol, 200 mg Co-N-C-PANI/AL catalyst, T: 60°C, F_{air}: 20 mL min^{-1}, speed of stirring: 300 rpm.

Experiment using Co-N-C-CoTMPP catalyst

Experimental data

$m_{catalyst} = 125\ mg$				
Times (min g ml^{-1})	[A], M	[B], M	[C], M	[D], M
0,00	0,13947	0,00288	0,00000	0,00000
0,09	0,13425	0,00836	0,00076	0,00000
0,18	0,12768	0,01131	0,00202	0,00000
0,26	0,12300	0,01329	0,00328	0,00000
0,34	0,11923	0,01459	0,00478	0,00000
0,42	0,12041	0,01610	0,00657	0,00000
0,49	0,11341	0,01610	0,00775	0,00000
0,56	0,11233	0,01675	0,00936	0,00001
0,63	0,11166	0,01730	0,01094	0,00004
1,83	0,09602	0,01868	0,02990	0,00011
3,58	0,08534	0,01842	0,04750	0,00025
5,22	0,07746	0,01741	0,05770	0,00036

Concentration of benzyl alcohol, benzaldehyde, methyl benzoate, and benzyl benzoate are denoted as [A], [B], [C], and [D], respectively.

Calculated concentration

$m_{catalyst} = 125\ mg$				
Times (min g ml^{-1})	[A], M	[B], M	[C], M	[D], M
0	0,13947	0,00288	0	0
0,091	0,134842	0,006817	0,00069	1,26E-07
0,178	0,130561	0,009963	0,001825	6,05E-07
0,262	0,126556	0,012501	0,00329	1,53E-06
0,342	0,122855	0,014524	0,004965	2,93E-06
0,419	0,119395	0,016152	0,006793	4,79E-06
0,492	0,116205	0,017442	0,00869	7,06E-06
0,561	0,113267	0,018459	0,010605	9,66E-06

Concentration of benzyl alcohol, benzaldehyde, methyl benzoate, and benzyl benzoate are denoted as [A], [B], [C], and [D], respectively

Result overview:

Coefficient's name	Value	95% confidence interval	t-value	Standard error
k1	3.7082e-01	+/- 2.4476e-02	3.1092e+01	1.1969e-02
k2	1.5457e+00	+/- 1.2506e-01	2.5099e+01	6.1155e-02
k3	3.4120e-02	+/- 5.1296e-03	1.3641e+01	2.5083e-03

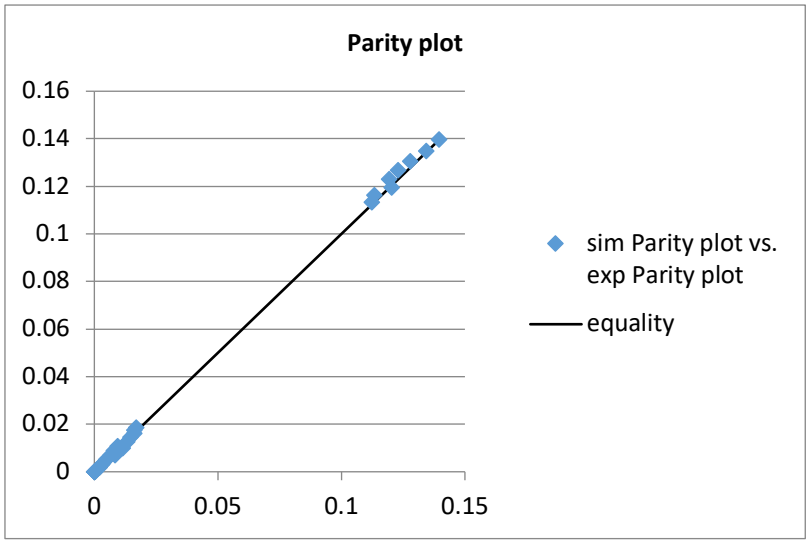

Figure 8-22 Parity plot from parameter estimation (PE) for experiment using Co-N-C-CoTMPP catalyst. Reaction conditions: 10 mmol Benzyl alcohol, 2 mmol K_2CO_3, 80 mL methanol, 125 mg Co-N-C-CoTMPP catalyst, T: 60°C, F_{air}: 20 mL min^{-1}, speed of stirring: 300 rpm.

Experiment using Co-N-C-PXP catalyst

Experimental data

$m_{catalyst} = 302\ mg$				
Times (min g ml^{-1})	[A], M	[B], M	[C], M	[D], M
0,00	0,14056	0,00418	0,00015	0,00000
0,22	0,12282	0,01383	0,00647	0,00000
0,44	0,11102	0,01519	0,01478	0,00004
0,66	0,10425	0,01467	0,02280	0,00006
0,88	0,09803	0,01448	0,03024	0,00010
1,10	0,08986	0,01341	0,03596	0,00013
1,32	0,08780	0,01301	0,04274	0,00012
1,54	0,08154	0,01199	0,04696	0,00013
1,76	0,07717	0,01136	0,05065	0,00015
5,28	0,04569	0,00775	0,08760	0,00026
10,54	0,02980	0,00560	0,10953	0,00057
15,79	0,02144	0,00443	0,11782	0,00055

Concentration of benzyl alcohol, benzaldehyde, methyl benzoate, and benzyl benzoate are denoted as [A], [B], [C], and [D], respectively.

Calculated concentration

$m_{catalyst} = 302\ mg$				
Times (min g ml^{-1})	[A], M	[B], M	[C], M	[D], M
0,00	0,14056	0,00418	0,00015	0
0,22	0,129043	0,010683	0,005158	2,85E-06
0,44	0,118508	0,013419	0,012937	1,3E-05
0,66	0,108825	0,014236	0,021767	3,12E-05
0,89	0,099926	0,014086	0,030764	5,67E-05
1,11	0,091784	0,013477	0,039454	8,78E-05
1,32	0,084336	0,012669	0,047639	0,000123
1,54	0,077486	0,011795	0,055286	0,000162

Concentration of benzyl alcohol, benzaldehyde, methyl benzoate, and benzyl benzoate are denoted as [A], [B], [C], and [D], respectively

Result overview:

Coefficient's name	Value	95% confidence interval	t-value	Standard error
k1	3.8500e-01	+/- 6.8590e-02	1.1449e+01	3.3541e-02
k2	2.8700e+00	+/- 5.1158e-01	1.1433e+01	2.5016e-01
k3	4.2000e-02	+/- 7.9992e-03	1.0661e+01	3.9116e-03

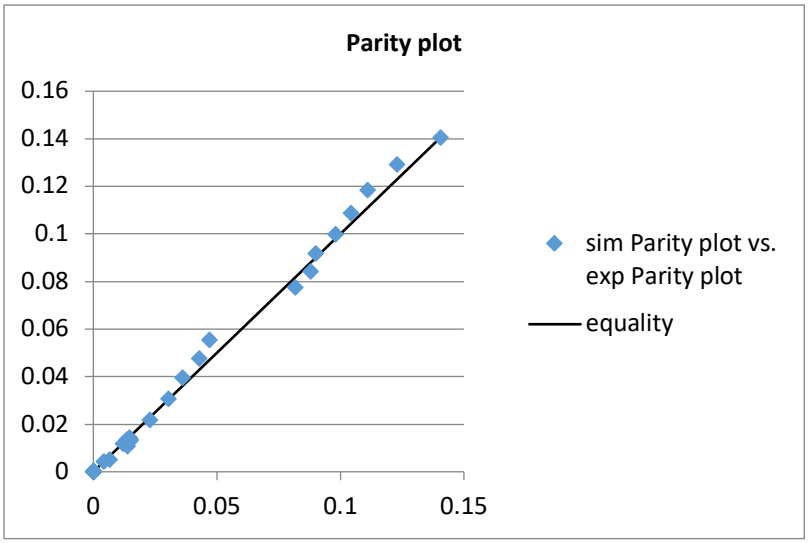

Figure 8-23 Parity plot from parameter estimation (PE) for experiment using Co-N-C-PXP catalyst. Reaction conditions: 10 mmol Benzyl alcohol, 2 mmol K_2CO_3, 80 mL methanol, 302 mg Co-N-C-PXP catalyst, T: 60°C, F_{air}: 20 mL min^{-1}, speed of stirring: 300 rpm.

Experiment using Co-N-C-PXP/AL catalyst

Experimental data

$m_{catalyst} = 284\ mg$				
Times (min g ml^{-1})	[A], M	[B], M	[C], M	[D], M
0,00	0,13687	0,00277	0,00000	0,00000
0,21	0,12377	0,01067	0,00439	0,00000
0,42	0,11622	0,01245	0,01058	0,00004
0,63	0,10710	0,01247	0,01680	0,00005
0,83	0,10411	0,01237	0,02304	0,00008
1,04	0,09409	0,01133	0,02719	0,00007
1,24	0,09348	0,01156	0,03290	0,00011

Experimental data (continued)

$m_{catalyst} = 284\ mg$				
Times (min g ml^{-1})	[A], M	[B], M	[C], M	[D], M
1,44	0,08873	0,01111	0,03804	0,00011
1,64	0,08809	0,01092	0,04307	0,00014
4,92	0,05205	0,00774	0,08101	0,00029
9,81	0,03504	0,00590	0,10730	0,00049
14,67	0,02645	0,00464	0,12854	0,00077

Concentration of benzyl alcohol, benzaldehyde, methyl benzoate, and benzyl benzoate are denoted as [A], [B], [C], and [D], respectively.

Calculated concentration

$m_{catalyst} = 284\ mg$				
Times (min g ml^{-1})	[A], M	[B], M	[C], M	[D], M
0,00	0,13687	0,00277	0	0
0,21	0,127787	0,008306	0,003542	2,11E-06
0,42	0,119379	0,010867	0,009373	1,04E-05
0,63	0,111516	0,011861	0,016211	2,62E-05
0,83	0,104233	0,01202	0,02329	4,88E-05
1,04	0,09745	0,011754	0,030282	7,74E-05
1,24	0,091133	0,011278	0,037007	0,000111
1,44	0,085249	0,01071	0,043385	0,000148

Concentration of benzyl alcohol, benzaldehyde, methyl benzoate, and benzyl benzoate are denoted as [A], [B], [C], and [D], respectively

Result overview:

Coefficient's name	Value	95% confidence interval	t-value	Standard error
k1	3.2691e-01	+/- 4.5564e-02	1.4721e+01	2.2281e-02
k2	2.8736e+00	+/- 4.7258e-01	1.2549e+01	2.3109e-01
k3	5.1557e-02	+/- 9.9537e-03	1.0190e+01	4.8673e-03

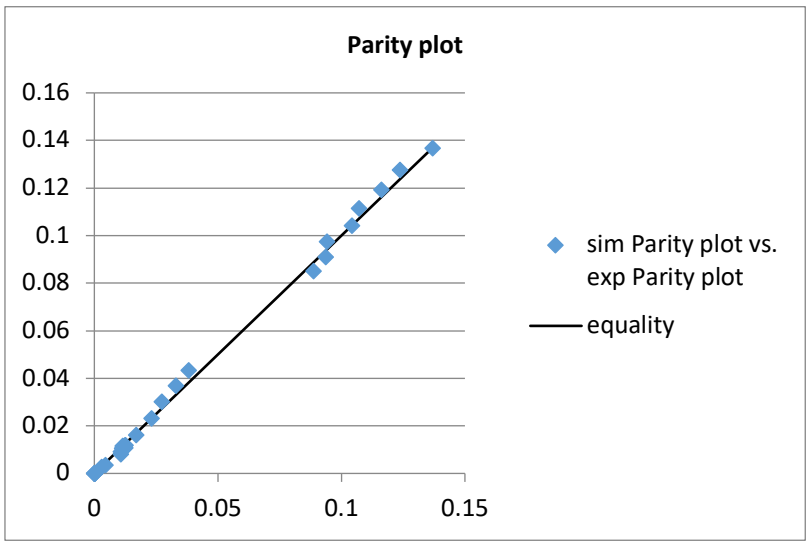

Figure 8-24 Parity plot from parameter estimation (PE) for experiment using Co-N-C-PXP/AL catalyst. Reaction conditions: 10 mmol Benzyl alcohol, 2 mmol K_2CO_3, 80 mL methanol, 284 mg Co-N-C-PXP/AL catalyst, T: 60°C, F_{air}: 20 mL min^{-1}, speed of stirring: 300 rpm.

8.7.4 Evaluation of kinetic in variation of base concentration

Table 8-2 Summary of rate constants from parameter estimation for reaction using Co-N-C/AL catalyst with variation of base concentration

Base concentration (mol %)	Catalyst mass (mg)	Rate constant (ml min^{-1} g_{cat}^{-1})	Estimated value	95% confidence interval	t-value	Standard error
Without base	500	k_1	2.5522e-01	+/- 3.6863e-02	1.3371e+01	1.8052e-02
		k_2	1.0835	+/- 2.0364e-01	1.0748e+01	9.9725e-02
5	500	k_1	4.5525e-01	+/- 5.4045e-02	1.6674e+01	2.6467e-02
		k_2	3.5882	+/- 7.2953e-01	1.1104e+01	3.5726e-01
20	500	k_1	1.2062	+/- 2.0944e-01	1.0817e+01	1.0686e-01
		k_2	6.4852	+/- 1.6051e+00	7.9550e+00	8.1893e-01
5	100	k_1	4.0744e-01	+/- 5.3489e-02	1.5512e+01	2.6194e-02
		k_2	4.0451	+/- 7.9087e-01	1.0380e+01	3.8730e-01
20	100	k_1	7.4458e-01	+/- 5.8131e-02	2.6107e+01	2.8468e-02
		k_2	8.1157	+/- 7.4604e-01	2.2139e+01	3.6535e-01